Fall 2014

Distinguishing Harmonic Behavior Of Longitudinal Resonant Combustion In A Variable Geometry Model Rocket Combustor

Sarah W. Hester
Purdue University

Graduate School Form 30
(Revised 08/14)

PURDUE UNIVERSITY
GRADUATE SCHOOL
Thesis/Dissertation Acceptance

This is to certify that the thesis/dissertation prepared

By Sarah W. Hester

Entitled

DISTINGUISHING HARMONIC BEHAVIOR OF LONGITUDINAL RESONANT COMBUSTION IN A VARIABLE GEOMETRY MODEL ROCKET COMBUSTOR

For the degree of Master of Science in Aeronautics and Astronautics

Is approved by the final examining committee:

William E. Anderson

Stephen D. Heister

J. Stuart Bolton

Matthew J. Casiano

To the best of my knowledge and as understood by the student in the Thesis/Dissertation Agreement, Publication Delay, and Certification/Disclaimer (Graduate School Form 32), this thesis/dissertation adheres to the provisions of Purdue University's "Policy on Integrity in Research" and the use of copyrighted material.

William E. Anderson

Approved by Major Professor(s): _____

_____

Approved by: William E. Anderson on behalf of Wayne Chen 10/16/2014

Head of the Department Graduate Program Date

DISTINGUISHING HARMONIC BEHAVIOR OF LONGITUDINAL RESONANT COMBUSTION IN A VARIABLE GEOMETRY MODEL ROCKET COMBUSTOR

A Thesis

Submitted to the Faculty

of

Purdue University

by

Sarah Hester

In Partial Fulfillment of the

Requirements for the Degree

of

Master of Science in Aeronautics and Astronautics

December 2014

Purdue University

West Lafayette, Indiana

To my family for their unwavering support and motivation.

ACKNOWLEDGEMENTS

This work would not have been possible without the support of many people. First and foremost, I would like to thank my advisor, Professor Bill Anderson. He has made my time at Purdue a truly educational experience and supported my need to explore the world. Special thanks are also due to Tom Feldman, who was the best mentor I could ask for. His guidance and introduction to the CVRC were invaluable. I'd also like to thank Justin Hardi for acting as a secondary mentor, teaching me the importance of doing things right and questioning everything. Additionally, I am very grateful to Professor Steve Heister for his support before I ever arrived at Zucrow Laboratories that has continued through my last day at Purdue.

A lot of the work done to support this study was outside of my area of expertise, and I am extremely grateful to the subject matter experts who helped me bridge the gaps in my knowledge. First, Matt Casiano from NASA MSFC was a constant resource for not only PC Signal Analysis but also as a general sanity check. Professor Michael Zoltowski of Purdue University eagerly attacked the problem of processing experimental data with me and provided insight into the world of digital signal processing. Professor J. Stuart Bolton of Purdue University helped clarify acoustic concepts for me and suggested ideas from a non-combustion standpoint. David Kittel spent three months developing a wavelet analysis supplemental code so that I didn't have to and was always willing to take the time

to walk through the process with me. And while I never worked directly with him, Jim Sisco's previous efforts helped guide my work, not just with the oscillation decrement but with the whole study in general.

I'd like to thank my lab mates, especially Tom Feldman, Justin Hardi, Mike Bedard, and Zach Hallum. Working with them was always enjoyable. Thanks also to Cheng Huang for letting me pick his brain on topics I didn't understand. Scott Meyer and Rob McGuire were tireless and infinitely helpful resources that I could always depend on. And a special thanks to the group at The University of Rome La Sapienza under Professor Marcello Onofri and Professor Francesco Nasuti. My time in Italy was a life experience I'll never forget, especially because of Dr. Marco Pizzarelli and Dr. Giovanna Gargiulo. Finally, I'd like to thank Steve Shark for his role as editor with all of my written works and his unconditional support.

This material is based upon work supported by the National Science Foundation Graduate Research Fellowship under Grant No. DGE-1333468. Any opinion, findings, and conclusions or recommendations expressed in this material are those of the authors and do not necessarily reflect the views of the National Science Foundation.

TABLE OF CONTENTS

Page

Page

Page

Page

LIST OF TABLES

LIST OF FIGURES

Figure Page

Figure Page

NOMENCLATURE

α	Exponential Growth Rate
BP	Band Pass Filter
CVRC	Continuously Variable Resonance Combustor
CWT	Continuous Wavelet Transformation (for Wavelet Analysis)
DSP	Digital Signal Processing
FDA	Filter Design and Analysis (for Matlab)
FFT	Fast Fourier Transformation
Δf	Frequency Resolution
GUI	Graphical User Interface
HP	High Pass Filter
IF	Instantaneous Frequency tracking (from PC Signal Analysis)
Lop	Oxidizer Post Length
#L	The #-th Longitudinal Mode
MSFC3	Test Series Test Number
ORSC	Oxygen-rich Staged Combustion
PSD	Power Spectral Density
PT	Pressure Transducer

ABSTRACT

Hester, Sarah W. M.S.A.A., Purdue University, December 2014. Distinguishing Harmonic Behavior of Longitudinal Resonant Combustion in a Variable Geometry Model Rocket Combustor. Major Professor: William E. Anderson.

Throughout the study of high frequency combustion instability in a single element Continuously Variable Resonance Combustor (CVRC), the excitation of the fundamental longitudinal mode is closely followed by the excitation of higher harmonic modes. In an attempt to establish a heuristic relationship between the appearances of the fundamental mode and its harmonics, several unstable fixed geometry and variable geometry tests from the CVRC are analyzed through traditional Fourier-based methods and alternative signal processing methods such as wavelet analysis and Instantaneous Frequency (IF) Analysis from PC Signal Analysis. Early results led to the conclusion that traditional Fourier-based analysis provides believable and consistent results for the first three modes. However, Fourier analysis is sensitive to effects from non-sinusoidal waveforms.

Further work using manufactured signals with both sinusoidal and steep-fronted waveforms established that it is unclear which parts of the calculated harmonic signals are data artifacts and which are true signal. Supplementary assessment of IF Analysis and the traditional Fourier-based analysis explored the applicability of each method, the inherent data artifacts, and

distinguishing behavior between the experimental data and those data artifacts. The results obtained from the IF Analysis provide good agreement with the traditional Fourier-based analysis, though one uses FIR filters and the other uses IIR filters. The validity of the results is sensitive to the settings chosen for these filters.

It is shown that harmonic modal content exists in the CVRC, but it is also shown that the current results include indistinguishable Fourier artifacts. Both methods are sensitive to the sinusoidal assumption and cannot correctly interpret steep-fronted waveforms. This supplementary assessment has shown that IF Analysis is no worse than traditional Fourier-based analysis, but it fails to provide additional useful information.

Qualitative modal behavior is distinguishable from the experimental data, including the sequential excitation of modes and the increasing growth rate with increasing mode number. However, quantitative results such as the growth rate or modal amplitude have been shown to be unreliable. The acoustic wave assumption is supported by the standing wave behavior observed in the CVRC, specifically the decreasing amplitude of a mode near its equivalent pressure node location and the relative phase between modal signals on either side of its equivalent pressure node. However, the shock-like wave assumption has not been completely disproved. Additional work needs to be done with wavelet analysis using steep-fronted wavelet shapes to assess the potential steep-fronted waveform.

CHAPTER 1. INTRODUCTION

Combustion instability within liquid bi-propellant systems continues to be a major subject of study as models have yet to be developed that can accurately and reliably predict the combustion dynamics of any given combustor design [1,2]. Combustion instabilities can be very destructive in rocket engines and can lead to the structural failure of the engine or catastrophic damage to the payload [3]. Due to the complex interactions between combustion kinetics, heat transfer, fluid dynamics, acoustics, viscosity, and other physical phenomena, analytical models to date have been largely heuristic and require experimental data to validate any modeling effort [2,4]. Despite this, significant advances have been made in understanding the mechanisms producing dynamic responses in liquid combustion systems [3,5]. Pursuing relationships for unstable combustion continues to be worthwhile as further knowledge of combustion dynamics brings researchers closer towards the ultimate goal of *a priori* instability knowledge.

1.1 Overview of Combustion Instability

There are two primary classes of unstable combustion, specified by frequency ranges. Low frequency combustion instability, more commonly referred to as “chug” or “pogo instability”, occurs below 1000 Hz and is most often due to interactions between the gas residence time and bulk mode of the chamber [1,3,6]. Chug is most

commonly seen in gas turbine systems which have a lower speed of sound (lower frequency) than rocket engines, though NASA's Apollo 13 lunar mission is a notorious example of pogo in rocket engines [3]. Of more interest in this study is high frequency combustion instability which often occurs in the 1000's of Hz range and is a result of spatial-temporal coupling between unsteady heat release and resonant acoustic modes of the combustion chamber, hence the name "resonant combustion" [1,3,7]. It is also known as "screeching" for the audible high-pitched sound during unstable combustion. A relationship between heat release and pressure was first established by Sir Rayleigh in 1874, where the relative phase between the two fluctuating combustion characteristics would dictate whether pressure oscillations would be excited or damped in a system [1,3,8]. More specifically, if the maximum heat release is in phase with the maximum pressure, a circumstance exists that allows for positive growth of the pressure oscillations [1]. In its simplest form, Rayleigh's criterion can be expressed as

$$\int_0^T p' * \dot{Q}' dt \tag{1.1}$$

where p' is the fluctuating pressure and $\dot{Q}'$ is the fluctuating heat flux[1,3,8]. In its expanded form,

$$\frac{\partial}{\partial t}\int_V \langle \frac{p^2}{2\rho_0 c^2} + \frac{\rho u^2}{2} \rangle \, dV + \oint_S (pu) dS = \frac{\gamma - 1}{c^2}\int_V \langle pQ \rangle dV \tag{1.2}$$

where bracket $\langle \quad \rangle$ refers to a time-averaged quantity [8]. In the 150 years since Rayleigh's criterion was first proposed, significant advances have been made in the understanding of high frequency combustion instability, yet Rayleigh's criterion continues to be integral in analytical models developed [1,3,9–11].

Two primary resources on combustion instabilities in liquid rocket engines are NASA Special Publication 194 (SP-194) entitled "Liquid Propellant Rocket

Combustion Instability", a 1974 compilation of current knowledge by Harrje and Reardon [1], and one of AIAA's Progress in Astronautics and Aeronautics books entitled "Liquid Rocket Engine Combustion Instabilities", a 1995 compilation of up-to date knowledge by Yang and Anderson [12] meant as an update to SP-194.

1.1.1 Modes of Instability

There are three modes of resonant combustion: tangential, radial, and longitudinal [1,3,13]. The mode(s) present is largely dictated by the internal geometry of the combustor and the chemical kinetics of the propellants. Tangential modes, where pressure oscillations travel back and forth from the combustor walls as illustrated in Figure 1.1a, can be the most destructive and are therefore studied most often [1,3,7]. The interactions between neighboring injector elements largely affect the occurrence of tangential modes while the frequencies of the modes seen depend on internal geometric features such as the diameter in a cylindrical combustion chamber. Less common and of less interest is the radial mode. Figure 1.1b demonstrates the first and second radial mode, which act like ripples in a pond as the pressure moves outward from the combustor axis and reflects on the combustor walls [1,3,14].

The focus of this study is longitudinal modes of instability. In a closed combustor, pressure waves reflect off of acoustic boundaries at the injector and nozzle as illustrated in Figure 1.1c. Longitudinal instabilities are thought to be dependent on a kinetics-based characteristic time lag and internal geometries such as the length of the combustion chamber and/or length of the injector [1,4,13,15]. Previous work has shown the tendency for the frequencies of pressure oscillations to couple with the chamber acoustic frequencies [1,4,7]. Other factors that affect all

modes include the propellant combination, equivalence ratio, injector type, and internal speed of sound [1,12,14,16,17].

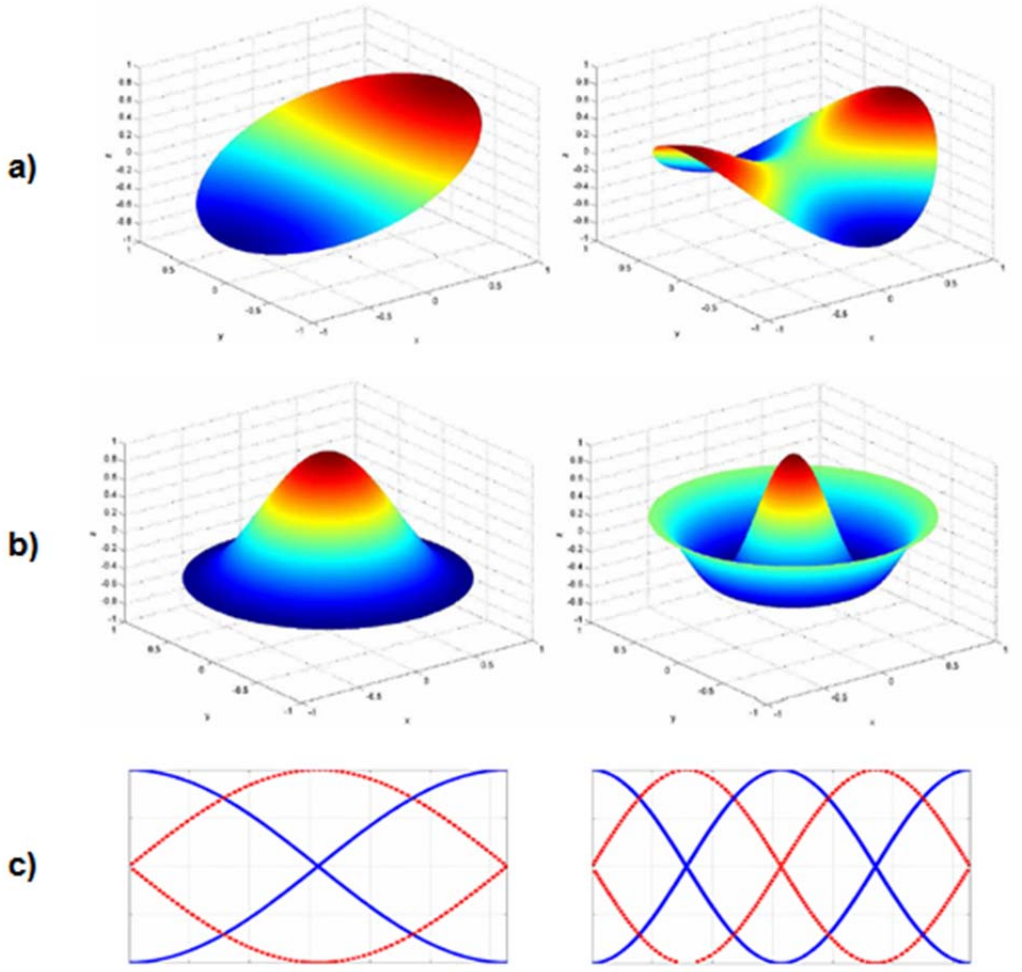

Figure 1.1 The first two modes of instability for a) tangential, b) radial, and c) longitudinal instability. [18]

Any reference to a "mode" from this point forward will be to a longitudinal mode unless otherwise specified. Numbering of modes such as second mode or 2L refers to the harmonic frequency of the longitudinal mode at $2*f_1$, where f_1 is the fundamental frequency. It is also important to note that 2L does not necessarily refer to the second natural acoustic mode of the chamber, and the fundamental

frequency here called 1L may couple with any mode of the chamber, such as the third natural acoustic mode [4]. See Ref.[4] for a detailed comparison of the excited frequencies observed and the calculated natural acoustic frequencies of the chamber.

1.2 Previous Related Work

1.2.1 Subscale Testing

As mentioned previously, *a priori* knowledge of the combustion dynamics of a rocket engine design does not currently exist and analysis of the designed combustor requires thorough testing to obtain empirical values to support heuristic modeling efforts. As computational power has increased, recent analysis has shifted towards computational fluid dynamics (CFD) validated by experimental data. However, high fidelity modeling and full-scale testing are expensive both in terms of cost and time. Because of these restrictions, new designs commonly use previous stable engine designs as a guide, limiting the range of designs and performance available [1,3,4,18]. For example, Russian liquid rocket engines operate at chamber pressures on the order of 2000 psi or more, while equivalent American designs are limited to half this [4]. This makes subscale testing an attractive option so long as the behavior of the full-sized engine can be represented in its smaller counterpart.

Replicating the full-scale behavior can be difficult, as most laboratory settings cannot run tests at the high operating chamber pressure (on the order of 1000 psi) and mass flow rates (on the order of 1-10 kg/s), so special attention must be given to the scaling method used [18]. Since longitudinal modes are the sole interest of this study, isolating this mode class is also highly desirable. In the development of oxygen-rich staged combustors (ORSC), the Russians had success

with subscale testing campaigns by developing a single injector element to isolate and study longitudinal instabilities [4,14,18]. The injectors tested at that time, the RD-170 and RD-180, have been used as a design guide for the gas-centered swirl coaxial injector used in this study, discussed in Section 1.2.3 [4,18–22]. See Ref. [4] and [23] for a more in depth summary of historical subscale testing and the design processes typically used.

The study of combustion dynamics in ORSC is especially of interest at American institutions due to the lack of historical experience; in the past, American liquid rocket engines utilized fuel-rich combustion systems while Russian liquid rocket engines utilized the more efficient but more difficult oxygen-rich combustion systems [4,14,18,24]. ORSC provide advantages in terms of weight and efficiency, but they are also more prone to instabilities and have more stringent material requirements due to the higher temperature and high pressure oxygen-rich environment [4,18].

Traditional instability modeling often includes a characteristic time lag as proposed by Crocco and Cheng, which for liquid propellant engines can include the time for droplets to form, vaporize, and mix [25,26]. In subscale testing, the length of the combustor is often not long enough for complete combustion of liquid propellants. In the case of ORSC, the oxidizer will have been through a pre-burner in full scale engines, so some combustion products will exist when injected into the main chamber and the injection temperature will be high (on the order of 1000 K) [18]. Subscale testing for ORSC can utilize decomposed peroxide in the study of staged oxygen-rich combustors as it simulates the pre-burner products of gaseous oxygen and water vapor at a decomposition temperature around 1200 ^{o}F (925 K). Earlier testing programs have shown comparable dynamic behavior using gaseous

propellants in place of liquid propellants as would be used in full-scale tests [16,17]. Both liquid and gaseous fuels may be used in subscale testing, with gaseous methane used in this study. Previous work by Miller [18], Smith [19], and Sisco [4] used liquid hydrocarbon fuel (JP-8), while work by Yu [20], Rosen [21], and Feldman [22] used gaseous fuels (CH_4 and H_2) for better comparison to CFD conditions. Similar single element ORSC work done by Pal et al. at Penn State used liquid RP-1 for direct comparison to full scale engines [27].

1.2.2 Variable Chamber Length

In the 1950's and 1960's, Zucrow and Osborn performed subscale testing at Purdue University to study longitudinal combustion instabilities, specifically the effect changing several parameters would have on the stability of a combustor [16]. One of these parameters was the length of the combustion chamber, and through this testing they established a relationship between the length of the combustion chamber and the stability of the combustor, as discussed in Sec. 2.3.

In more recent work done in 2005, Miller also studied longitudinal combustion instabilities utilizing a single element combustor and discretely variable chamber length [18]. The combustor was designed to encourage self-excited instabilities, with a rear-facing step at the dump plane to encourage vortex shedding and an oxidizer post designed to remove the minimum amount of energy, shown in Figure 1.2. The design focused on acoustic coupling between the oxidizer injector post and combustion chamber [18]. The experimental work qualitatively agreed with a linear model of a coupled acoustical system. Smith supplemented Miller's experimental work with 1D CFD modeling, using both Euler equations and Reynolds Averaged Navier-Stokes (RANS) equations [19].

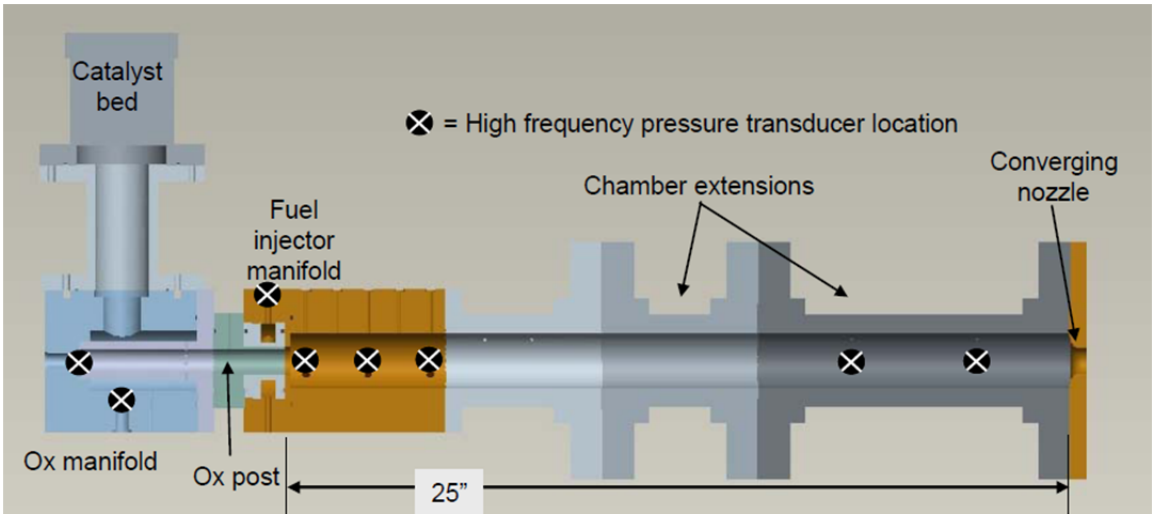

Figure 1.2 Cross section of Miller's variable chamber length experiment. [18]

Miller's work was expanded by Sisco, who continued experimental investigations, this time into the effect of the injector face width, while developing both linear and nonlinear acoustic models for comparison [4]. Of most interest are the models developed, which build off work done by Culick for linear acoustic analysis [2] and Zinn and Lores for nonlinear stability analysis utilizing a normalized Galerkin method (see Sec. 2.3) [28,29].

1.2.3 Variable Oxidizer Post Length

In the last five years, longitudinal combustion instability research has centered on a Continuously Variable Resonance Combustor (CVRC), a second generation device that builds off Miller's work [18,20–22]. The CVRC is able to change the oxidizer post length during a test, as illustrated in Figure 1.3. This allows for the study of the coupling between the length of the oxidizer post and the combustion chamber length. Original experimental and analytical work was performed by Yu in 2009 [20], and design specifications on both the hardware and

equipment used in the CVRC as well as the data acquisition (DAQ) design can be found in Ref. [20–22]. Significant features of the CVRC include: 1) a translating shaft to actively vary the length of the oxidizer post by moving the sonic inlet, 2) a backward-facing step at the dump plane to encourage acoustically-induced vortex shedding and consequent instabilities, and 3) modular chamber sections to allow for optical study of combustion by replacing one chamber section with a quartz tube.

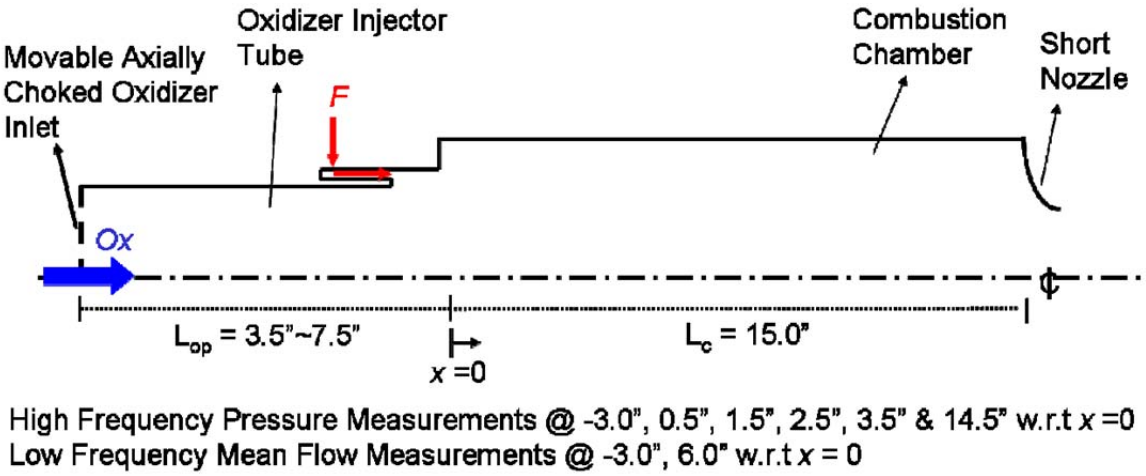

Figure 1.3 Schematic of the CVRC with instrumentation locations. [20]

Figure 1.3 and Figure 1.4 illustrate the cross section of the CVRC hardware and relevant instrumentation locations. Of particular interest is the location of high frequency pressure transducer (PT) ports, at the oxidizer manifold, the oxidizer post, the fuel manifold, and at 0.5 in, 1.5 in, 2.5 in, 3.5 in, 9.5 in, and 14.5 in along the axial length of the combustion chamber. Primarily, investigations have been done using data from the 14.5 in location, as this corresponds to a pressure anti-node [20]. To test for transverse or radial instabilities, a second transducer is placed at the 0.5 in location at a 60° angle to the other axial ports. The geometry

of the combustor was chosen based on the results in Miller and Sisco's theses, as self-excited instabilities are the objective of this design [4,18,20].

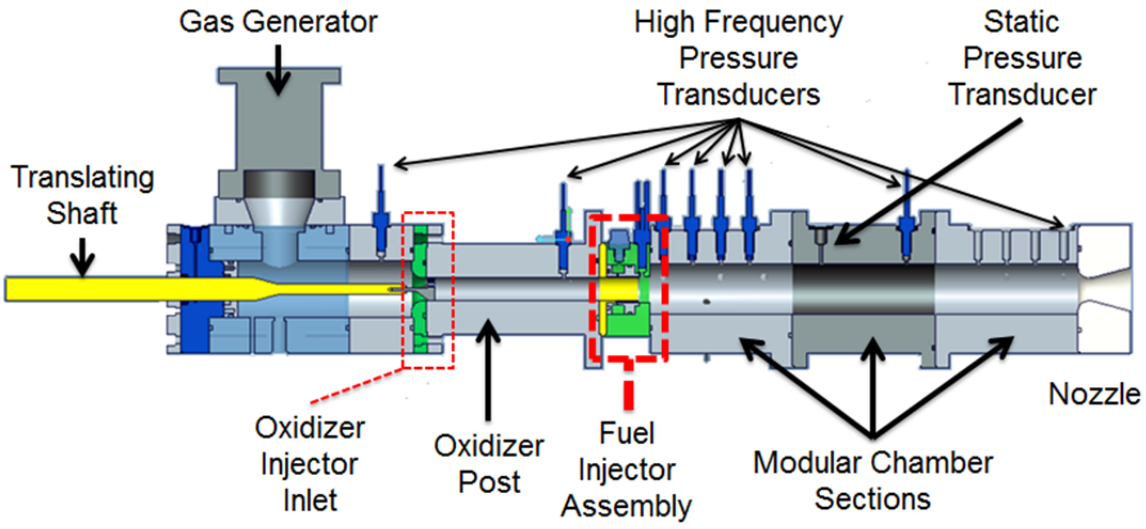

Figure 1.4 Cross section of the CVRC experiment. [30]

The CVRC has been a useful validation tool for CFD and analytical models due to its straightforward design and isolation of longitudinal instabilities that arise from oxidizer post length – chamber length coupling effects [30,31]. Yu made comparisons between the frequency and mode shapes estimated by the Linearized Euler Equations (LEE) and observed from experimental pressure data at various axial positions along the combustor [20,32]. Yu's linear acoustics model took into account mean flow effects and some entropy effects. Yu found three regions of stability with this combustor that represent linear and nonlinear regimes, which the author called stable, unstable, and marginally stable. In the transition from linear to nonlinear instability, the near-synchronized appearance of higher harmonics up to the tenth mode was observed. Furthermore, in the transition back to stable (linear) combustion, the harmonics disappeared sequentially from highest

to lowest until a two-mode system remained with 1L and 2L. Rosen, too, observed the sequential appearance and disappearance of harmonic modes at the transition regions [21].

Rosen performed further work with LEE and the CVRC to study the transition region from stable to unstable combustion and vice versa [21]. With a 10 kHz high speed camera to capture line of sight optics for the first 5 in of the combustion chamber, the author used CH* chemiluminescence to calculate the change in the center of intensity during the transition to and from stability. Rosen found that the center of intensity moves up to 1 in towards the injector face as the combustor transitions to instability and the flame front moves towards the injector. Coupled with high frequency pressure data and LEE results, Rosen was able to determine Rayleigh Index values at different oxidizer post lengths and stability conditions, though the validity of the calculated Rayleigh Index values are directly tied to the validity of the LEE model.

Further work with the CVRC by Feldman found a correlation between wave resonator values and the occurrence of unstable combustion of the fundamental and first two harmonic modes [22]. The belief with acoustic coupling of the oxidizer post and the chamber is that maximum damping occurs at a ¼ Wave Resonator and minimum damping occurs at a ½ Wave Resonator, assuming no mean flow effects. Using LEE and experimental results, Feldman established correction factors for this axiom based on Mach number, demonstrated in Figure 1.5.

Feldman also used Large Eddy Simulation (LES) to model the unsteady heat release and fluctuating pressure to study the physical interaction between these two variables that sustains and propagates pressure oscillations [22]. This

theory is based on fundamental acoustics, assuming a traveling pressure wave and closed acoustic boundaries at the oxidizer inlet and sonic nozzle. The work presented the viability of determining empirical relationships to characterize longitudinal combustion instability.

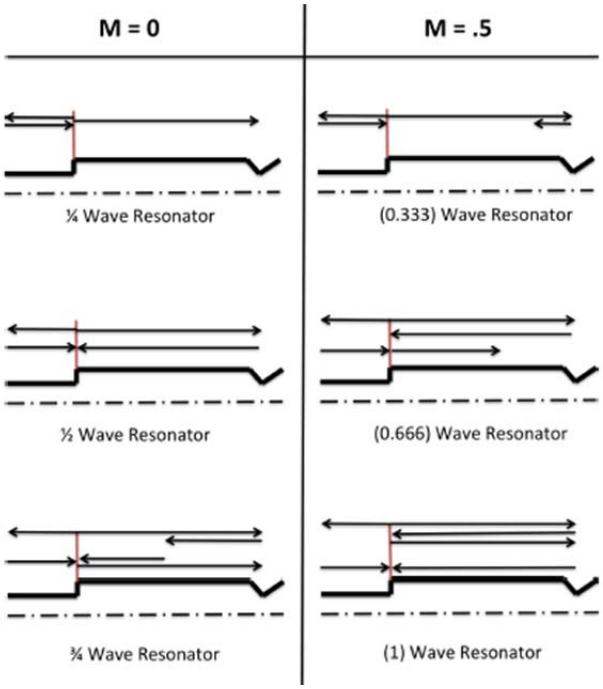

Figure 1.5 Wave resonator relationships for the first three longitudinal modes, without and with mean flow effects. [22]

1.3 Current Study

Ample work has been done with the CVRC, as outlined in Sec. 1.2.3, to establish relationships between stability behavior and combustor geometry. From previous studies, Sisco postulated that longitudinal instabilities seen in the CVRC are primarily due to a combination of acoustics (such as acoustically-induced vortex shedding) and mixture ratio inhomogeneity [4]. The current study focuses on harmonic modes in self-excited longitudinal instabilities. As will be discussed in

Sec. 2.3, it is unclear whether harmonics exist or if the use of them in theory is solely for simplification of analysis of discontinuous shock-like waves. If it can be shown that the modal behavior observed is real, defining a heuristic relationship between the excitation of the fundamental mode and higher harmonics may provide a better insight to supplement existing analytical and computational models.

1.3.1 Motivation

Multiple harmonics have been observed in previous CVRC testing and speculations have been made as to whether the excitation of harmonic frequencies are tied to the excitation of the fundamental frequency either in terms of the number of cycles, the amplitude of the fundamental oscillations, or some other unknown characteristic of the oscillations [20–22]. As will be discussed in Sec. 2.2, Lang made correlations between the ratio of the fundamental oscillation's amplitude and the steady-state chamber pressure as well as the ratio of the first harmonic oscillation's amplitude and the fundamental oscillation's amplitude [33]. Furthermore, Lores and Zinn described a transient-process energy transfer from the fundamental mode to higher harmonic modes until a limit cycle behavior is reached [28,29]. Additionally, related uni-element ORSC experiments performed by Pal et al. indicate the presence of harmonics showing decreasing intensity with increasing modes [27]. The further study of harmonics of fundamental resonant frequencies may provide better insight into the behavior of instabilities after initial excitation and support improvements to existent models.

As Hefner demonstrated in Ref. [1], the simultaneous study of multiple modes in data is non-trivial, and at the high frequencies seen, problems arise when

distinguishing resonant behavior of multiple modes from noise in the signal. The last time a similar study was performed was Bowman's 1967 PhD Thesis entitled "Experimental Investigation of High Frequency Longitudinal Combustion Instability in Gaseous Propellant Rocket Motors" [34]. Bowman's Fourier-based data processing found the presence of harmonic modes, and the author concluded that chemical kinetics is the driving mechanism in the specific case of high frequency longitudinal resonant combustion in gaseous rockets.

1.3.1.1 Universal Behavior

To verify that a common relative modal behavior exists in unstable CVRC tests and that the high-mode pressure signals are not an artifact of spectral analysis trying to match a rapidly changing signal (see Sec. 2.3), a few simplistic comparisons were made between the primary mode (1L) and each resonant mode up to the sixth longitudinal mode (6L). A second-order Butterworth band pass filter was applied to the raw pressure data around each resonant frequency. These filtered pressure signals were normalized by their maximum amplitude, and then each signal was plotted on top of the primary mode's signal in the time domain for three test cases.

At this base analysis, the lead-lag behavior of each mode with respect to the primary mode was recorded, looking at the two ignition events and the growth to limit cycle of each mode. The behavior observed was compared across two unstable tests to verify that observed relationships could be considered universal across these unstable cases. One stable test case was also analyzed and compared to confirm that any phenomena observed could be attributed to unstable cases and not just the general performance of the CVRC.

As seen in Figure 1.6, the onset of the second resonant mode occurs after the onset of the primary mode. This was seen in the signal overlays for each mode in all of the unstable tests considered. In the stable test, any perturbations in the signals occur at the same time at every mode, as illustrated in Table 1.1. This simple analysis quickly confirms a common behavior exists between the observed harmonic modes.

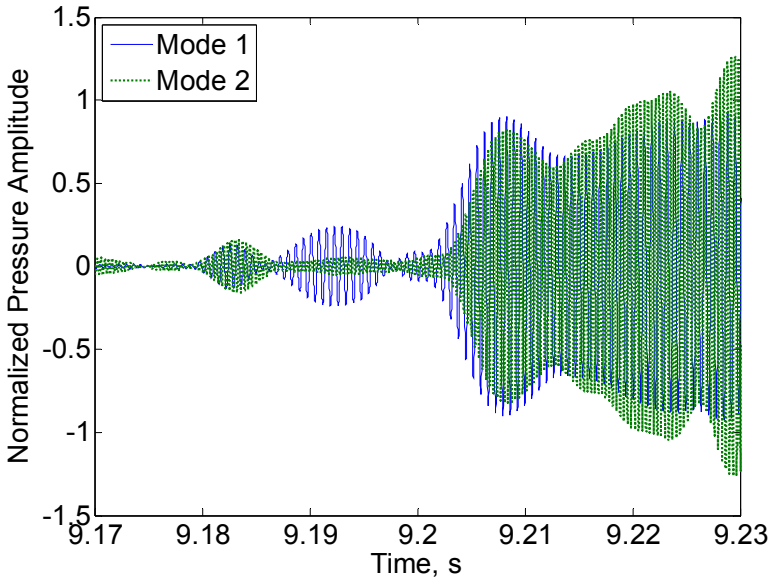

Figure 1.6 Comparison of Mode 1 and Mode 2 pressure oscillation behavior near onset of instability.

Table 1.1 Modal behavior relative to the primary mode for two unstable cases and one stable case.

	Fixed 5.1 in (unstable)	**Fixed 5.1 in (2) (unstable)**	**Fixed 7.85 in (stable)**
2nd Mode f = 2820 Hz	Lead – Lag – Lag	Lead – Lag – Lag	Same as 1st Mode
3rd Mode f = 4230 Hz	Lead – Lead – Lag	Lead – Lead – Lag	Same as 1st Mode

1.3.2 Objective of the Study

The objective of this study is to establish a digital signal processing (DSP) method to reliably and repeatedly distinguish transient behavior of fundamental and harmonic modes via highly sampled experimental pressure data, focused on the time of modal onset and growth rate of the oscillations. Two subsequent objectives are to determine: 1) if the observed higher harmonics are real, and 2) whether the excitation source of these higher modes is acoustic and/or combustion. Specific requirements include a time resolution on the order of 1 ms and insensitivity to user bias. Important parameters to be obtained for each mode include the time of initial oscillation growth (a.k.a. onset time), growth rate of the oscillation amplitude, time when limit cycle is reached, and limit cycle amplitude.

1.3.3 Approach

Experimental data sampled at a rate of 100 kHz using water-cooled piezo-resistive pressure transducers are taken at several axial locations along the combustor length, as shown in Figure 1.4Figure 1.4 Cross section of the CVRC experiment. [30]. Multiple tests were performed in previous test campaigns using fundamentally the same combustor configuration. Fixed geometry tests (referred to as fixed) at stable, unstable, and marginally stable configurations as well as variable geometry tests (referred to as translating) are considered in this study.

To evaluate the signal processing methods under review, one unstable fixed test is analyzed with each method. If the method is able to distinguish the individual transient behavior of the first three modes, a second fixed test and a

translating test are evaluated as well. A fake signal is also analyzed to check for bias and artifacts contributed by the data processing method.

1.4 Outline

Chapter 2 reviews of relevant longitudinal combustion instability theory. Chapter 3 presents the digital signal processing (DSP) methods assessed and examples of results for these methods using both experimental data and a manufactured signal. Initial observations from the experimental results are discussed. Chapter 4 uses manufactured signals with both sinusoidal and steep-fronted waveforms to further evaluates potential DSP methods as well as potential and existing issues with the method(s) chosen. Chapter 5 covers observations from the results presented and outstanding issues are discussed. Chapter 6 summarizes the work done and draws conclusions from the work presented. Future tasks to continue this work are proposed.

CHAPTER 2. LONGITUDINAL COMBUSTION INSTABILITY THEORIES

2.1 Overview

In high frequency combustion instability, frequencies of pressure oscillations observed during unstable combustion relate to natural acoustic modes of the combustion chamber [1,3,8]. There exist two schools of thought on the wave behavior of longitudinal instabilities: essentially acoustic or essentially shock-like. Even within SP-194, the seminal text on liquid rocket engine instabilities, theorized wave behavior changes section to section based on the contributing author(s) [1]. Both classifications are broken into linear and nonlinear regimes based on the analysis required.

Linear analysis methods are employed when pressure oscillations spontaneously grow from combustion noise [1]. Characteristics of linear instability include continuous sinusoidal waves and pressure oscillations less than 10% of steady-state pressure (i.e. $p'/p_c<0.1$). The response to finite amplitude disturbances (known as triggered instability or subcritical bifurcation) resulting in rapidly growing pressure oscillations is treated using nonlinear analysis and is thus known as nonlinear instability [1,2,35]. Nonlinear analysis is also required to model the transition from growth to limit cycle amplitude, as this behavior is attributed to nonlinear effects [2,29]. Additionally, the distortion of the pressure waveform as harmonic frequencies are excited is considered a nonlinear effect [1]. This so-called

nonlinear instability is characterized by pressure oscillations greater than 10% of steady-state pressure (i.e. $p'/p_c>0.1$) and non-sinusoidal waves. It is possible for instabilities to start in a linear regime and transition to a non-linear regime, as demonstrated in Figure 2.1, or the instabilities may begin in the nonlinear regime [1,3,36].

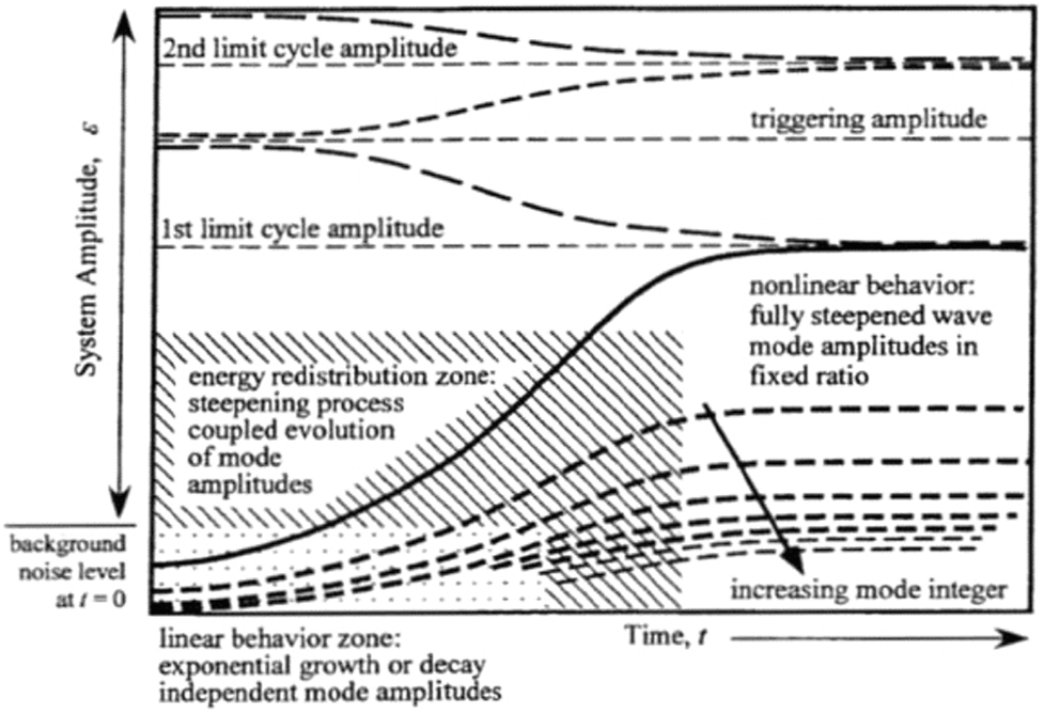

Figure 2.1 Evolution of behavior during onset of instability. [36]

The qualitative behavior of these combustion instabilities can be closely approximated by an infinite series of harmonic periodic acoustic waves subject to linear and nonlinear analysis [1,3]. And while many believe shock behavior is present, some choose to represent the behavior using harmonic acoustics for ease of analysis and modeling [17,37]. For example, Flandro et al. strongly support the shock-like behavior in high amplitude longitudinal instabilities, but their model

assumes the steep-fronted traveling wave under consideration is composed of standing acoustic modes of the chamber to avoid difficulties in shock analysis [36,38].

Both acoustic and shock-like theories often incorporate the idea of a time lag, typically sensitive to pressure. The theory of a combustion time lag was first proposed by von Karman, based on early liquid engine work [3]. The idea was further developed by Crocco and Cheng (1956) concurrent to Zucrow and Osborn's efforts at Purdue University, creating the linear sensitive time lag theory [16,25]. Based on empirically obtained values, they presented a model based on the characteristic time for the combustion to respond to perturbations. This linear n-τ model has been a cornerstone of many discontinuous instability models [17,26,28,29,39,40]. Lores and Zinn describe the interaction index n as "a measure of the sensitivity of the combustion process to flow oscillations" and the sensitive time lag τ as "representative of the time required for the unsteady combustion process to respond to flow perturbations" [29].

2.2 Acoustic Wave Theory

Culick has established both linear and nonlinear acoustic models to study longitudinal instabilities in rocket engines [1,2,41]. The linear acoustic model fundamentally states that linearized problems should be considered as the classical acoustic wave problem in a closed tube, with growth and decay rates most easily modeled as exponential [1]. This baseline linear acoustic model assumes low amplitude continuous periodic waves (no shocks) and may not be suitable for higher amplitude and/or "strongly nonlinear" oscillations [41]. Otherwise, in Culick's linear model, the combustor is treated as a simple harmonic oscillator

subject to nonlinear losses and gains and evaluated through traditional acoustic analysis.

Combustion instabilities can be approximated using the traditional acoustic and fluid dynamic analyses in the classic representation of combustion dynamics [2,8]. The wave equation is given as

$$\frac{\partial^2 p}{\partial t^2} - c^2 \frac{\partial^2 p}{dx^2} = \rho_0(\gamma - 1)\frac{\partial Q}{\partial t} \tag{2.1}$$

where c is the speed of sound and $\frac{\partial Q}{\partial t}$ is the heat release from combustion [8]. The wave is represented using the complex eigenvalue form,

$$\omega = 2\pi f + i\alpha \tag{2.2}$$

so that the oscillatory pressure can be represented as

$$p' = \hat{p}e^{i\omega t} = \hat{p}e^{-i(2\pi f + i\alpha)t} = \hat{p}e^{-i2\pi ft} * e^{\alpha t} \tag{2.3}$$

where $e^{-i2\pi ft}$ represents the periodic behavior of the wave and $e^{\alpha t}$ represents the exponential growth or decay of the oscillation amplitude [8]. Simplifying assumptions include linear acoustics, inviscid flow, unit area, and no body forces. Second order terms and higher are ignored, and pressure, density and temperature are represented as a mean term and oscillatory term, where

$$p = \bar{p} + p' \tag{2.4}$$

$$\rho = \bar{\rho} + \rho' \tag{2.5}$$

$$T = \bar{T} + T' \tag{2.6}$$

and mean velocity is assumed to be zero, so the velocity term is purely the oscillatory velocity [8]. An additional assumption is

$$\left|\frac{p'}{\bar{p}}\right| \ll 1, \left|\frac{\rho'}{\bar{\rho}}\right| \ll 1, \left|\frac{T'}{\bar{T}}\right| \ll 1$$

Combined with a linearized equation of state, the conservation equations are linearized to yield:

mass conservation in 1D,

$$\frac{\partial \rho'}{\partial t} + \bar{\rho}\frac{\partial u'}{\partial x} = 0 \tag{2.7}$$

momentum conservation in 1D,

$$\bar{\rho}\frac{\partial u'}{\partial t} = -\frac{\partial p'}{\partial x} \tag{2.8}$$

and the acoustic energy corollary in 1D,

$$\frac{\partial}{\partial t}\left[\frac{1}{2}\bar{\rho}u'^2 + \frac{1}{2}\frac{p'^2}{\bar{\rho}c^2}\right] + \frac{\partial}{\partial x}[p'u'] = 0 \tag{2.9}$$

Then the wave equation for the pressure fluctuations in 1D becomes

$$\frac{1}{c^2}\frac{\partial^2 p'}{\partial t^2} = \frac{\partial^2 p'}{\partial x^2} \tag{2.10}$$

The three dimensional wave equation to describe the oscillatory pressure behavior with an unsteady heat source is

$$\frac{\partial}{\partial t}\int_V \left\langle \frac{p^2}{2\rho_0 c^2} + \frac{\rho u^2}{2} \right\rangle dV + \oint_S (pu)dS = \frac{\gamma - 1}{c^2}\int_V \langle pQ \rangle \, dV \tag{2.11}$$

and derivation of this result can be found in Ref. [8].

As evidenced above, linear acoustic analysis requires many simplifying assumptions. However, linear analysis can yield good approximations of the potential frequencies and mode shapes of the oscillatory pressure, as demonstrated through Purdue's LEE model mentioned in Sec. 1.2.3 [20,32,41]. Nonlinear analysis is required when more interest is given to limit cycle amplitude and growth behavior of the mode [35,37,42]. Acoustic theory states that limit cycle amplitudes are reached due to nonlinear losses and/or higher order nonlinear acoustics in the system, which may include localized energy losses and coupling between unstable and stable modes [2,3,8]. It is important to note that Culick specifically states that his acoustic theory is largely heuristic, unlike some models presented in Sec. 2.3

[41]. In addition, it may provide inadequate approximations for cases with large amplitudes or focus on velocity coupling. For more details on Culick's linear and nonlinear acoustic theories, refer to Refs. [1,2,5,8,12,41].

Sterling and Zukowski built off Culick's nonlinear acoustic model with a heavy emphasis on the effect of Rayleigh's criterion to model instabilities seen in subscale combustors [43,44]. Their work is applicable mainly to combustors whose instabilities can be attributed to periodic vortex shedding at the dump plane. Sisco previously attributed instabilities in the CVRC to acoustically-driven vortex shedding, so Sterling and Zukowski's theory is applicable to the current study [4]. As previously discussed, Culick attributes the transition to limit cycle to nonlinear acoustics, though Sterling contends that this behavior is due to nonlinear combustion processes [2,41,43]. Specifically, vortex shedding at the dump plane occurring at the acoustic frequencies of the chamber induces oscillatory heat release, which governed by Rayleigh's criterion can couple with the chamber pressure to support instabilities [43,44]. Moreover, limit cycle is reached when nonlinear coupling between the excited mode and subharmonic modes cause an energy loss to the process. In contrast to Sterling's subharmonic coupling hypothesis, many papers mention coupling between the fundamental and harmonic modes of higher frequency [1,2,12,14,33].

Margolis supports the concept of coupling between the fundamental and higher harmonic modes [45]. In his work with model pulse combustors, Margolis demonstrated a resonant-like coupling between any growing mode and its first harmonic mode (in his application, $3*f_1$). The author further inferred that finite limit cycle amplitude is achieved though "a nonlinear resonant coupling between

the linearly unstable (growing) mode and the linearly stable (decaying) mode," where the stable mode is a harmonic of the growing mode.

On the interpretation of experimental data, Hefner in SP-194 equated longitudinal instabilities to traveling "acoustic" waves in a closed-closed cylinder [1]. For two sinusoidal traveling waves, amplitudes would approach zero at pressure nodes of an equivalent standing wave in the tube. More pertinent to this study, Hefner attributed the double peak seen in experimental data to the asymmetry of non-sinusoidal acoustic waves traveling in the cylindrical combustion chamber, illustrated in Figure 2.2. Unlike sine waves, the amplitudes of the distorted waves will never cancel out completely, leading to a high-low double peak between node and anti-node locations. The distance between the two peaks decreases as it approaches the end of the tube where a pressure anti-node exists. This is in direct contrast to Tsuji and Takeno's shock theory presented in the following section [17].

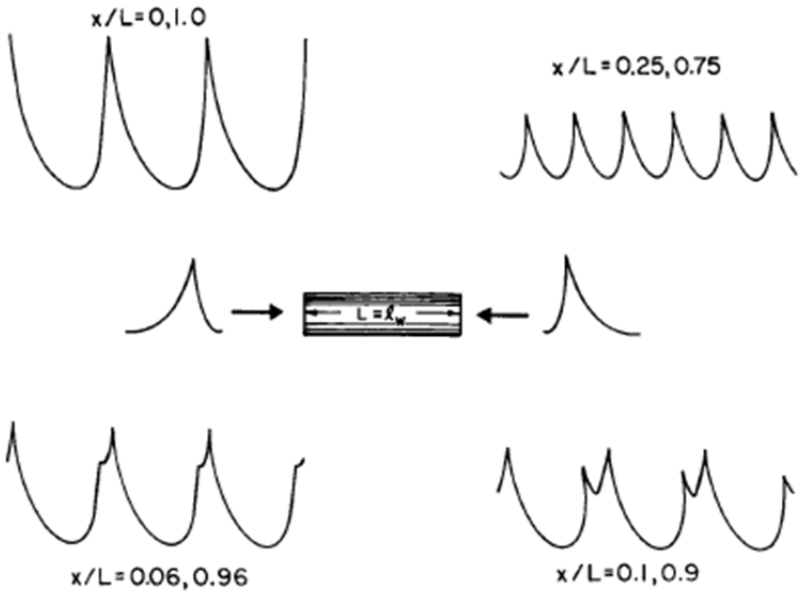

Figure 2.2 Appearance of distorted traveling waves versus axial location. [1]

In his 1991 paper, Lang presented behavior of the fundamental frequency and the conditions that would encourage harmonics in oscillatory flames [33]. Working from the basis of a nonlinear system subject to a periodic excitation, Lang modeled the system response y as

$$\begin{aligned} y(x) &= a_0 x_0 \sin(\omega t) + a_1 x_0^2 \sin^2(\omega t) \\ &= a_0 x_0 \sin(\omega t) + \frac{1}{2} a_1 x_0^2 + \frac{1}{2} a_1 x_0^2 \cos(2\omega t) \end{aligned} \tag{2.12}$$

where a is amplitude components of the nonlinear system, x_0 is the amplitude of the periodic excitation, and ω is the frequency of the excitation [33]. From this, Lang claims that the amplitude of the harmonic frequency is directly related to that of the fundamental frequency. At small amplitudes, harmonics do not exist and the wave is sinusoidal. As the total amplitude increases, harmonics appear and the wave shape becomes distorted. The harmonics seen are tied through amplitude and phase to the fundamental frequency. The concept of threshold amplitude is discussed as a determinant of harmonics (and nonlinear behavior).

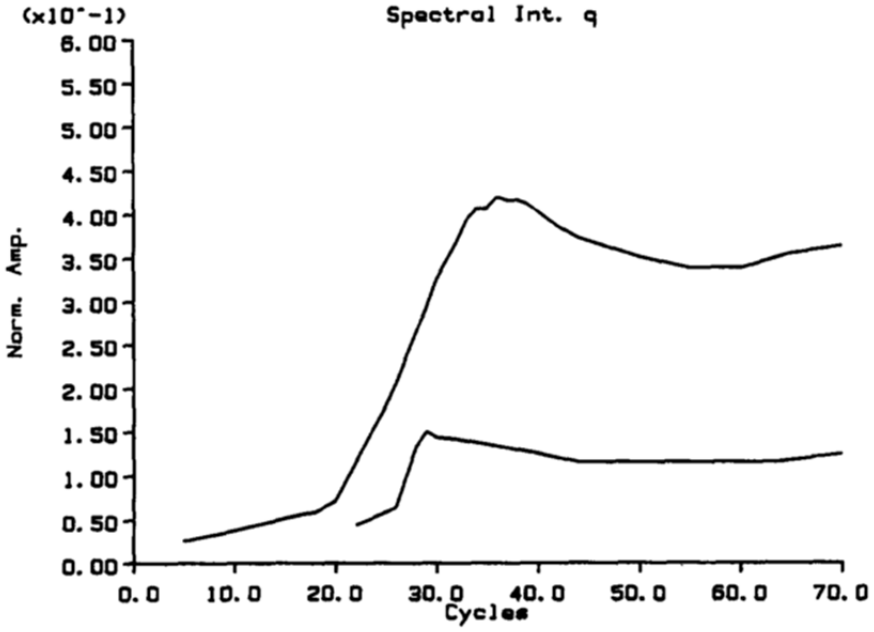

Figure 2.3 Proposed behavior of 1L and 2L as a function of 1L cycles. [33]

Some of Lang's results are shown in Figure 2.3, where the fundamental and first harmonic behavior are presented as normalized spectral intensity as a function of 1L cycles. The fundamental mode, represented in the upper curve, is normalized with the static chamber pressure, while the first harmonic, represented in the lower curve, is normalized with the amplitude of the fundamental mode. The time between excitation of the fundamental and first harmonic are presented in terms of cycles of the fundamental frequency. Lang's acoustic nonlinear theory most closely relates to the theorized behavior of the CVRC modes and supports the idea that a heuristic relationship between the modes may exist.

2.3 Shock-like Wave Theory

Early experimental work such as that done by Zucrow and Osborn at Purdue University in 1958 [16], Tsuji and Takeno at University of Tokyo in 1965 [17], and Bowman at Princeton University in 1967 [34] employed simplified model combustors with premixed gas propellants to study the effects of chamber length, steady-state chamber pressure, and equivalence ratio on longitudinal oscillations. These separate experimental efforts yielded comparable results that a relationship exists between both the chamber geometry and chemical kinetics of the propellants with the amplitude and frequency of longitudinal pressure oscillations.

Zucrow and Osborn specified two principle categories of longitudinal instabilities: "shock" type and "sinusoidal" type [16]. These categories often correspond to nonlinear instability and linear instability as described in Sec. 2.1, with the terms being used interchangeably in later literature. While shock-like instabilities are nonlinear, nonlinear instabilities are not necessarily shock-like. They characterized the shock-type oscillations as traveling detonation waves fed by

rapid energy addition behind the shock front from the unsteady combustion, leading to high amplitude self-propagating oscillations. Zucrow and Osborn postulated that instabilities occurred as a result of accumulated unburned and burned propellant near the injector end being compressed and combusted by the shock wave reflected from the nozzle [16]. Their experiment found a minimum chamber length for instabilities to occur but did not reach a maximum length limit. From this, it was concluded that there exists a minimum kinetically-driven time scale that would promote the growth of oscillations.

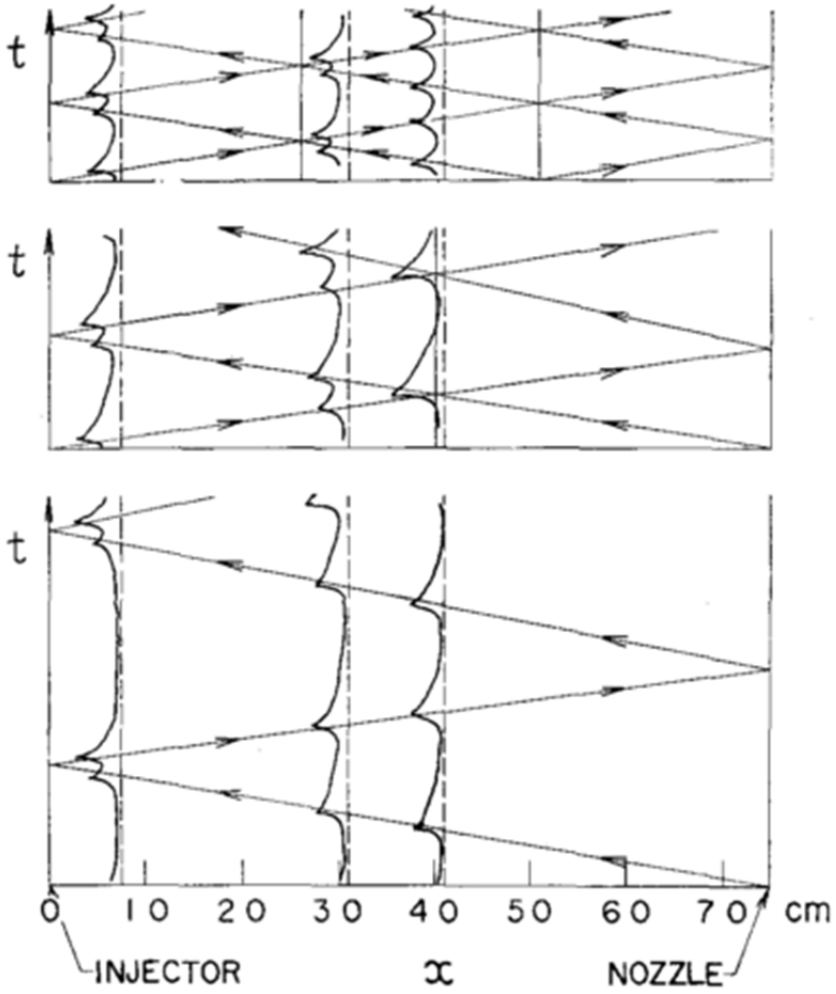

Figure 2.4 Traveling shock behavior of 1L, 2L, and 3L (from bottom to top). [17]

Tsuji and Takeno also observed shock type oscillations with harmonics but treated the traveling shocks as standing waves since the shocks were found to reflect at velocity nodes of equivalent standing waves [17]. This behavior is illustrated in Figure 2.4 from Tsuji and Takeno's 1965 paper, which demonstrates this traveling shock wave behavior and how the data from pressure transducers would appear at different axial locations along the combustor for, from bottom to top, the first (1L), second (2L), and third (3L) longitudinal modes.

These results can be compared to the theory presented by Hefner in SP-194 [1]. Both assume a traveling wave that would have equivalent standing wave characteristics. However, where Hefner states that the distorted wave shape of the two traveling waves cause the double peak experimentally observed, Tsuji and Takeno contend that the double peaks are an indication of the traveling shock wave reflecting from an acoustic boundary and traveling back [1,17].

As discussed by Harrje, shock waves with a constant period are often observed experimentally, but models (especially for "triggering") avoid shock theory as much as possible and create linear and nonlinear periodic waves that qualitatively agree with experiments [1,37]. However, shock theory is incorporated in analytical models developed by Sirignano [46] and Mitchell, Crocco, and Sirignano [26]. In previous work, Sirignano derived a relationship between "β, …the ratio of the thermal relaxation time …to the wave travel time," and the shock amplitudes and peak-to-peak amplitudes of the oscillations [46]. This work found that for small β values, continuous (shockless) solutions that appear as "distorted-sinusoidal waveforms" exist, as earlier established by Crocco and Cheng, while shock-like solutions exist for larger β values (corresponding to shorter time lag

values) [25]. In later work, continuous (shockless) periodic solutions were shown to only be valid in close proximity to the neutral stability limit [26].

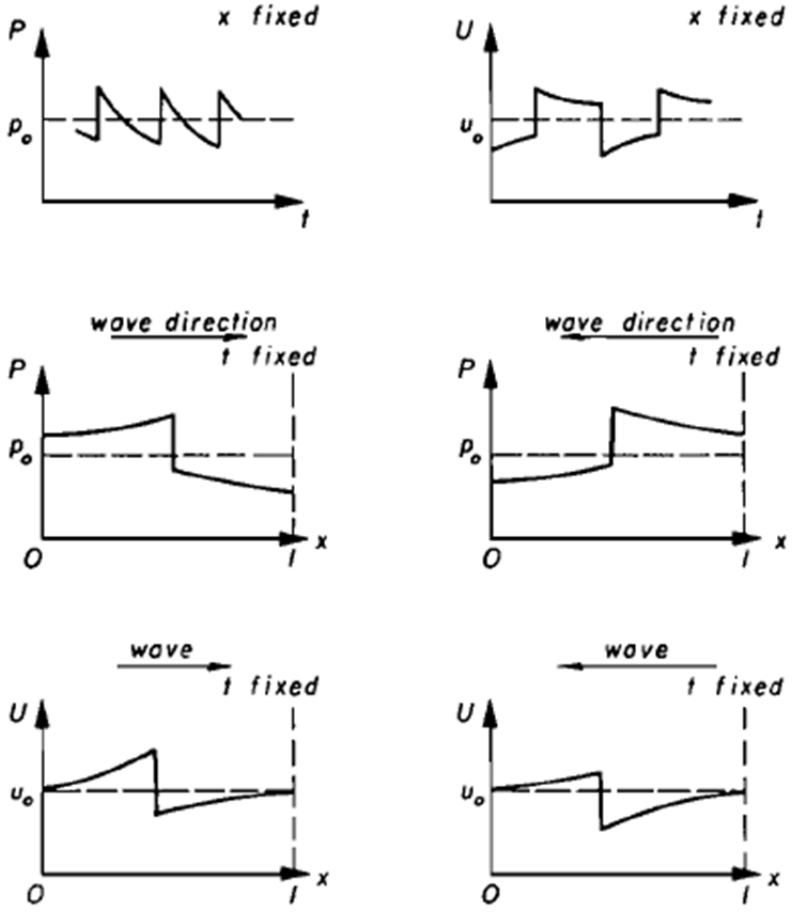

Figure 2.5 Wave shapes for traveling shock-like waves. [26]

In their 1969 paper, Mitchell et al. presented two analytical models for continuous (sinusoidal) and discontinuous (shock-like) solutions with and without Crocco's pressure-sensitive time lag theory [26]. First, a nonlinear model for periodic traveling shock waves with no time lag was introduced, providing analytical estimations for shock velocity and shock strength. The appearance of these shock waves at constant location or constant time presented by Mitchell et al. is shown in Figure 2.5. The model anticipates the appearance of a shock

discontinuity followed by an exponential decay, with observed behavior changing based on the direction of travel. In this model, only one frequency is considered.

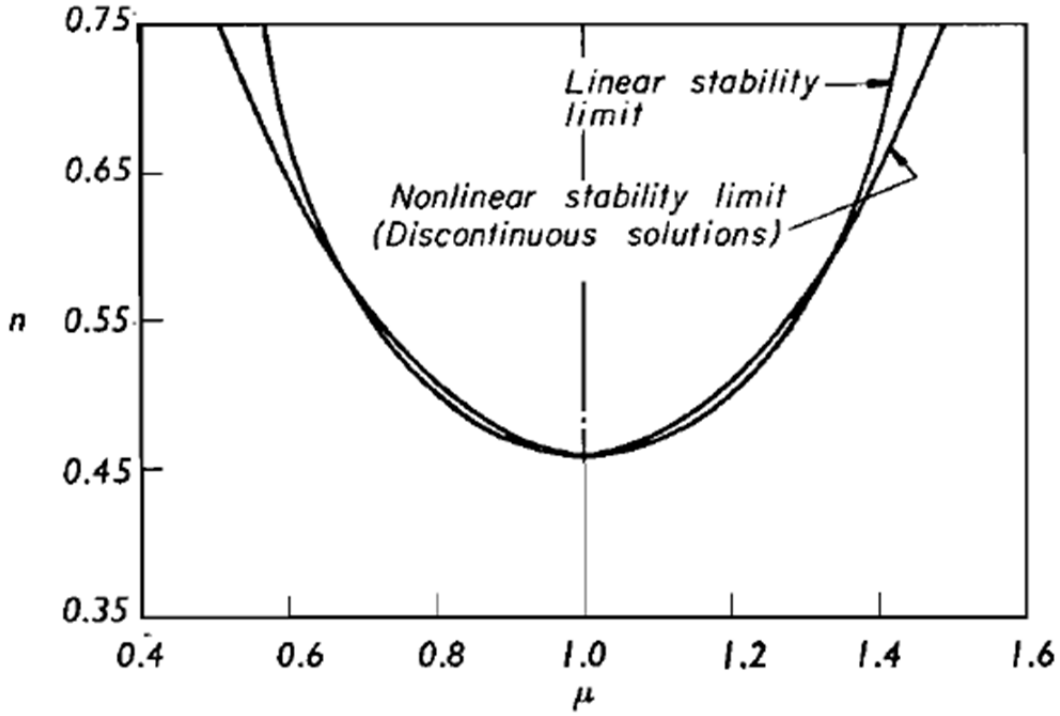

Figure 2.6 Linear and nonlinear stability limits. [26]

The second model presented addresses Crocco's n-τ model, specifically creating a nonlinear model that supports discontinuous solutions to supplement Crocco's original linear model [25,26]. Figure 2.6 demonstrates the behavior of these models as a function of interaction index n and extended time lag μ. Shockless solutions are supported near the stability limit, as earlier proved by Sirignano, while shock solutions are the predicted response to small perturbations for most other areas of the n-μ plane [26,40].

A significant portion of shock-like theory for combustion instabilities has built off of the work done by Crocco's group at Princeton University [25,26,37,39,40], and the idea that nonlinear and linear stability limits exist as a

function of n-τ to this day continues to be a critical cornerstone of combustion instability theory. Figure 2.7 demonstrates some of the ensuing complex analytical models developed from this initial work, here done by R. J. Priem in SP-194 [1].

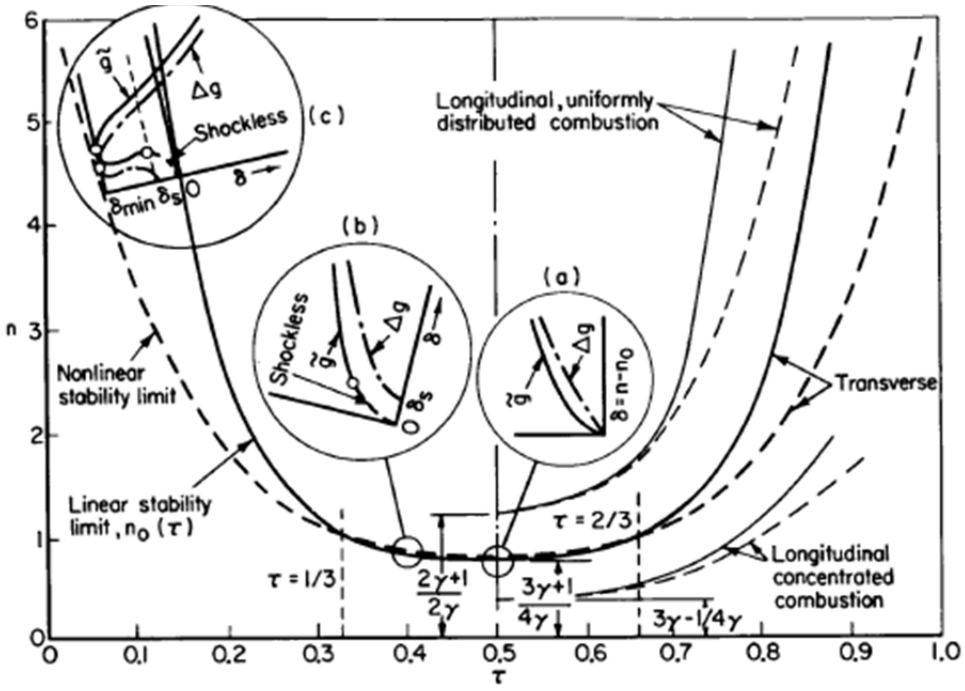

Figure 2.7 Detailed linear and nonlinear behavior. [1]

One of the difficulties with distinguishing between shock-like behavior and continuous wave behavior is that shock velocities are closer to the speed of sound than anticipated. As explained by Bracco in SP-194, this is due to the effects of non-uniform axial temperature [1]. Bracco further explored this effect for both traveling shocks and standing acoustics in Ref. [11], working from linearized conservation equations.

The contemporary opposition to Culick's acoustic theory, Flandro et al. make the assertion that low amplitude standing acoustic waves grow and distort into shock-like disturbances [36]. Because of this traveling shock behavior,

unsteady combustion processes may be affected by detonation-like mechanisms, as earlier hypothesized by Zucrow and Osborn [16,36,38]. The main argument against using traditional acoustic models such as those presented by Culick is the assumption of irrotational acoustic waves, which may not take into account additional acoustic energy added by rotational processes like vortex shedding [2,36]. Culick's model explicitly states that it cannot handle shock-like behavior [41]. Their conjectures are supported by behavior seen in solid rocket motors and work in the mid 1960's by Clayton et al. at JPL on rotating detonation-like combustion [38,40,47,48]. In this model, nonlinear loss effects leading to limit cycle amplitude are entropy gain and energy loss associated with the shock front. The existence of harmonic content in the frequency domain is used to further support the argument of steep-fronted wave behavior, as the Fourier-based analysis attempts to represent the steep wave front. It is worth noting, though, that some of the model relies on the assumption that the composite steep-fronted traveling wave is made up of standing acoustic waves for ease of computation [36].

Zinn and Lores of Georgia Tech proposed the application of the Galerkin method for the analysis of longitudinal modes [28,29]. Their work supports analysis of transient AND limit cycle behavior for the change from continuous (sinusoidal) to discontinuous (shock-like) periodic waves, with the conclusion that most longitudinal instabilities result in shock-like behavior. This capability is unique, as generally both nonlinear and linear analyses need to be performed to separately model or analyze these distinct regions. This work is built off of Crocco's linear n-τ model and other time lag work done at Princeton [25,26,37,39], with qualitative agreement between the results found and parent models, with the added ability to model transient behavior and more than one mode at a time.

2.4 Application to Current Study

Contemporary study of longitudinal combustion instabilities in liquid rocket engines at Purdue University (see Ref. [4,18–22]) has integrally assumed an acoustics-based instability theory with traveling pressure waves that act as standing waves. This has led to the belief that the harmonic frequency content observed from experimental data analysis is authentic and tied to the behavior of the fundamental mode. As discussed in Sec. 1.3.1, the conclusions drawn from previous CVRC work has led to this current study. But as shown in Sec. 2.3, there is a sizable group within the combustion instability community who believe that for large amplitude instabilities, the harmonic frequency content observed is a consequence of the Fourier-based signal processing responding to a steep wave front as opposed to extant harmonic modes. If this can be shown to be true, the main objective of this study may be invalidated. Therefore, the existing theories and their relevance to this current study are of interest.

The amplitude of pressure oscillations observed in the CVRC categorizes most of the unstable combustion as a nonlinear instability, having peak to peak magnitudes upwards of 45% steady state pressure. This brings in the possibility that shock waves may exist in the chamber and legitimizes the continued investigation into both the existence of harmonics and the ability to distinguish real harmonic signals from composite steep-fronted waves.

CHAPTER 3. DIGITAL SIGNAL PROCESSING METHODS

One of the primary concerns when evaluating digital signal processing (DSP) techniques is how the method handles the data and what artifacts, biases, or irregularities the method may introduce to the results, as this directly impacts the reliability and repeatability of the method [49]. Other considerations include computational costs, time resolution, and ease of use. For detailed information on any of the methods discussed, see Ref. [49–52].

3.1 Traditional Analysis Methods for Combustion Instability

Experimental data are often more useful in the frequency domain when discussing combustion instabilities. Transforming data from the time domain to the frequency domain can assist in identifying the spectral content (and therefore dominant modes) present throughout the test [49,50]. The resultant frequencies can then be further used to isolate the signal of each mode of interest for study of other instability characteristics such as amplitude and relative phase.

3.1.1 Fourier Analysis

The most commonly used DSP method to study instabilities at an experimental level is Fourier analysis. The Fourier transform assumes that a

complex signal can be represented by a series of sine waves of harmonic frequencies and various phase and amplitude,

$$x(t) = \frac{a_0}{2} + \sum_{n=1}^{\infty} M_n \cos(2\pi n f_1 + \phi_n) \tag{3.1}$$

where x is the time-dependent reconstructed signal, $\frac{a_0}{2}$ is the mean value of the signal (a.k.a. DC level), f_1 is the fundamental frequency, M_n is the amplitude of the frequency component at nf_1 (a.k.a. n^{th} mode), and ϕ_n is the phase of the frequency component at nf_1 [49]. A common analysis technique to transform a signal in the time domain into the frequency domain, the Fourier transform is only as valid as the assumption that the signal is made up of sinusoidal components. While several theories such as those presented in Sec. 2.3 refute the existence of sinusoidal waves, many find the Fourier method most convenient to represent the complex wave behavior (see Sec. 2.3). And as Zeytinoglu and Wong state, "the main motivation of using the Fourier method has been the need to transform the received signal into a spectral representation where its harmonic structure will be unveiled" [53].

3.1.1.1 Power Spectral Density (PSD)

A typical analysis when studying frequency content is the Power Spectral Density (PSD) function, which calculates the intensity of frequencies that are present in a specified portion of the time-varying signal. There are three main methods to estimate the PSD function; only the one used by the Matlab function "periodogram" will be discussed, though further information on PSD analysis can be found in Ref. [49,50]. Matlab uses a non-parametric method that estimates the PSD values by the Fast Fourier Transform (FFT) of the biased autocorrelation sequence, given as

$$\hat{P}(f) = \frac{\Delta t}{N}\left|\sum_{n=0}^{N-1} h_n x_n e^{-i2\pi fn}\right|^2, -\frac{1}{2}\Delta t < f \leq \frac{1}{2}\Delta t \tag{3.2}$$

where Δt is the sampling interval, N is the number of points, x_n is the signal being analyzed, and h_n is the window function (in this study, a Hanning window) [50].

Since high frequency content is the primary interest in this study, a second order high pass (HP) Butterworth filter at 500 Hz is applied to remove potential electrical noise in the signal prior to PSD analysis. As the combustion transitions to instability, the frequencies that are present change, so PSD analysis is applied to 0.1 s of data once limit cycle amplitude has been reached. Figure 3.1 presents results of the HP filter and PSD of the unstable fixed test case under examination. Strong harmonics are seen up to 10L with a fundamental frequency of 1450 Hz. As shown by Sisco, this value corresponds closely with one of the natural acoustic modes of the cylindrical chamber [4].

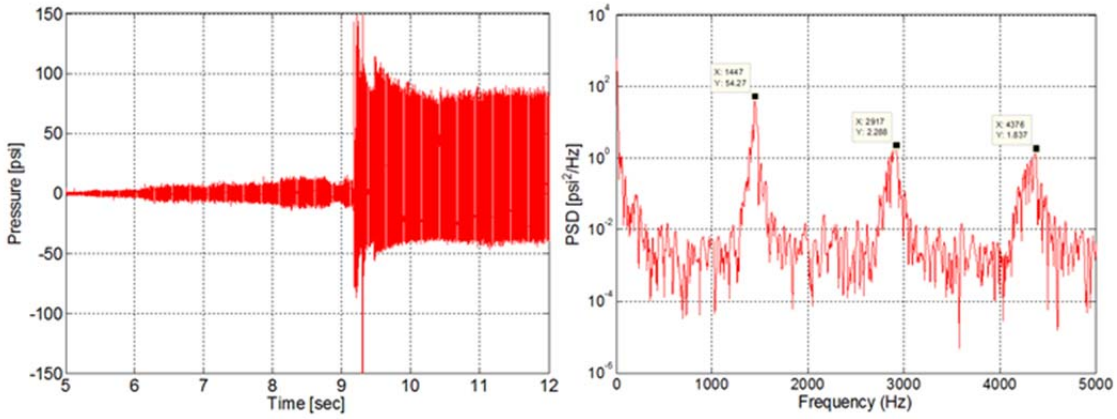

Figure 3.1 For the unstable fixed test case, a) the HP pressure and b) PSD showing 1L, 2L, and 3L with a frequency resolution Δf of 6 Hz.

3.1.1.2 Spectrogram

Another Fourier analysis technique, the spectrogram uses the same principles as the PSD function to represent the frequency content as a function of time. Matlab's "spectrogram" function performs a short-time Fourier transform (STFT) on the data using a sliding window to provide the time-dependent Fourier transform results [50]. This analysis technique is especially useful when applied to translating tests, since the geometry of the combustor is changing over the time of the test. Figure 3.2 demonstrates spectrogram results for a translating test that starts at an oxidizer post length of 7.7 in and ends at an oxidizer post length of 3.7 in. The color intensity is a measure of the spectral density on a logarithmic scale. The blue line shows the length of the oxidizer post during the test. Notice how the frequency content organizes as the combustion transitions to instability near Lop of 6.1 in and returns to marginally stable combustion near Lop of 4.2 in.

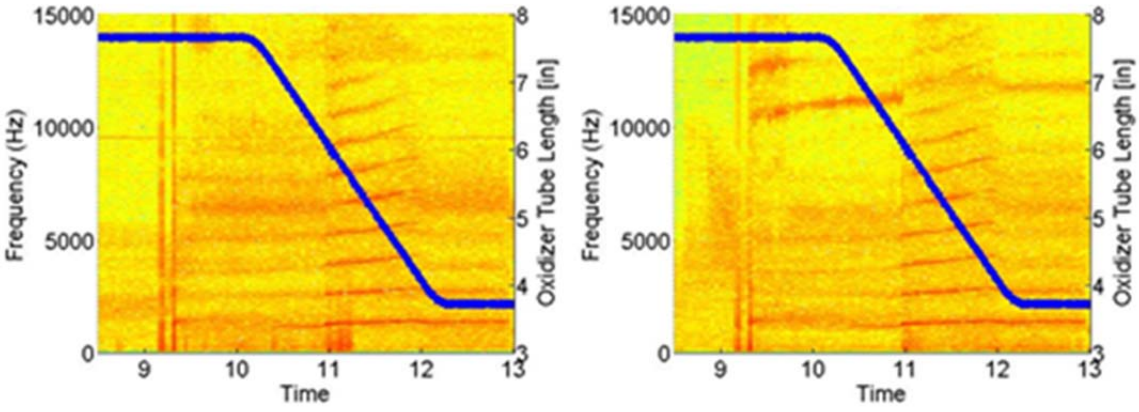

Figure 3.2 Spectrogram for a translating test at a) the aft end and b) the head end of the combustor.

As mentioned in Sec. 1.2.3, pressure was sampled at multiple axial locations, and while the PT at 14.5 in has been used in past studies, locations closer to the dump plane can offer additional information. For example, spectrograms of data taken near the injector (see Figure 3.2b) show frequency content near 12 kHz before and after the period of large amplitude unstable combustion, which corresponds to the first transverse mode (1T) of the chamber. This is not seen downstream at the 14.5 in location, nor in the oxidizer or fuel manifolds or inside the oxidizer post. It is worth noting that in the spectrograms at both locations, a two mode system of 1L and 2L can be seen past 12 s once the system achieves marginal stability, which agrees with Yu's observations [20].

3.1.2 Digital Filters

With the popularity of digital DAQ systems, digital filters become vital to remove system noise, exclude frequency content not of interest, and isolate a specific frequency range of interest. The digital filter output y(k) is related to input x(k) by convolution with its impulse response h(k) [50],

$$y(k) = \sum_{l=-\infty}^{\infty} h(l)\, x(k-l) \tag{3.3}$$

Depending on the filter type (low pass, high pass, band pass, or band stop), the characteristics of the filter are defined by filter design type (i.e. Butterworth), cutoff frequency ω_c, pass band frequencies, stop band frequencies, allowable ripple in the pass band R_p, allowable ripple in the stop band R_s, and filter order. An ideal filter acts as a "brick wall", with a magnitude of 1 in the pass band and 0 in the stop band [50]. In the design of a filter, there is a trade-off between the filter order, the transition width, and the allowable pass band/stop band ripple [51]. The lowest filter order that can meet the performance requirements is most desirable due to

the increasing computational cost with increasing filter order [51]. Design considerations and filter characteristics are detailed in Ref. [49–51].

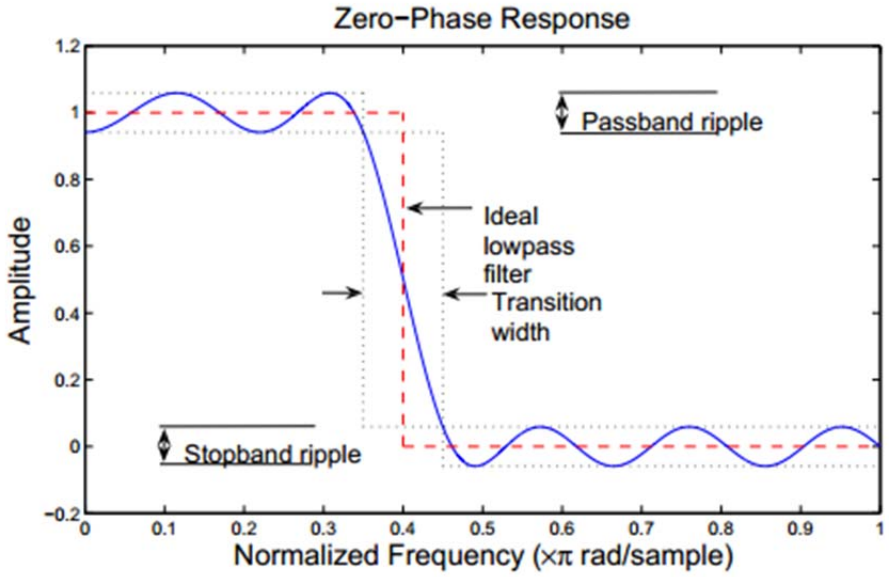

Figure 3.3 Definition of non-ideal digital filter characteristics. [51]

Some of the features of a digital filter are illustrated in Figure 3.3, where the pass band and stop band frequencies are normalized by the Nyquist frequency, $f_n = f_s/2$, where f_s is the sampling frequency. A zero-phase filter, like the one in Figure 3.3, eliminates nonlinear phase distortion that can occur in digital filters. Matlab's "filtfilt" function provides a non-causal zero-phase filter and is recommended to minimize or eliminate group delay (time delay of the filter as a function of frequency) and phase distortion [50].

3.1.2.1 Low/High Pass Filter

Low and high pass filters are used to exclude frequency content above and below a cutoff frequency ω_c, respectively [51]. A low pass filter keeps all content below ω_c and is used to filter high frequency content such as white noise. Typical

characteristics of a low pass filter are illustrated in Figure 3.4. Previous experimental analysis by Miller utilized a low pass filter for exclusion of content above 25 kHz to isolate the frequency range of interest [18]. High pass filters, as used here, allow for the exclusion of lower frequency content such as electrical noise at 60 and 120 Hz.

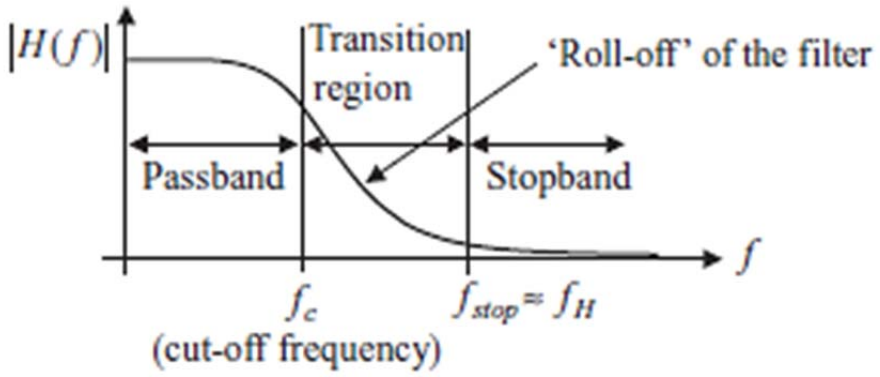

Figure 3.4 Definition of digital filter characteristics. [49]

3.1.2.2 Band Pass Filter

To look at a specific frequency or frequency range, a combination of low and high pass filters known as a band pass (BP) filter excludes content above a certain frequency (low pass filter) and below another frequency (high pass filter) [51]. The pass band is the width of the frequency range centered on the frequency of interest, defining the frequency content of interest. Figure 3.5 is a diagram of the characteristics used for the design of a digital band pass filter in Matlab. A_{stop1} and A_{stop2} correspond to R_s, the allowable ripple present in the stop band in dB units, in this study 10 dB. A_{pass} corresponds to R_p, the allowable ripple present in the pass band in dB units, in this study 1 dB. The difference between F_{pass1} and F_{pass2} represents the pass band width, while the difference between F_{pass} and F_{stop} defines

the transition width. In this study, F_{pass} is defined as +/- 100 Hz around the frequency of interest (i.e. 1L = 1450 Hz so F_{pass1} = 1350 Hz and F_{pass2} = 1550 Hz) and the transition width is 100 Hz (i.e. F_{stop1} = 1250 Hz, F_{stop2} = 1650 Hz).

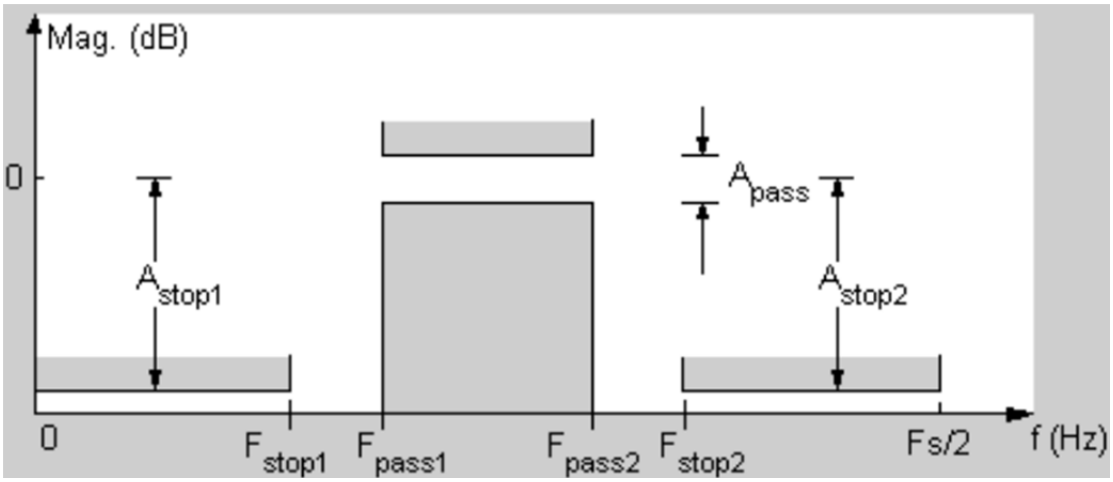

Figure 3.5 Filter characteristics used in Matlab's FDA Toolbox. [50]

In traditional analysis methods, band pass filters are used to decompose the signal into the identified Fourier components of interest. Section 4.3 discusses and compares several design types of digital filters, though a Butterworth filter is utilized for the current study based on previous analysis performed by Sisco [4]. A Butterworth filter is desirable when the quantitative behavior of the instability, such as the limit cycle amplitude, is of interest, as it has a maximally flat response in the pass band (i.e. negligible pass band ripple) [51]. Advantages and disadvantages of several filter types are further discussed in Sec. 4.3. Figure 3.6 demonstrates the change in wave behavior perceived as a result of no filter, a high pass filter, and a band pass filter.

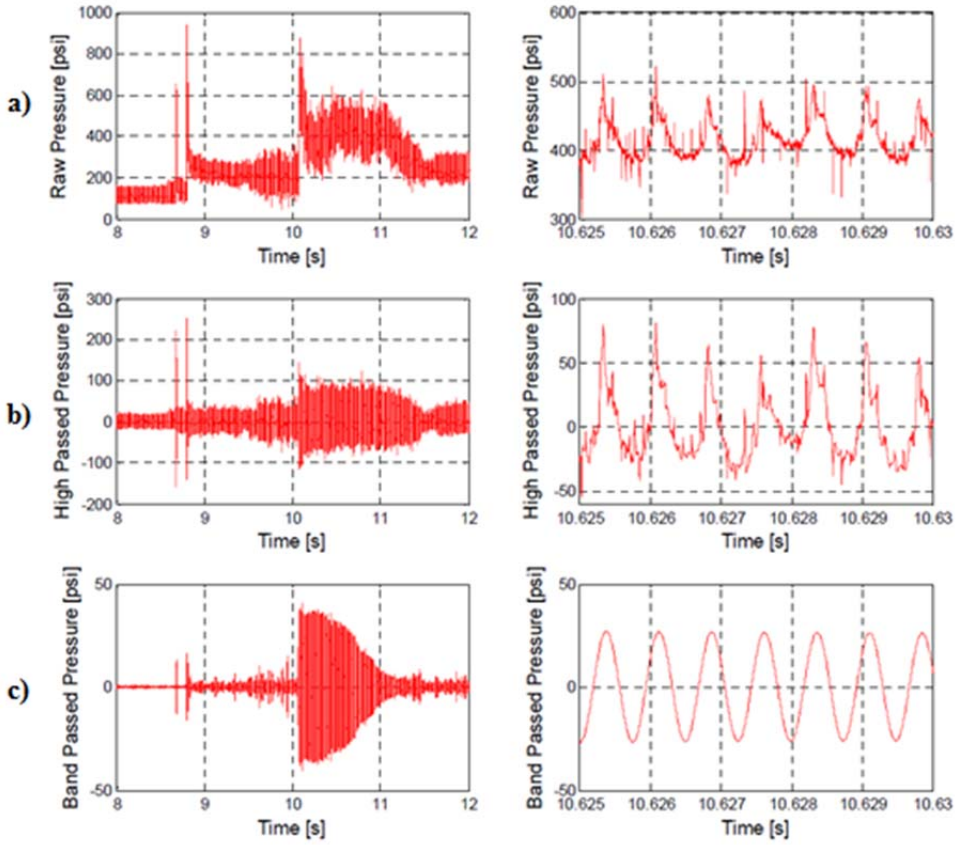

Figure 3.6 Comparison of a) unfiltered, b) HP filtered, and c) BP filtered experimental data. [21]

3.1.3 Hilbert Transform

The Hilbert transform decomposes an analytic signal into complex parts,

$$x = x_r + i * x_i \tag{3.4}$$

where x_r is the real part and x_i is the imaginary part of the signal [50]. The envelope of the original signal can then be found by

$$\hat{e}(t) = \sqrt{x^2 + xi^2} \tag{3.5}$$

where x is the original data and x_i is the Hilbert transformed data [50]. A built-in Matlab function "hilbert" provides the complex decomposition of the signal. The "instantaneous" amplitude, A(t), of the signal can then be found by

$$A(t) = |hilbert(x)| \tag{3.6}$$

Figure 3.7 demonstrates results from a Fourier-based Matlab routine, where the signal is band pass filtered around the frequency found from the PSD, then the Hilbert transform is applied to yield the instantaneous amplitude of the BP signal to decrease the number of data points under analysis.

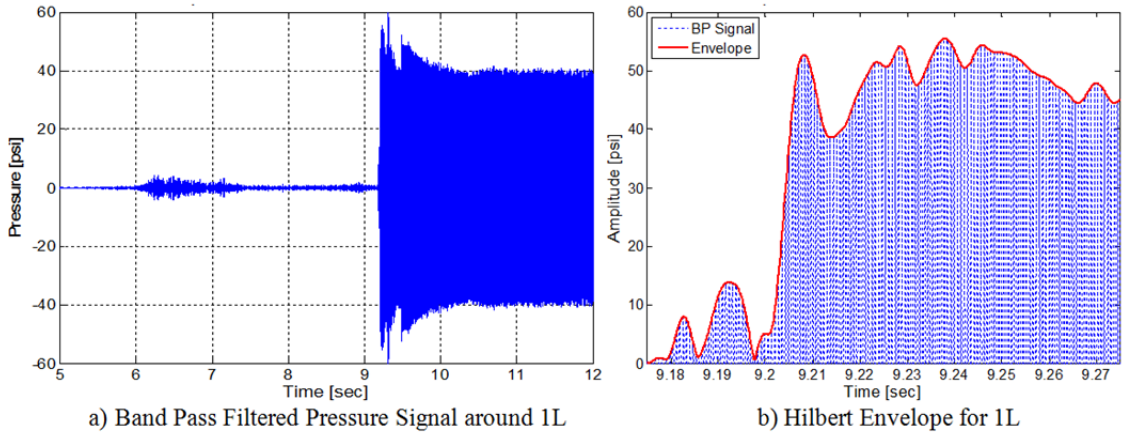

a) Band Pass Filtered Pressure Signal around 1L

b) Hilbert Envelope for 1L

Figure 3.7 For the unstable fixed test case, a) the BP pressure of 1L and b) the Hilbert envelope of 1L.

3.1.4 Statistical Noise Threshold

As is often the case, experimental data can be difficult to process at small time scales on the order of 10 ms and frequencies at 1 kHz or higher that include system noise and ringing from high amplitude ignition events. The system noise appears in the BP signals, potentially obscuring the onset time of each mode, demonstrated in Figure 3.8. In an attempt to combat this, the standard deviation

of the BP signal envelope is calculated from the beginning of the data up to the rapid rise in oscillation amplitude. A statistical noise threshold is established, where 95% of the noise falls below this 2σ value. When the BP signal rises above the statistical threshold, it is assumed that the signal is not simply system noise. Onset of each mode is distinguished as the last instance when the envelope is less than or equal to the threshold value prior to when the limit cycle amplitude is reached. This statistical analysis helps to eliminate potential user bias in the results.

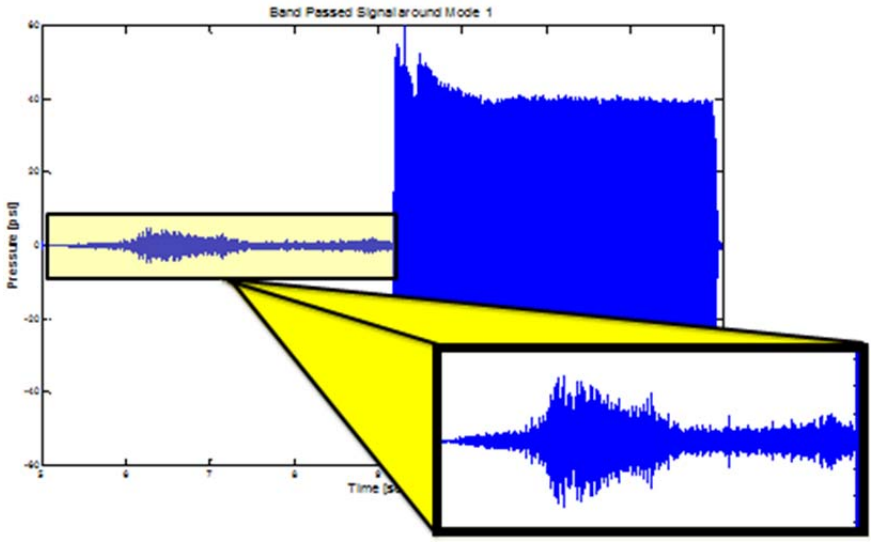

Figure 3.8 System noise in BP pressure signal of 1L.

3.1.5 Preliminary Results

The general analytical procedure used in this Matlab routine is as follows: first, the raw pressure signal is run through a second order Butterworth high pass (HP) filter to remove low frequency noise below 150 Hz. Second, to define dominant frequencies in the oscillatory signal, the PSD is calculated for 0.1 s of the HP signal once high amplitude pressure oscillations begin. Figure 3.1 shows an

example of these results. Third, the raw pressure signal is run through a custom Butterworth band pass (BP) filter, where the pass band frequency and stop band frequency are specified as a 200 Hz and 400 Hz window, respectively, around the modal frequency, normalized by the Nyquist frequency of the signal. For ease of analysis, the envelope of each BP signal is found using the Matlab function "hilbert", which decomposes the signal into real and imaginary parts. Figure 3.7 demonstrates that the magnitude of the Hilbert transformed data provides a good approximation of the instantaneous amplitude of the input time signal [50].

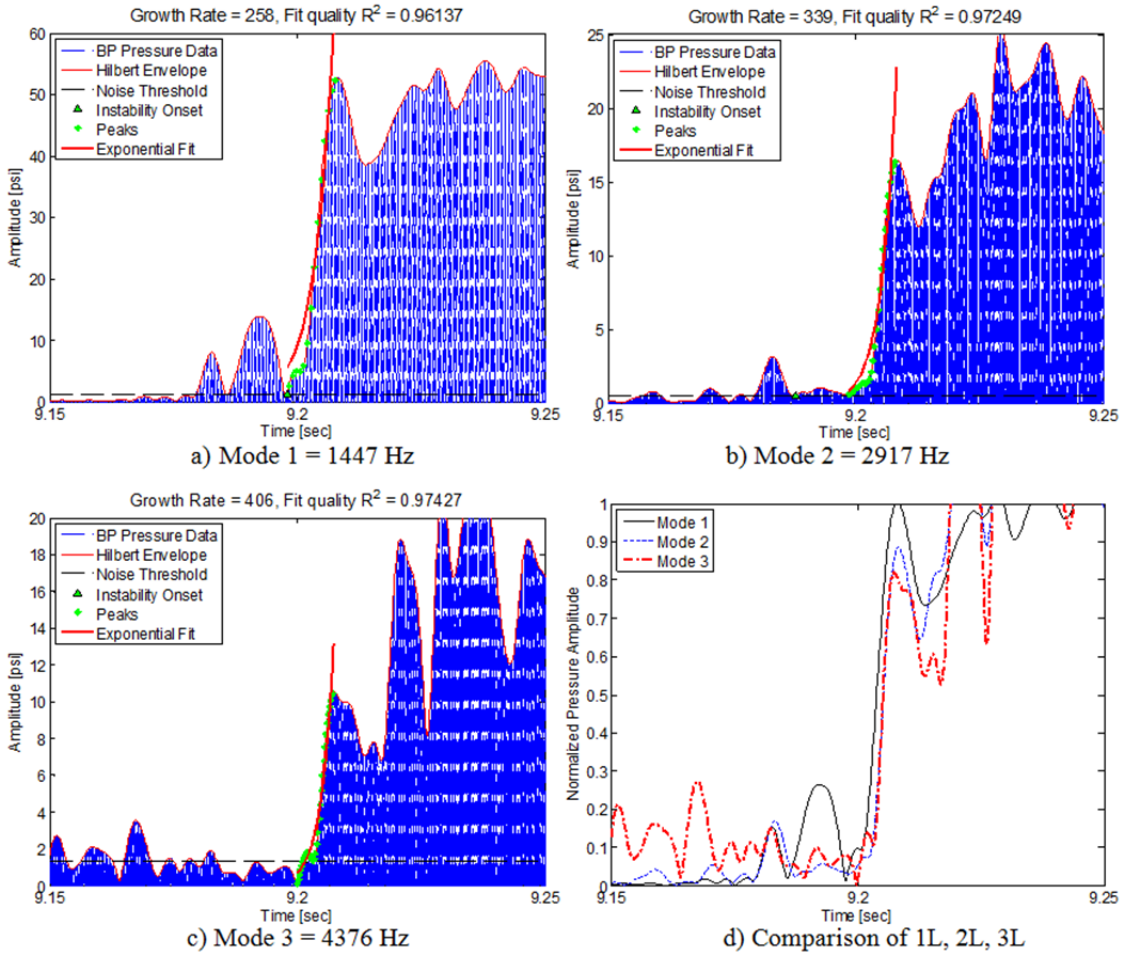

Figure 3.9 For an unstable fixed test case, traditional instability analysis of a) 1L, b) 2L, and c) 3L with d) a comparison of 1L, 2L and 3L.

When applied to the first three modes, the Fourier method presented in Sec. 3.1.1 is repeatable across different test cases and test series. Figure 3.9 demonstrates the results for the unstable fixed test that will be analyzed with every method reviewed. Onset time, growth rate, and goodness of fit are calculated for the fundamental frequency and the first two harmonic frequencies. From these results, it can be seen that the growth behavior of 2L and 3L are similar enough as to be nearly indistinguishable, with calculated onset times less than 1 ms apart. Additionally, the oscillation amplitude grows more rapidly for each subsequent mode. Assuming that a fixed energy source is exciting and sustaining the instability, modes with a higher frequency would traverse past the energy source more often and have energy added more frequently, so once the mode is excited it would grow faster than a mode with a lower frequency. Also, while the time of modal excitation is different (2 to 4 ms apart), the time each mode reaches limit cycle amplitude (end of rapid growth) is within 1 ms of the others.

More interest is given to translating test cases. The modal behavior when the combustion transitions from stable to unstable and vice versa while the oxidizer post length changes is particularly interesting and unique to the CVRC. While the instability seen in the fixed test cases may have been triggered by vestigial ignition events (a subcritical bifurcation), onset of instability in translating tests occurs more than one second after main ignition. As opposed to triggered instability, the translating test results present self-excited longitudinal instability based on combustor geometry.

Figure 3.10 illustrates the results from a translating test case. Growth behavior of each mode appears to be different than that seen in the unstable fixed test case in Figure 3.9. While the rate of oscillation amplitude growth is still higher

for each higher mode, the growth rates themselves are much less rapid than in the unstable fixed case in Figure 3.9. Yet for both fixed and translating cases, the time each mode reaches limit cycle amplitude is within 1 ms of the others. Additionally, the behavior of 2L and 3L are still comparable in the variable case but a distinguishable time difference exists between the onset and growth of each mode on the order of 5 ms.

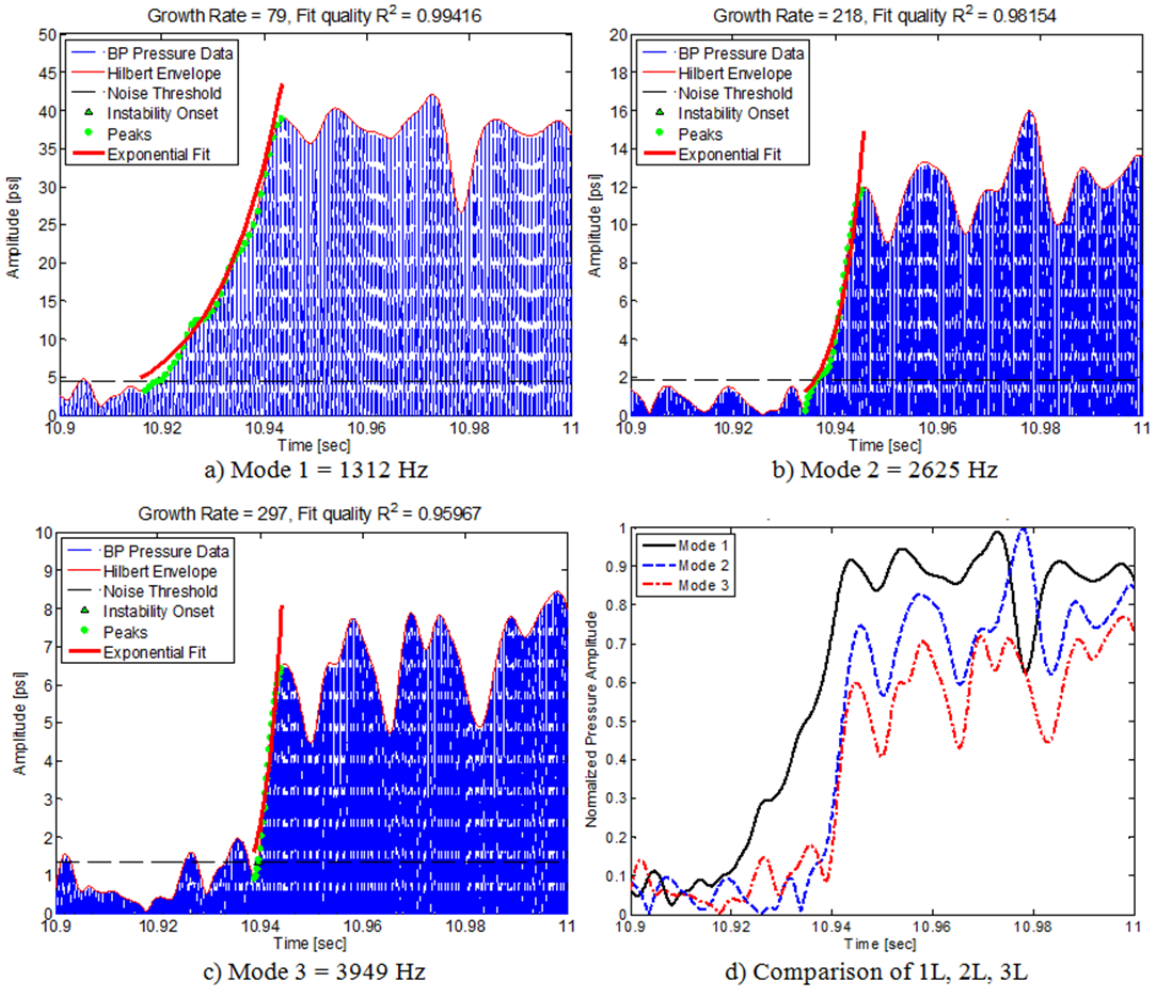

Figure 3.10 For a translating test case, traditional instability analysis of a) 1L, b) 2L, and c) 3L with d) a comparison of 1L, 2L and 3L.

It should be noted that in the fixed case the oxidizer post length (Lop) is 5.1 in (13 cm), a highly unstable geometric configuration as shown in previous testing and analysis. The translating test case transitions to unstable combustion at an oxidizer post length near 6.25 in (15.9 cm) as the inlet choke point translates from an oxidizer post length of 7.83 to 3.80 in (19.9 to 9.7 cm) over the course of two seconds, with unstable combustion at oxidizer post lengths from 6.25 to 4.75 in (15.9 to 12.1 cm). Thus, comparison of modal onset behavior would be more appropriate with fixed test cases at or near the geometry at onset of instability for the translating test case.

A manufactured signal, similar to the ones used to validate the oscillation decrement results in Sec. 3.2.1, was employed to verify the reliability of results from this preliminary analysis. Of particular concern was whether or not the HP and BP filters remove relevant information from the pressure signal, as the HP-filtered pressure data are used to find the dominant frequencies while the BP-filtered pressure data are used to find the onset time and growth rate for each mode. The envelopes of BP signals filtered around frequencies identified from the PSD were compared to the original signals that made up the composite signal. For sine waves, this analysis closely represents the original signal. However, if the component signal(s) is a steep-fronted wave, this analysis fails to correctly capture the component wave behavior.

Whether or not harmonic content exists in the manufactured signal, this analysis method indicated the presence of powerful harmonic frequencies for steep waves. Analytical models and experimental work presented in Sec. 2.2 support the assumption that in the case of longitudinal oscillations with harmonic modal content, the individual harmonic waves are continuous and can be treated as

sinusoidal. In this application, then, the method applied in this section appears to be both repeatable and believable across the three test cases analyzed. If, however, the individual harmonic wave behavior is discontinuous (non-sinusoidal), this signal processing method may need to be re-evaluated. Specifically, for a steep-fronted wave, the question remains whether or not the artificial harmonic signal can be separated from the existent modal behavior. This question is further explored in Sec. 4.1.

Several other observations were made in the analysis of the manufactured signal. In cases with and without harmonic content for a steep-fronted wave, the false harmonic signals did not follow a pattern with respect to the order in which each mode grows or the growth rate of each mode, unlike that seen in these preliminary results. Additionally, due to its slow roll-off property, it appears that the Butterworth filter fails to correctly represent the growth behavior of the modal oscillation for a steep-fronted wave, especially in the case of rapid growth to limit cycle amplitude, as seen here. This may indicate the need for different digital filter types to be investigated, as is done in Sec. 4.3.1.

3.2 Alternative Digital Signal Processing Methods

While Fourier-based analysis is most commonly used in combustion instability analysis, that does not necessarily mean it is the best DSP method for this study focused on harmonic content. As such, several alternative DSP methods were reviewed, including oscillation decrement, wavelet analysis, and an Instantaneous Frequency (IF) analysis in the PC Signal Analysis software.

3.2.1 Oscillation Decrement (Signal Autocorrelation)

The oscillation decrement, previously used in Russian engine development and gas turbine work, is a passive method to estimate system damping using dynamic pressure signals [4,14]. A non-dimensional damping factor, the oscillation decrement, δ_nT, is calculated using the decay rate of the autocorrelation of the pressure signal.

$$C_n(\tau) = e^{-\zeta_n \tilde{\omega}_n \tau} * \cos(\tilde{\omega}_n \tau) = e^{-\delta_n \tau} * \cos(\tilde{\omega}_n \tau) \tag{3.7}$$

C_n is the autocorrelation of the pressure signal, τ is time lag, ζ_n is a damping coefficient, $\tilde{\omega}_n$ is the adjusted angular frequency, δ_n is the damping factor, and T is the period of the oscillation [4]. Following past Russian subscale work, Sisco applied the oscillation decrement to determine when the combustor transitions to unstable combustion [4]. See Ref. [4] for further discussion of the oscillation decrement and results obtained looking at 1L. This analysis was applied to an unstable fixed test and the results are shown in Figure 3.11a.

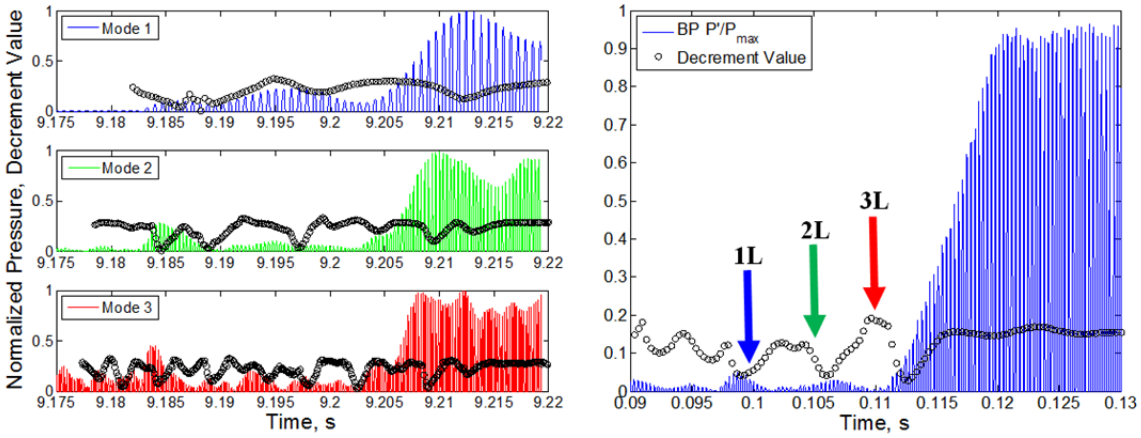

a) Experimental Data b) Fake Signal

Figure 3.11 The oscillation decrement analysis results for a) an unstable fixed test case and b) 3L of a manufactured signal.

It can be seen from the plots in Figure 3.11a that the oscillation decrement analysis produces results open to misinterpretation. If the beginning of unstable combustion is indicated by decreasing decrement values, Figure 3.11a suggests onset occurs before 9.2 s for 1L, near 9.2 s for 2L, and between 9.2 to 9.205 s for 3L. However, without the normalized pressure data superimposed it could also have been concluded that onset occurs between 9.21 to 9.215 s for 1L, before 9.21 s for 2L, and before 9.21 s for 3L. Additionally, it is unclear whether the beginning of instability should be interpreted from a valley or peak in the decrement value.

Manufactured signals were fed into the same analytical code. Three sinusoidal signals of frequency on the same order of magnitude as the first three modes were created to grow non-linearly at different "onset" times. The fake signals were combined along with low frequency system noise at 10% of the amplitude of the main signal before being processed through the oscillation decrement code. The procedure was repeated with the three signals at the same onset time. In the fake signal analysis, artifacts from the lower frequencies appear in the results of higher harmonic frequencies. This is illustrated in Figure 3.11b, as the onset times of the first (at 1 ms) and second signal (at 1.05 ms) dominate the decrement values calculated for the third signal (at 1.1 ms).

The fake 1L signal analysis reveals that onset is indicated by a minimum decrement value prior to rapid pressure amplitude growth, but for the fake 3L signal, onset is indicated by a maximum decrement value prior to amplitude growth. It is possible that either the criterion for instability changes for each mode or the results are only viable for the first mode. Another significant observation from the fake signal analysis is that for sinusoidal wave shapes, the decrement values tend to display a sinusoidal behavior, creating false points of high and low

damping. The uncertainty as to whether or not a result is from the data or an artifact of the analysis makes the oscillation decrement an unsuitable method for this application.

3.2.2 Wavelet Transformations

Wavelet analysis is one of the most convenient techniques in practice, as Matlab has an extensive Wavelet GUI and separate Wavelet Toolbox, documented through User Guides and reference material [50,52]. Similar to Fourier analysis, the general concept behind wavelet analysis takes a defined shape chosen by the user and attempts to fit a frequency-based hierarchical family of these shapes specified by scale values to a time-domain signal, transforming it into the frequency-domain [49,52]. Examples of typical wavelet shapes are shown in Figure 3.12. The output represents how well each wavelet within the family fits to the signal over time.

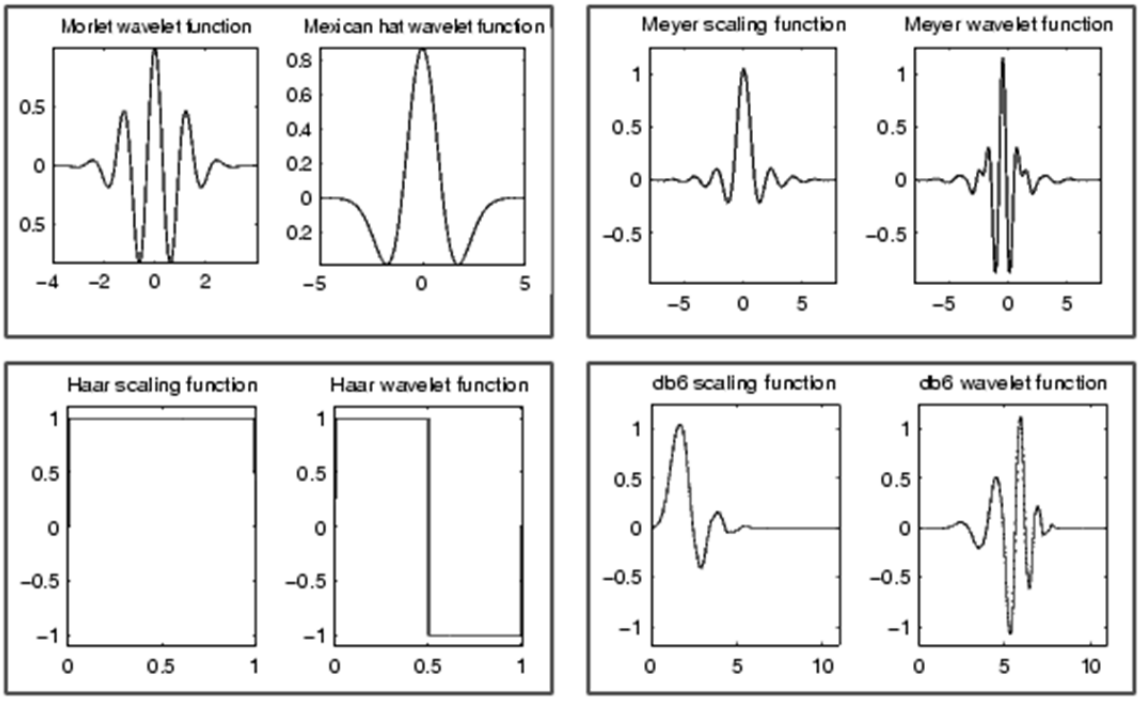

Figure 3.12 Typical wavelet shape families. [54]

One of the advantages of wavelet analysis is the ability to reconstruct the entire signal from the decomposition. Results from an analytical technique that manipulates the original signal to the point where the raw data cannot be distinguished may need to be reconstructed in order to verify that any interpretations are based on the data rather than the data processing.

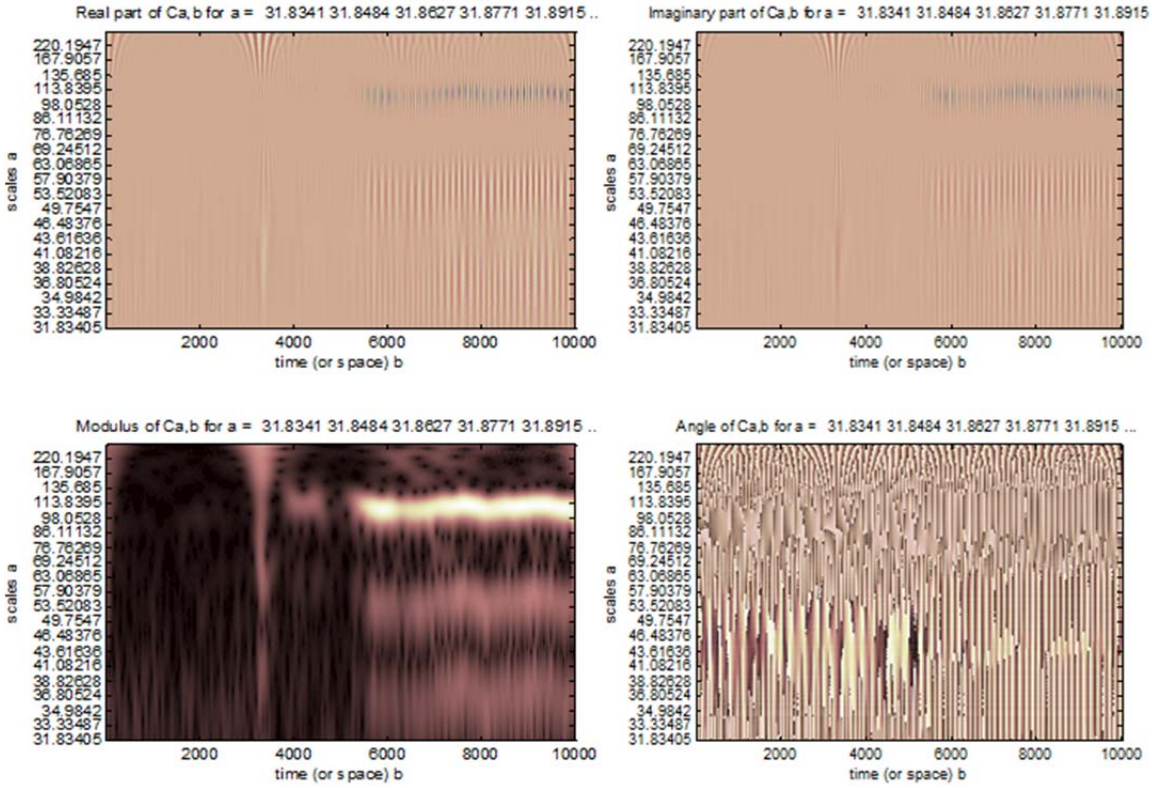

Figure 3.13 CWT decomposition results of an unstable fixed test from Matlab's Wavelet GUI.

The outputs from the Matlab tools previously mentioned are difficult to interpret for novice users, as results are presented in terms of scale families as opposed to frequency. Figure 3.13 provides an example of the continuous wavelet transform (CWT) decomposition results of the unstable fixed test from Matlab. The decomposed signal is shown in its real and imaginary parts, accompanied by

the moduli and angles for the scales, each of which represents one of the frequency-sized wavelets in the wavelet family applied [52]. Here, strong components are observed near scale 114 from 5500 data points to the end of the signal. This indicates when the frequency content organizes as resonant modes are excited, though the frequency and time indicated in Figure 3.13 would need to be back calculated based on the inputs given to the GUI and the relationship between scale values and frequency.

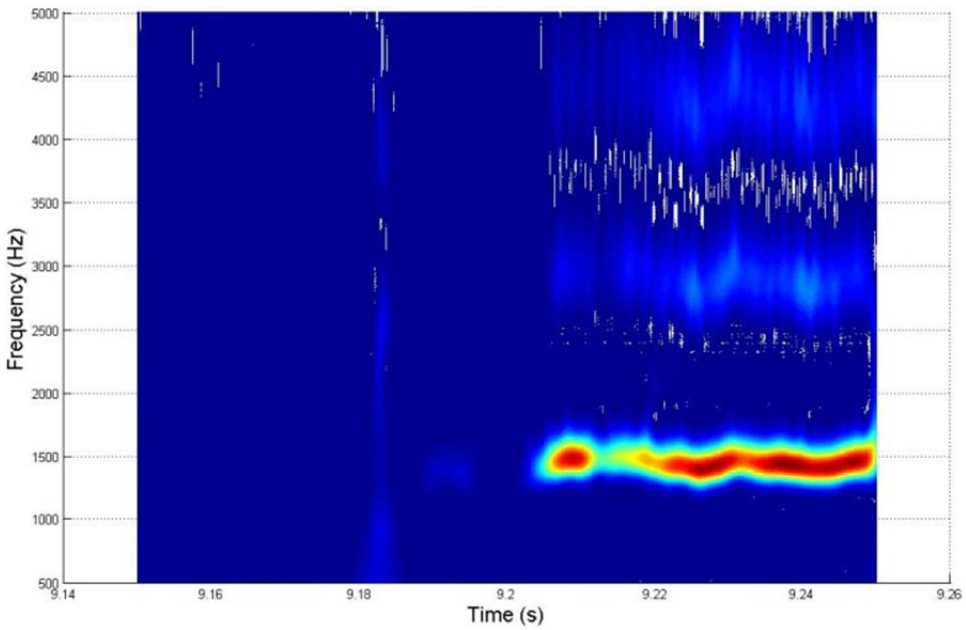

Figure 3.14 For an unstable fixed test case, scalogram of formatted CWT results.

Using a routine developed by Kittel to format the Matlab toolbox output into time-frequency information allows for the individual analysis of each mode, as a frequency range of interest (here 0.5 to 5 kHz) can be specified within the program [55,56]. An example of these outputs is presented in Figure 3.14, showing results for the first three modes. The strength of the 1L components washes out the results for the two harmonic modes seen, so it would be better to limit the

frequency range of interest around each modal frequency being studied. Here, a Gabor wavelet of shape factor Gs = 10 is used.

The wavelet analysis is appealing due to its ability to track multiple potentially non-sinusoidal frequencies over time, but two issues remain. First, the user chooses the type of wavelet to be applied, making *a priori* knowledge of the wave shape very desirable for the most accurate results. Second, results are highly dependent on the input settings as the shape factor directly affects the time-frequency resolution and the input settings may need to be changed on a test case or test series basis [55,56]. For example, changing the shape factor applied in Figure 3.14 could move the perceived onset of instability of a modal frequency by up to 20 ms. This makes comparison between tests more difficult if the same analysis (with the same bias) is not performed on each set of data, otherwise the onset information could be obscured due to user input settings. Furthermore, as the shape factor approaches infinity, the wavelet transform begins to act like a Fast Fourier Transform (FFT) [55,56].

It should be noted that for test environments with low signal to noise ratio, wavelet analysis has an advantage over traditional techniques as it can better distinguish signal from noise, but in the CVRC data, signal to noise ratio does not tend to be an issue [20–22,30,49,52,55,56]. In addition, Matlab's Wavelet GUI requires substantial computational power beyond the capability of many desktop PC's. However, while wavelet analysis has a basis in traditional Fourier analysis, it is not confined to a sine wave assumption and may be more appropriate for the steep-fronted waveform observed in unstable combustion pressure signals. For sinusoidal components waves, there does not appear to be a significant advantage for using wavelet analysis over the more common Fourier transforms in this

application. However, if it can be shown that the wave behavior is more shock-like and/or steep-fronted, wavelet analysis may have an advantage with the ability to apply steep-fronted wavelet shapes to the dynamic pressure signal.

3.2.3 Matched Filtering

Since the frequencies of the acoustic modes are known, a matched filter technique was attempted. The matched filter technique assumes that since each frequency occurs and reaches sinusoidal-like limit cycle behavior, each band pass filtered signal can be additionally filtered with something akin to a step function looking for a long (on the order of 1 s) sine wave with modal frequency [49]. However, the frequency content of the pressure signal is unorganized until the modes are fully excited. The transition time can be on the order of 100 ms with non-sinusoidal and/or nonlinear behavior during that period.

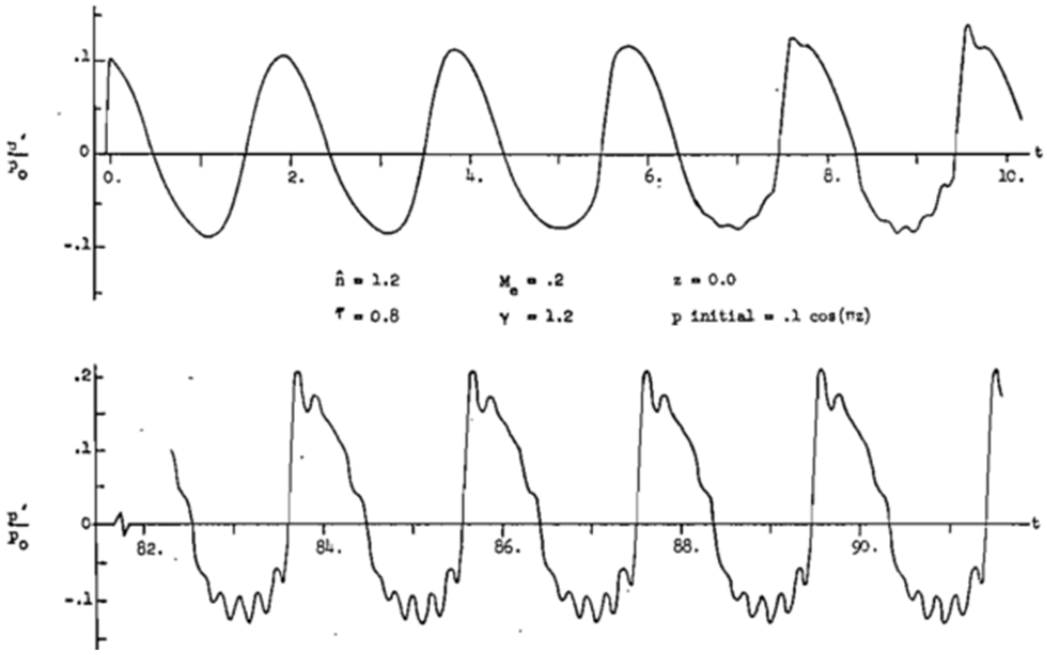

Figure 3.15 Distortion of pressure waveform at onset of instability. [28]

As discussed by Zinn and Lores, experimental investigations have shown that the pressure oscillations initially appear as continuous sinusoidal waves but quickly distort into discontinuous shock-like waves, with this discontinuous behavior fully established by the time limit cycle amplitude is reached [28,29]. The transient and limit cycle behavior of the pressure oscillations are shown in Figure 3.15 from their 1971 paper [28]. For a purely sinusoidal signal, such as one tested for reference, the matched filter technique produces useful results, but in this application, any output results do not provide the desired onset information. Additional information on the matched filter technique can be found in Ref [49].

3.2.4 PC Signal Analysis Software

The program PC Signal Analysis from AI Signal Research is a dynamic signal processing software package designed for engineering applications such as turbine rotor vibration analysis or static rocket test analysis [57,58]. It has an extensive GUI with more specific data processing abilities than Matlab, especially in the case of real and noisy experimental data. However, the program works as a black box, and there is limited software documentation on unique capabilities such as the Instantaneous Frequency (IF) Tracking Analysis used in this study. Because of this, results from IF Analysis were exported to Matlab for any continued examination.

3.2.4.1 Instantaneous Amplitude Tracking

In the case of amplitude from IF Analysis, the program looks for the most "dominant" frequency near each user-specified frequency (in this case, the resonant modal frequencies) and calculates the amplitude of the signal as a function of time.

Figure 3.16 presents a comparison of the results from a) IF Analysis and b) the Fourier analysis presented in Sec. 3.1. As the comparison demonstrates, the results from the two signal processing methods are comparable, though the results from IF Analysis appear to be less affected by signal noise than those obtained using the Matlab routine.

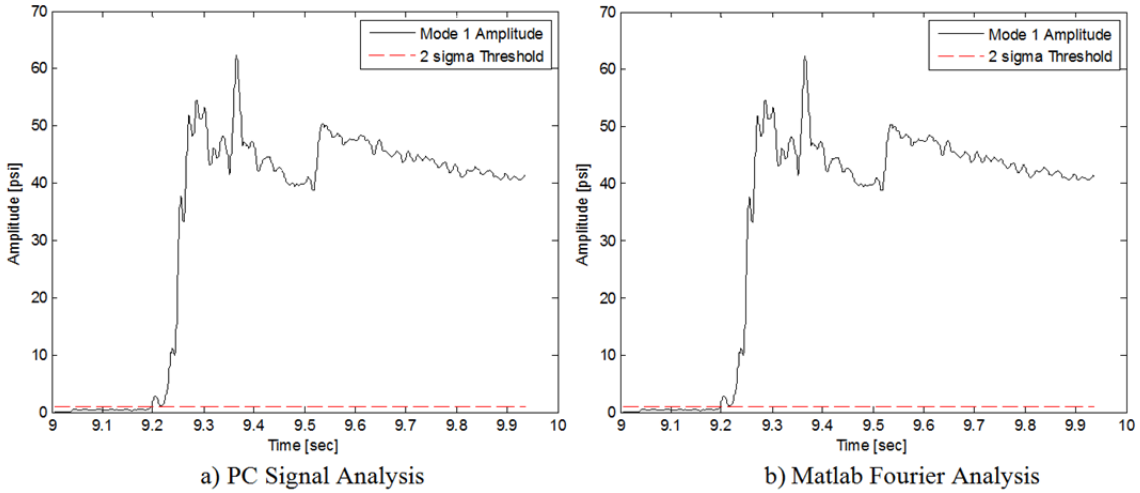

Figure 3.16 For an unstable fixed test case, instability analysis of 1L from a) PC Signal Analysis and b) traditional Fourier analysis.

However, when comparing the results for 2L and 3L in Figure 3.9d and Figure 3.17, IF Analysis provides significantly different information than the Matlab routine. It may be possible that for the harmonic modes, the large amplitude response seen near 9.3 s is a DSP artifact from the rapid onset of 1L, while the true excitation for 2L begins around 9.55 s and 9.75 s for 3L. This would give an onset time difference on the order of 100 ms, two orders of magnitude larger than other DSP methods have shown. Further investigation into this potentially significant difference is performed in Sec. 4.2.

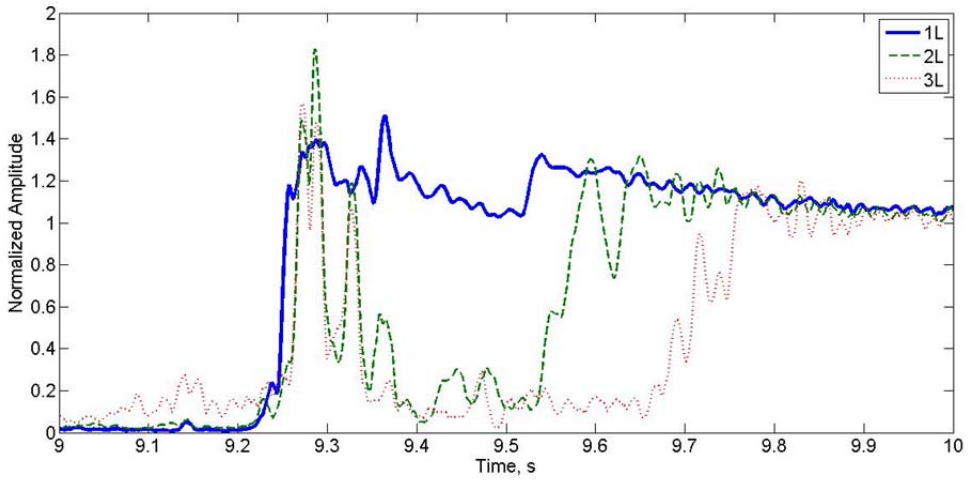

Figure 3.17 For an unstable fixed test case, amplitude from IF Analysis of 1L, 2L, and 3L.

3.2.4.2 Instantaneous Frequency Tracking

The ability to handle experimental data is a significant advantage that PC Signal Analysis software offers, especially in the case of the frequency tracking from IF Analysis, as traditional analysis methods used in Matlab such as the Hilbert transform are sensitive to noise from experimental data and cannot provide the same information without potentially large errors. It was speculated that frequency coherence could be an indication of the excitation of the unstable mode. To test this, PC Signal Analysis's IF Analysis is applied to the signal, looking at a 200Hz pass band centered on the 1L frequency.

Preliminary analysis using the IF Analysis for 1L provides the results shown in Figure 3.18 for the unstable fixed test. While it appears that the standard deviation of the frequency significantly decreases during unstable combustion, this does not occur until approximately 0.5 s after the onset times found using the

other DSP methods presented, including the amplitude results from IF Analysis in Sec. 3.2.4.1. Taking a closer look at the frequency coherence of 1L, 2L, and 3L, the IF Analysis shows identical variance in normalized frequency once limit cycle amplitude is reached, seen in Figure 3.18b. It is unclear as to whether or not this supports or refutes the existence of harmonics.

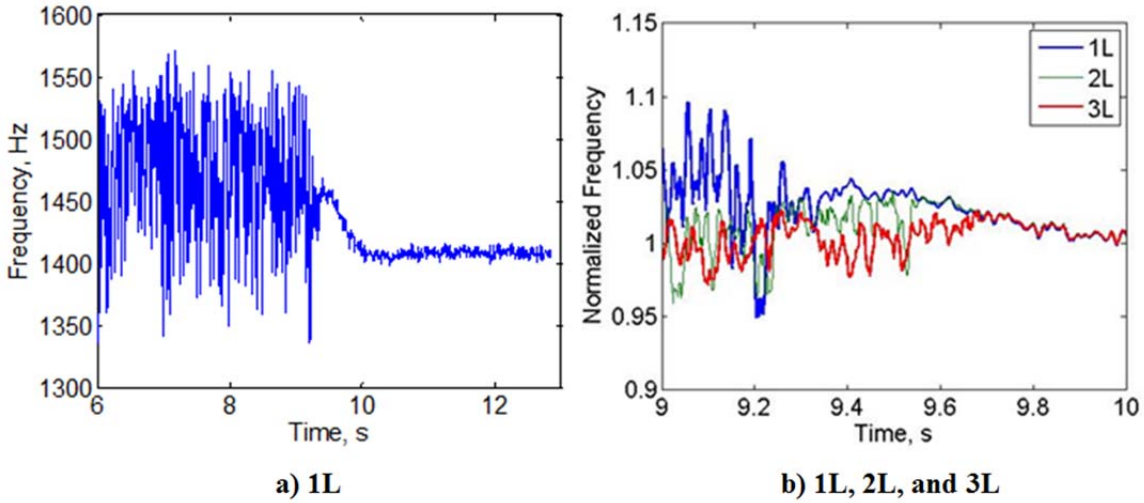

Figure 3.18 For an unstable fixed test, frequency from IF Analysis of a) 1L and b) 1L, 2L, and 3L.

3.2.4.3 Instantaneous Phase Tracking

Another unique ability of PC Signal Analysis is phase tracking from IF Analysis, shown in Figure 3.19. While the results do not provide quantitative information, it is interesting to note the sequential organization of phase per mode. From Figure 3.18, spectral organization occurs around 9.25 s for 1L, 9.5 s for 2L, and 9.75 s for 3L. From Figure 3.17, this corresponds to the times at which each mode reaches limit cycle.

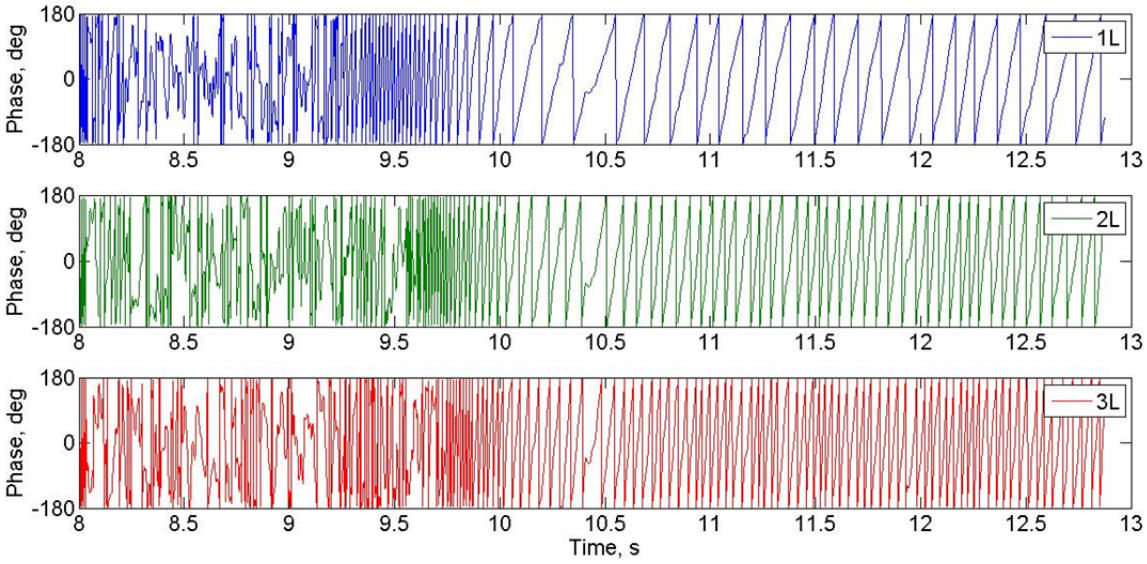

Figure 3.19 For an unstable fixed test case, phase from IF Analysis of 1L, 2L, and 3L.

3.2.4.4 Summary of Results

Now the three main results from IF Analysis are shown for each mode of interest. The frequency shift at onset of instability, the amplitude of the pressure oscillations, and the instantaneous phase are presented in Figure 3.20 – Figure 3.22. From these comparisons, a correlation between these characteristics can be seen, though perhaps not quantified. It is also worth noting that IF Analysis results do not match Matlab's Fourier analysis results as covered in Sec. 3.1.5 for 2L and 3L, as the point of onset for the harmonic modes does not occur immediately after the fundamental excitation.

Closer inspection of the raw data shows that the steep-fronted wave behavior exists by 9.2 s, the onset time of 1L. Yet if the results from PC Signal Analysis are valid, this opens up the possibility that 1L may be nonlinearly excited,

causing a distortion in the continuous waveform prior to the excitation of harmonic modes. Then, the steep-fronted wave behavior would not be attributable to harmonic acoustics.

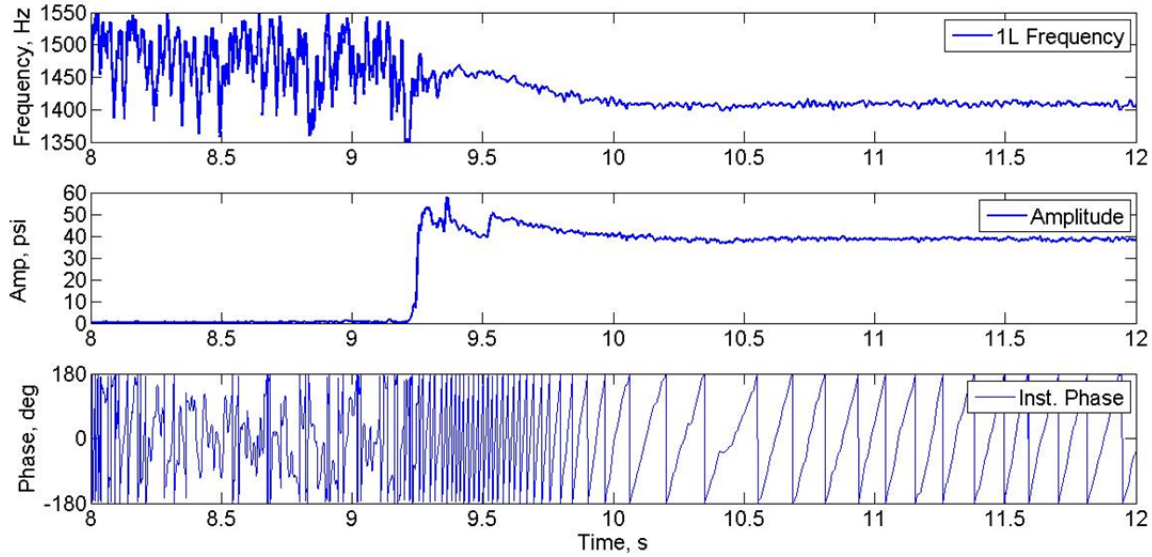

Figure 3.20 Summary of IF Analysis results of 1L for an unstable fixed test case.

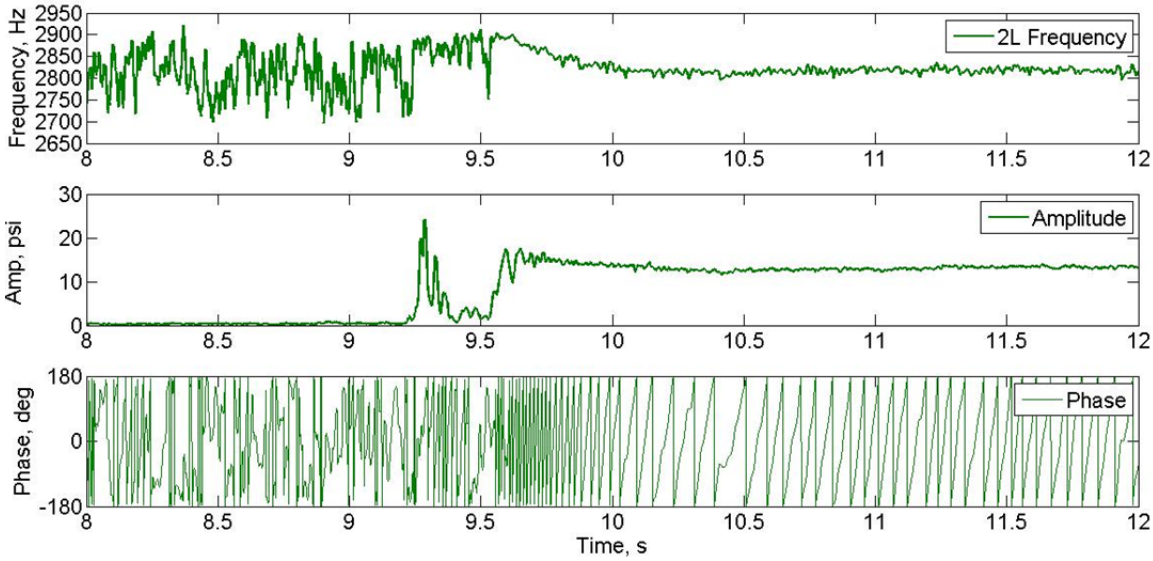

Figure 3.21 Summary of IF Analysis results of 2L for an unstable fixed test case.

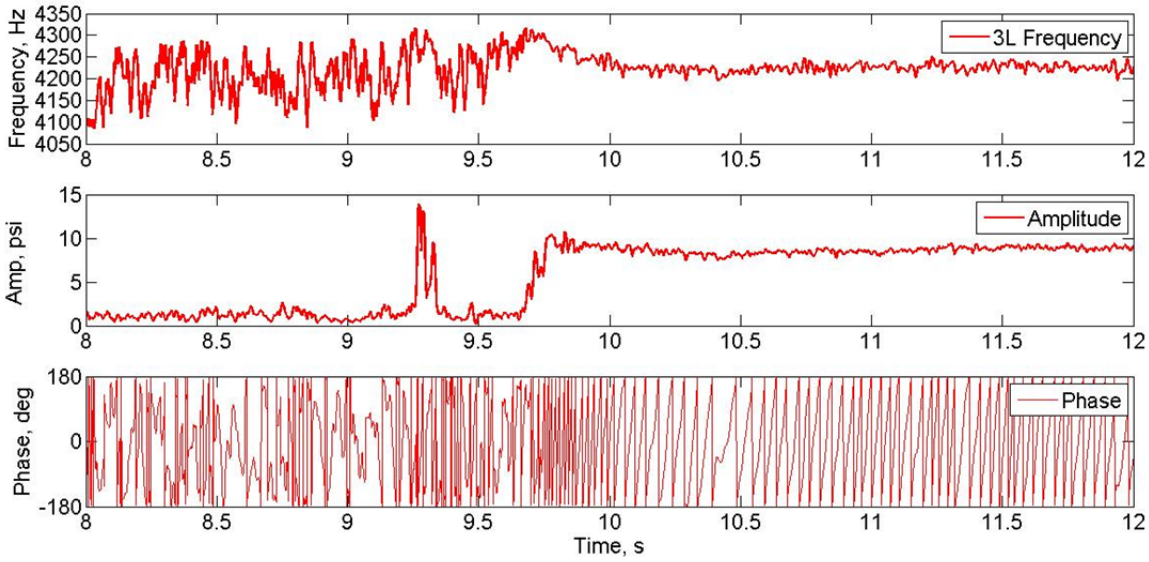

Figure 3.22 Summary of IF Analysis results of 3L for an unstable fixed test case.

The results presented here are unique from the other DSP methods and may or may not be distinguishing the extant modal behavior from the dynamic pressure signal. If this is the case, then IF Analysis becomes highly desirable for this study. However, application of "black box" software to a research problem is difficult when a full understanding of the process is not readily available. If more extensive documentation and tutorials become available for the software and specifically its unique signal processing modules, this method may become the most suitable method for this application, but as of right now, the benefits over the Matlab routine previously discussed must be significant to justify the time investment needed for confident use. As with the Wavelet GUI, IF Analysis requires substantial computational power beyond the capability of many desktop PC's. That, combined with the current need to export results to Matlab for further analysis, presents potential difficulties when applied to this research problem.

3.3 Initial Conclusions from DSP Review

In the case of high frequency digital signal processing on experimental pressure data obtained from CVRC instability tests, several signal processing techniques were reviewed: Fourier transformations with Butterworth filtering, oscillation decrement, wavelet transformation, matched filtering, and IF Analysis from the software PC Signal Analysis.

If it can be shown that the harmonic frequencies are not artifacts of the signal processing method, traditional Fourier analysis provides rational results up to the third modal frequency and offers a sufficient time resolution for this application when combined with band pass filters and statistical noise thresholds. Other methods may provide less noisy results but require substantial computational power.

Oscillation decrement has proven to be unsuitable for the study of multiple frequencies, especially in the case of sine waves. Artifacts from lower frequencies appear in the results of higher frequencies, potentially obscuring relevant information. Time resolution is also a concern.

Wavelet transformations offer potential advantages over traditional signal processing methods, but are most relevant when the data has a low signal to noise ratio, which is not the case in this application. It is a complex method that requires significant computational power, while the user-specified wavelet type and shape factor strongly impact the results; specifically, wavelet shape factor directly affects the time-frequency resolution.

IF Analysis from the software PC Signal Analysis offers similar results with less sensitivity to noise near onset of each modal frequency but requires significant

computational power. Due to the general "black-box" nature of the software routines, results were exported into Matlab for further analysis. While powerful, the software has a steep learning curve and requires significant direct interaction with the company as a result of limited documentation. If it can be shown that the distinguishing behavior for 2L and 3L observed in Sec. 3.2.4.1 is consistent across several tests and/or the instantaneous phase and frequency provide relevant information to further study the modal relationships, IF Analysis may become the more attractive signal processing method.

3.4 Initial Observations

Preliminary results were presented in Secs. 3.1.5 and 3.2.4.4 for the onset of instability for the first three longitudinal modes. Initial observations discussed here were attained from the preliminary results from the Fourier-based Matlab routine. For both fixed and translating tests, the fundamental mode goes unstable first, followed sequentially by the second and third mode. The time difference in both cases is significantly smaller between the second and third mode than between the first and second mode, on the order of 1 ms versus 10 ms. It is possible that some of the harmonic behavior observed here can be attributed to Fourier artifacts from the steep-fronted wave. Higher modes demonstrate faster growth rates than lower modes which could be attributed to a fixed energy source in the longitudinal path traveled by the resonant modes.

Comparison between the fixed and translating tests showed a slower growth rate for the translating case, though this might be due to the onset occurring at an oxidizer post length closer to the stability limit of the combustor while the fixed case is performed at a highly unstable condition. Another conceivable difference

between the two test cases may be the source leading to high amplitude pressure oscillations. In the case of the fixed test, transition to instability occurs within 5 ms of main ignition, where the high-pressure short-duration ignition event could potentially act as a trigger for sustained pressure oscillations. In the case of the translating test, transition to instability occurs nearly 1 s into a 4 s hot fire duration, so self-excited oscillations are more likely to be present.

CHAPTER 4. COMPARISON AND ASSESSMENT OF METHODS

The initial analysis performed and presented in Chapter 3 raised several questions, prompting supplementary investigation into the traditional Fourier analysis, PC Signal's IF Analysis, the digital filters used, and the existence of harmonic modes.

4.1 Steep-fronted Wave Analysis

Traditional Fourier analysis makes the assumption that the signal under consideration is sinusoidal or composed of sinusoidal component signals [49]. However, many prevailing theories discussed in Sec. 2.3 suggest that nonlinear effects cause a compression of the pressure wave followed by an expansion leading to shock-like behavior and that this is responsible for the non-sinusoidal wave behavior as opposed to the excitation of harmonic frequencies. This proposed behavior brings in to question the validity of traditional analysis methods that are based on a sinusoidal assumption. Specifically, Gibb's phenomenon states that

> *When a function is approximated by a partial sum of a Fourier series, there will be a significant error in the vicinity of a discontinuity, no matter how many terms are used for the partial sum* [49].

If a true discontinuity exists, the Fourier analysis would indicate strong artificial harmonics in an attempt to represent the steep-fronted wave behavior seen.

4.1.1 Initial Study

To investigate whether or not Fourier artifacts are affecting the results from this study, a steep-fronted wave is manufactured using an exponential growth followed by an exponential decay, as illustrated in Figure 4.1. The time between peaks corresponds to the fundamental frequency observed (on the order of 1.5 kHz), while the times of growth and decay are based on experimental data, here 3 ms to maximum amplitude and 5 ms to minimum amplitude for the fundamental frequency. The waveform then exponentially grows until it reaches a limit cycle.

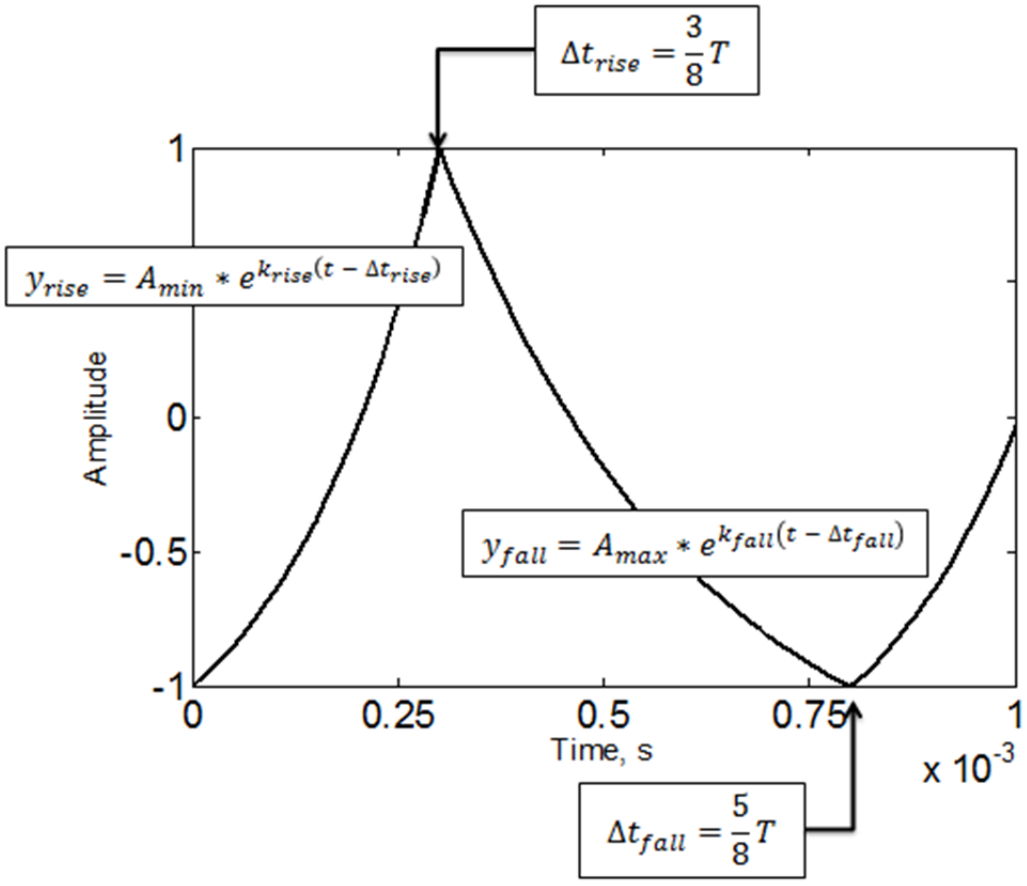

Figure 4.1 Design procedure for making steep-fronted waves.

This baseline study exhibited strong harmonics, shown in Figure 4.2b, for a single steep-fronted waveform while only the fundamental frequency was observed for a single sine waveform, shown in Figure 4.2a. These initial results prompted a more detailed investigation.

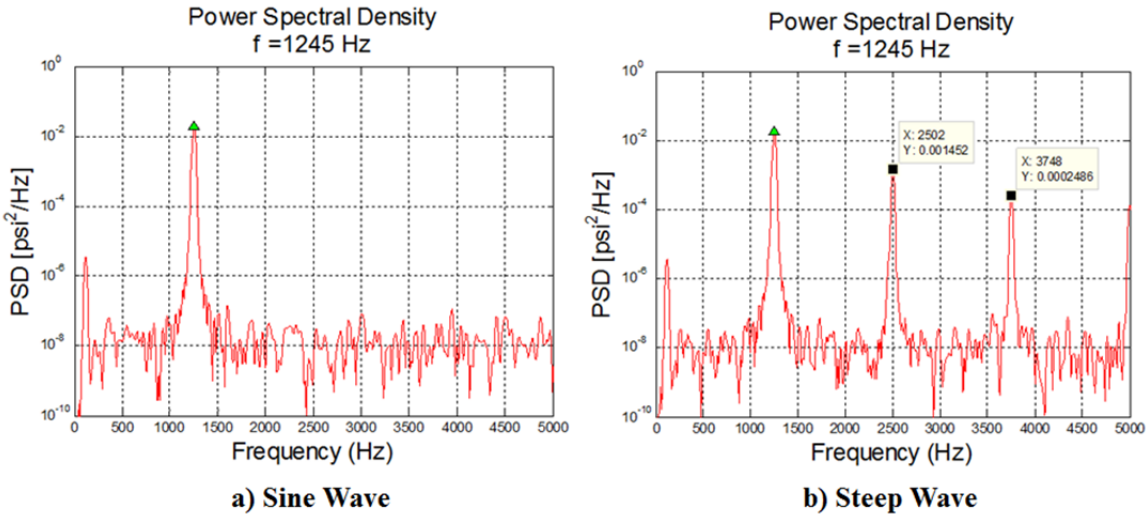

Figure 4.2 PSD results from manufactured signal analysis of a) sine waveform and b) steep-fronted waveform, both with $\Delta f = 6$ Hz.

4.1.2 Design

Five waveforms were manufactured to investigate how the traditional analysis would present the original signal for different variations of steep waves and sine waves with and without harmonics. Each manufactured waveform is then run through the same design process, illustrated in Figure 4.3. The signal begins to grow exponentially at a constant onset time of 0.05 s, overshoots at t_{max}, before exponentially decaying to the limit cycle amplitude by t_{limit} of 0.1 s. The growth and decay rates, α_1 and α_2, are determined by the value of t_{max}, as shown in Figure 4.3. In the cases presented, t_{max} occurs at 0.055 s for each manufactured signal.

This gives a growth rate of α_1=183.3 [1/s] and decay rate of α_2 = -10.2 [1/s] that are on the order of magnitude as observed experimentally. The growing and decaying signal is combined with a 10% noise level with high and low frequency content. Then the traditional analysis method put forth in Sec. 3.1 is applied to each manufactured signal.

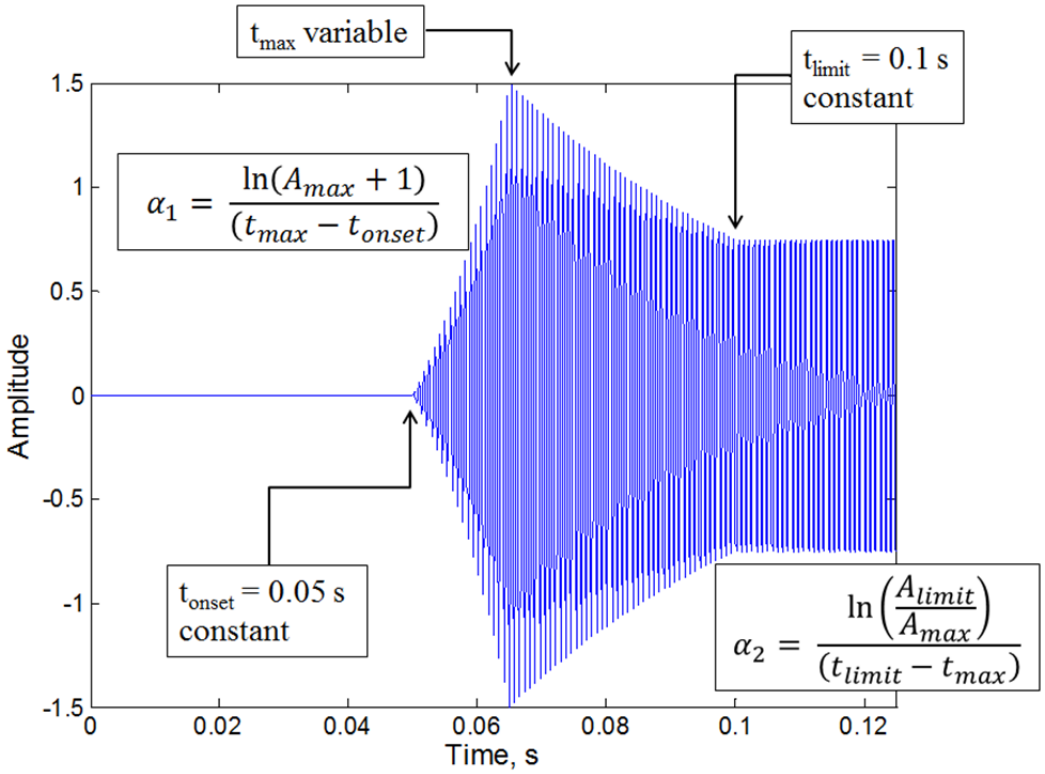

Figure 4.3 Design procedure of manufactured signal.

4.1.3 Comparison of Manufactured Signal Results

As previously described in Sec. 4.1.2, five signals were manufactured to investigate how the traditional analysis would interpret different variations of a steep wave versus a sine wave, with harmonics. The baseline waveform composed of a variation of steep and sine waves are processed through the same code to

create a signal like that shown in Figure 4.3. As best as possible, the waveforms are normalized and amplitude and phase differences are consistent between 1L and its harmonics based on empirical observations.

Several results to pay attention to are the frequencies and powers from the PSD plots, the calculated amplitude of each mode, and the calculated growth rate of each mode. In the case of signals without harmonic components, any harmonic frequencies shown are exclusively DSP artifacts. Regardless, the growth rate and onset time for each mode should be the same, since they make up components of a single waveform that grows and reaches limit cycle amplitude. Table 4.1 summarizes the design and results for the five signals.

Table 4.1 Overview of the five manufactured signals.

	1L	**Harmonics**	**Actual α**	**Calculated α**
Signal #1	Steep	N/A	183.3 [1/s]	272 [1/s]
Signal #2	Steep	1L Steep	183.3 [1/s]	277 [1/s]
Signal #3	Steep	2L and 3L Steep	183.3 [1/s]	272 [1/s]
Signal #4	Steep	2L and 3L Sine	183.3 [1/s]	330 [1/s]
Signal #5	Sine	2L – 7L Sine	183.3 [1/s]	285 [1/s]

4.1.3.1 Signal #1 Single Steep Wave

The common speculation is that the pressure waveform in longitudinal combustion instabilities is either a traveling shock-like wave (see Sec.2.3) or a compilation of harmonic sine waves (see Sec.2.2). A single steep wave is constructed based on experimental data, with an exponential rise time to maximum amplitude followed by an exponential fall to minimum amplitude as

discussed previously. The final signal with the growing waveform and system noise at both low and high frequencies is shown in Figure 4.4a. The traditional analysis presented in Sec. 3.1 is applied to the manufactured signal to yield the dominant frequencies as given by the PSD and the components of the signal as band pass filtered around the first three dominant frequencies.

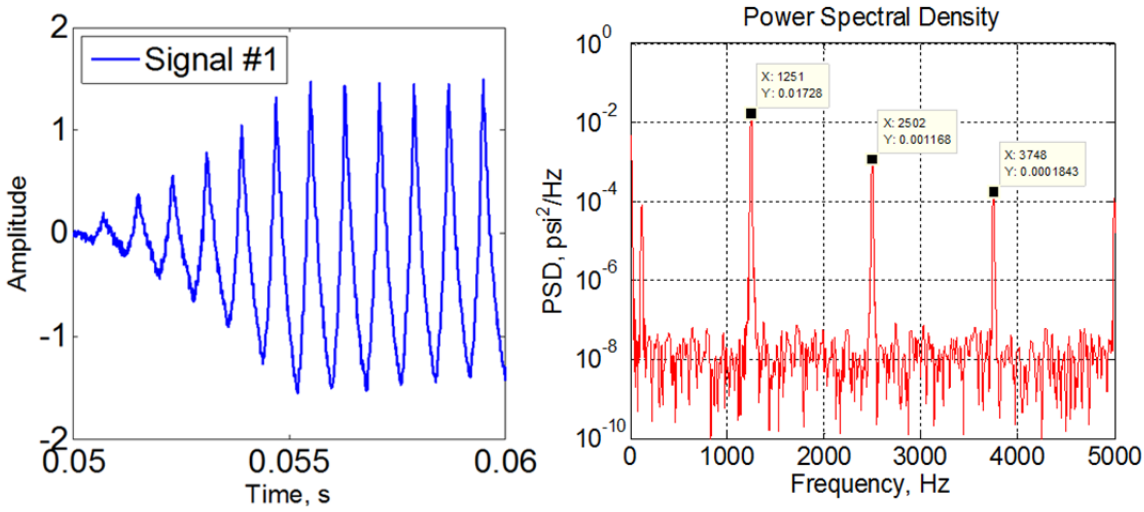

Figure 4.4 For a single steep-fronted wave, a) the manufactured signal and b) PSD showing the first three dominant modes detected, $\Delta f = 6$ Hz.

Figure 4.4b depicts the PSD results for Signal #1 which exhibit the presence of strong harmonics of decreasing intensity, though no harmonics are truly present in the original waveform. The results from the traditional analysis can be seen in Figure 4.5. What is concerning about these results is not only that strong harmonics appear, but also that the relative amplitude for the first three frequencies is similar to that seen in experimental results.

Figure 4.5a displays the components of the composite waveform, which in the case of Signal #1 is simply a single steep-fronted wave at 1250 Hz. Figure 4.5b, c, and d show the results from the traditional analysis for the first three frequencies

detected on the PSD in Figure 4.4b, which in this case corresponds to 1L and two artificial harmonic modes. All three analyses approximately show the true time of onset (constant at 0.05 s) and reach maximum amplitude at approximately the right time (in these cases, 0.055 s).

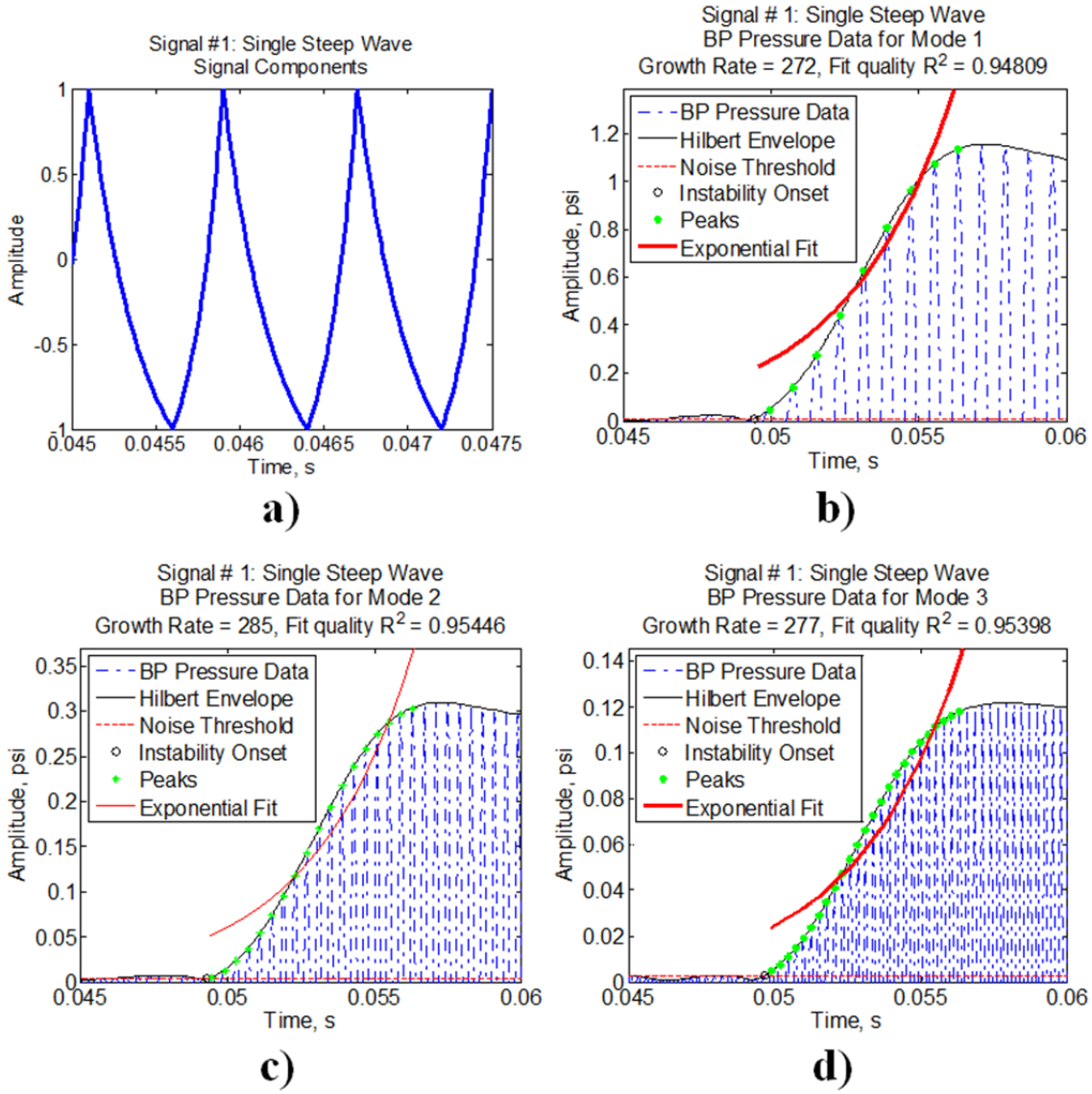

Figure 4.5 For a single steep-fronted wave, a) waveform components and traditional analysis results of calculated b) 1L, c) 2L, and d) 3L.

It is also important to note that all three calculate a similar growth rate, since there are not multiple signals with multiple growth rates. Interestingly, though the signal was subject to a purely exponential growth from 0.05 s to 0.055 s, the analysis is unable to correctly capture this behavior and overpredicts the growth rate, illustrated in Table 4.1.

4.1.3.2 Signal #2 Several Steep Waves

The work in Sec. 4.1.3.1 legitimizes any concern that the harmonics observed in the CVRC to date may in fact be Fourier artifacts. However, Signal #1 does not accurately reflect the steep-fronted pressure oscillations seen in the CVRC data. Figure 4.7 is a sample of the unfiltered pressure data for reference, where small-amplitude peaks can be seen out of phase with the primary waveform.

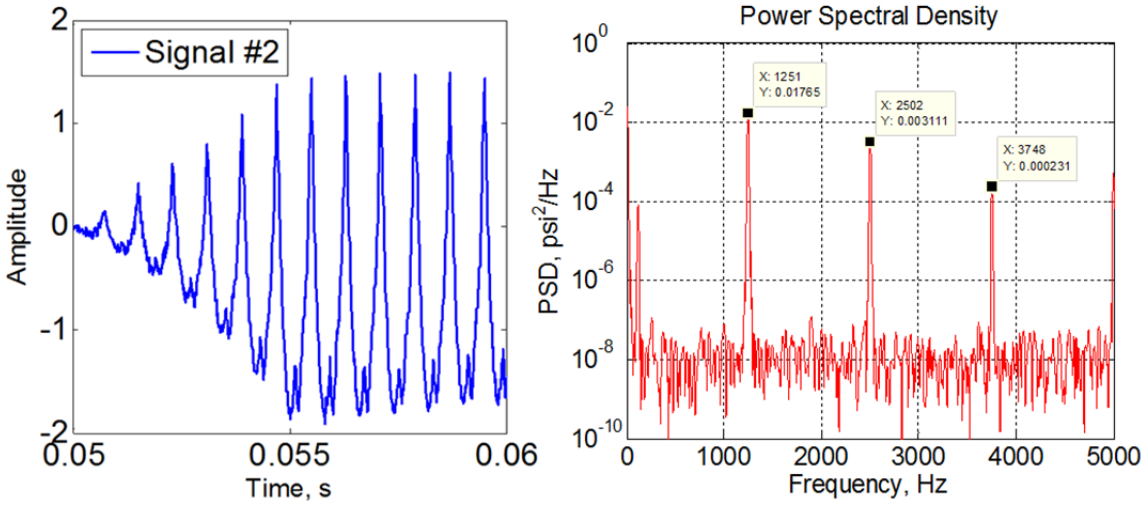

Figure 4.6 For several steep-fronted waves, a) the manufactured signal and b) PSD showing the first three dominant modes detected, $\Delta f = 6$ Hz.

Because of this, three steep-fronted waves at the 1L frequency of 1250 Hz were combined, with the second and third waves having amplitudes and phases

based on experimental observations from the CVRC. For a 1L amplitude of 1, the second wave's amplitude is then 0.35 and the third's is 0.2. These values are later used in Signals #3-5 for the relative amplitudes of 2L and 3L, respectively. The final signal with the composite steep-fronted waves is shown in Figure 4.6a, while the waveform components are illustrated in Figure 4.8a for reference.

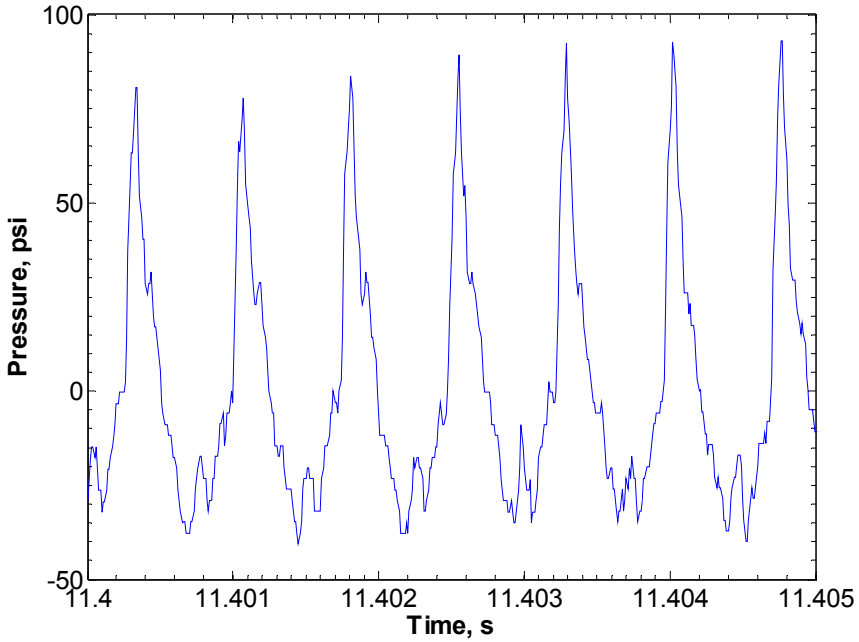

Figure 4.7 Sample from an unstable fixed test of unfiltered pressure data during limit cycle instability.

Compare the spectral intensities calculated for Signal #1 and Signal #2 in Figure 4.4 and Figure 4.6. The calculated intensity for the artificial 2L increases along with its apparent growth rate and amplitude, shown in Figure 4.8c. However, the extracted 1L and artificial 3L are largely unaffected by the additional out-of-

phase steep waves. This can also be seen when comparing Figure 4.5b with Figure 4.8b.

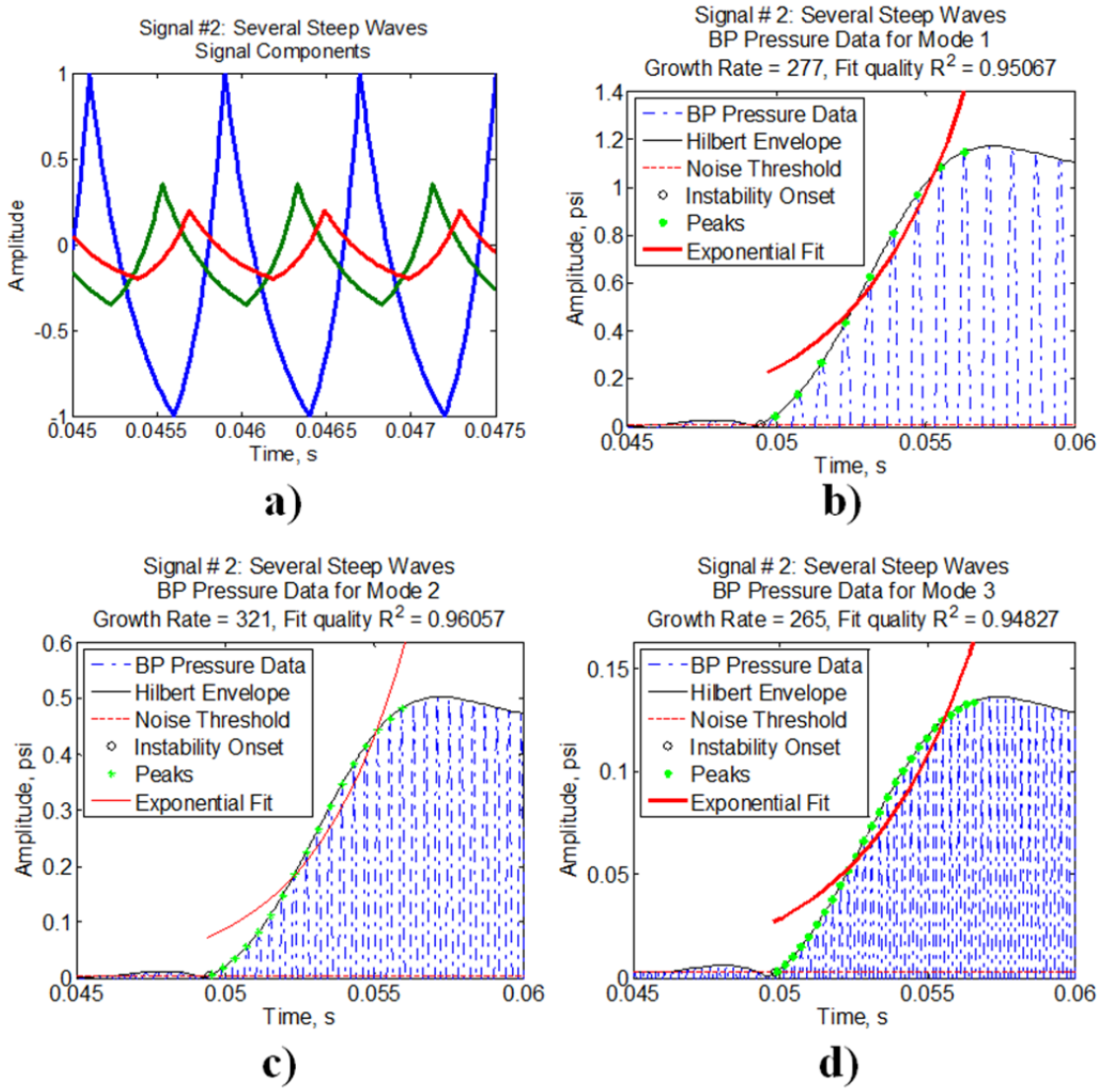

Figure 4.8 For several steep-fronted wave, a) waveform components and traditional analysis results of calculated b) 1L, c) 2L, and d) 3L.

4.1.3.3 Signal #3 Steep 1L with Steep Harmonics

Tsuji and Takeno in their work with longitudinal combustion instability, discussed in Sec. 2.3, experimentally observed a traveling shock-like wave at the fundamental frequency accompanied by traveling shock-like waves at harmonic frequencies [17]. Signal #3 works from these findings, with a steep-fronted wave at the 1L frequency of 1250 Hz combined with a steep-fronted wave at the 2L frequency of 2500 Hz and a steep-fronted wave at the 3L frequency of 3750 Hz. As in Signal #2, the amplitudes and phases of the 2L and 3L waves relative to the 1L wave are based on experimental observations from the CVRC.

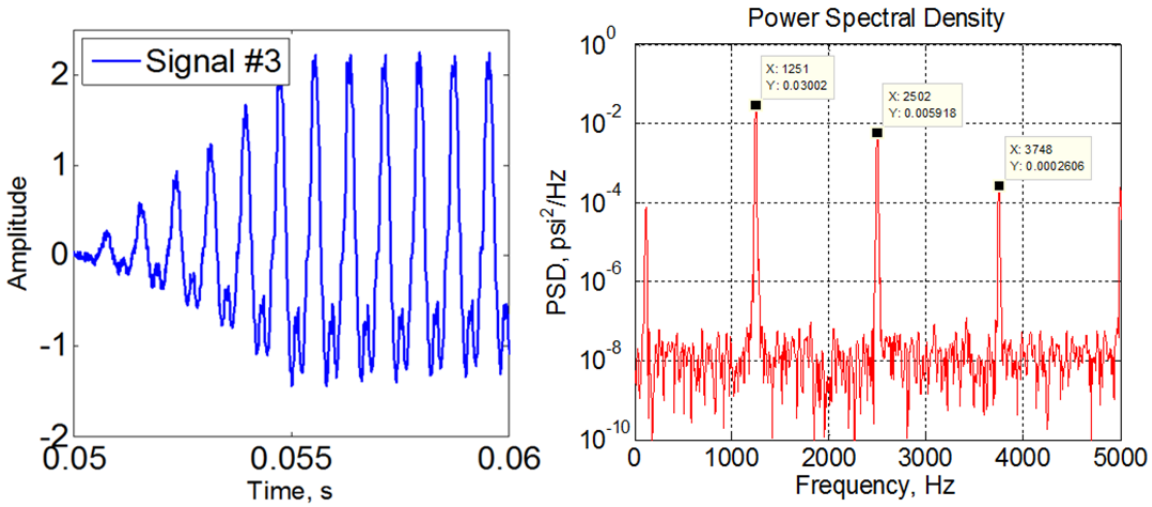

Figure 4.9 For a steep-fronted wave with steep-fronted harmonics, a) the manufactured signal and b) PSD showing the first three dominant modes detected, $\Delta f = 6$ Hz.

Figure 4.9a shows the final manufactured signal and Figure 4.10a shows the components of the waveform for reference. Any difference in amplitude between Signal #3 and the other manufactured signals is due to the normalization process

used on each waveform, so amplitude values from other signals should not be directly compared here.

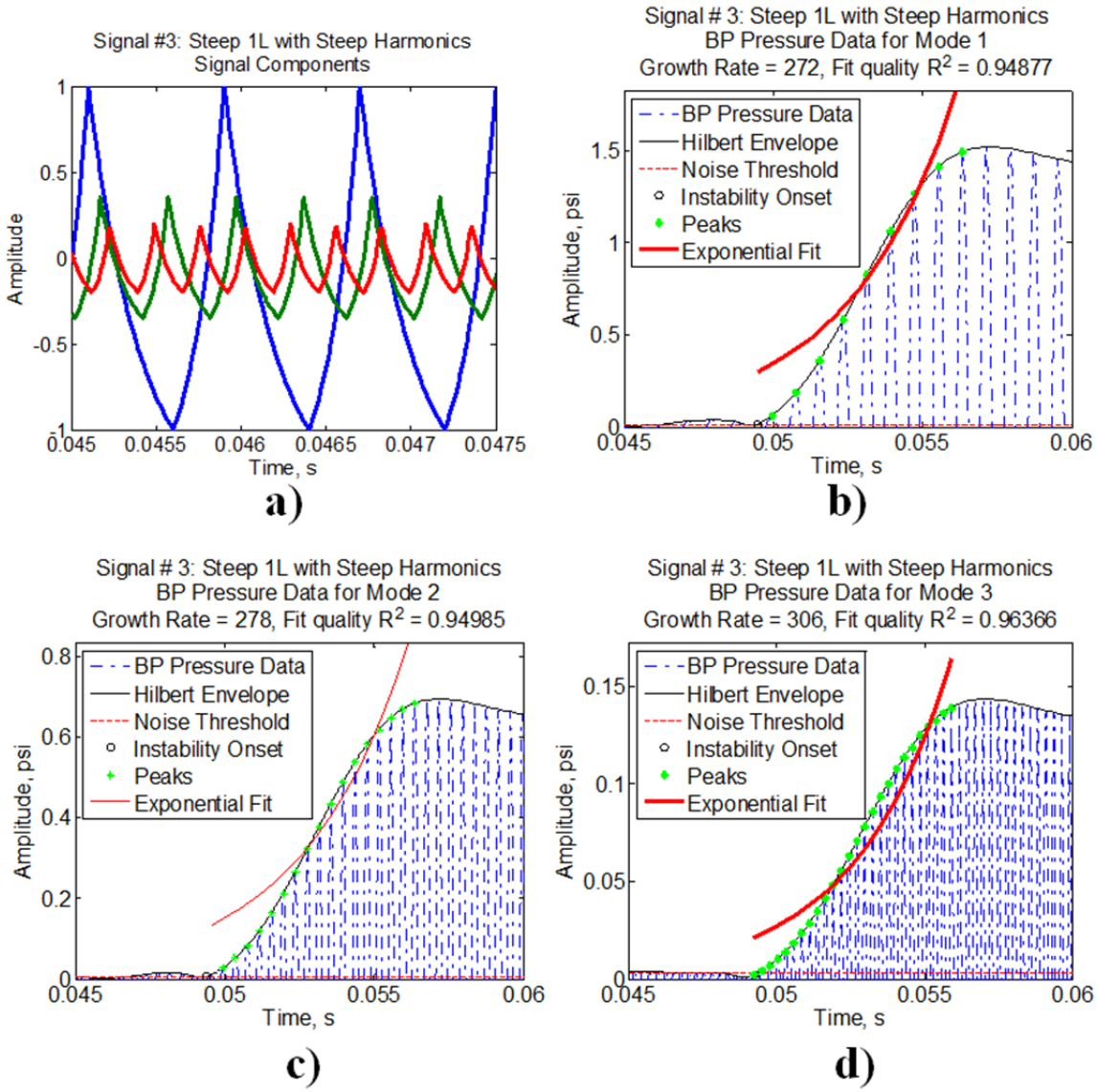

Figure 4.10 For a steep-fronted wave with steep-fronted harmonics, a) waveform components and traditional analysis results of calculated b) 1L, c) 2L, and d) 3L.

Again, looking at Figure 4.10, the traditional analysis is able to correctly approximate the onset time for all three modes, though the time to maximum

amplitude is incorrect, possibly indicating a slow response from the Butterworth filter. The growth rates are consistent with previous results, with the exception of 3L, which calculates a faster modal growth.

4.1.3.4 Signal #4 Steep 1L with Sine Harmonics

Zinn and Lores in their work on establishing a nonlinear model for axial combustion instability problems raise the idea that while 1L may be discontinuous, this does not necessarily preclude the harmonic mode(s) from being continuous [28].

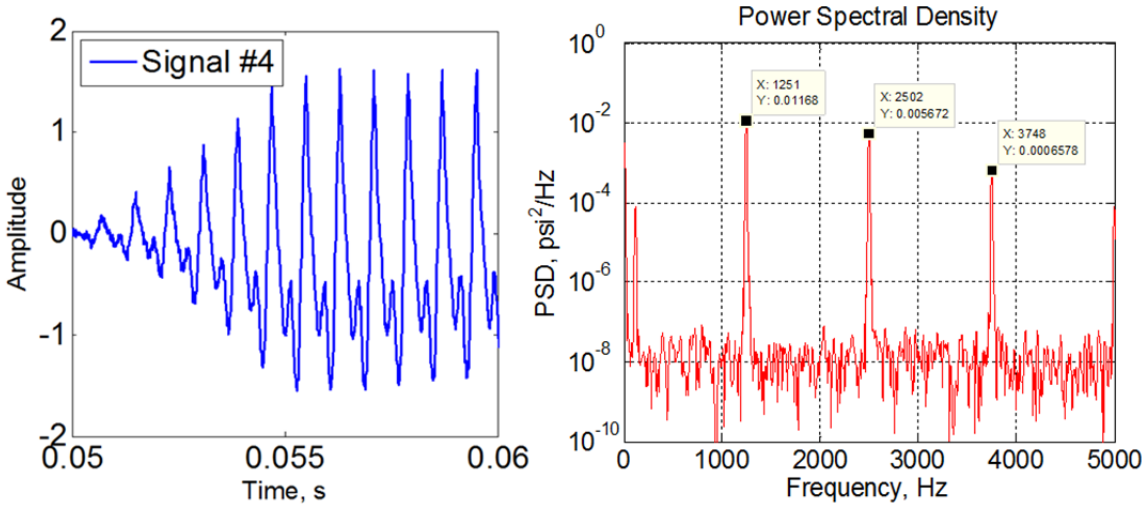

Figure 4.11 For a steep-fronted wave with sine harmonics, a) manufactured signal and b) PSD showing the first three dominant modes detected, $\Delta f = 6$ Hz.

Though their work largely supports the shock-like wave theory (see Sec. 2.3), it introduces an interesting possibility. From this, the waveform in Signal #4 was developed, using a steep-fronted wave at 1L frequency of 1250 Hz combined with a sine wave at 2L frequency of 2500 Hz and a sine wave at 3L frequency of 3750 Hz. Again, the amplitudes and phases of the 2L and 3L waves relative to the 1L wave

are based on experimental observations from the CVRC. The resultant manufactured wave for Signal #4 is shown in Figure 4.11a.

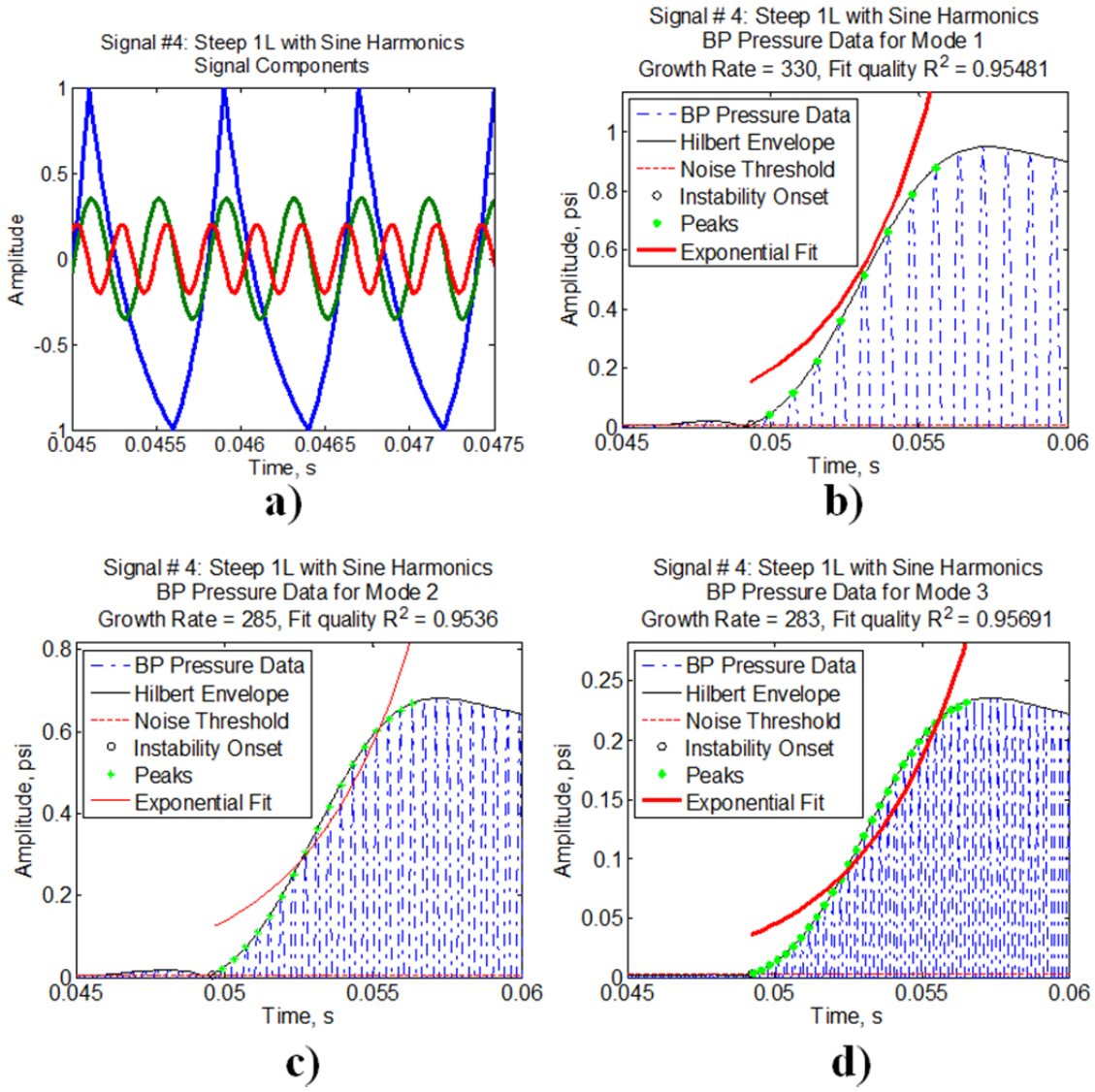

Figure 4.12 For a steep-fronted wave with sine harmonics, a) waveform components and traditional analysis results of calculated b) 1L, c) 2L, and d) 3L.

Several observations can be made from the results for Signal #4 in Figure 4.12. First, this is the first manufactured signal in which the traditional analysis is

able to more accurately determine the amplitude of 3L, as shown in Figure 4.12d. This raises the possibility that an effect of artificial modal information may be the underrepresentation of higher modal amplitudes. The limit cycle amplitude of 1L shown in Figure 4.12b is below the expected value of 0.95, with a calculated growth rate nearly double the actual value.

Finally, the amplitude of 2L shown in Figure 4.12c is nearly double the expected value of 0.33, which may indicate that signal components most likely intended for 1L or 3L have been contributed to 2L. These results are the least like those from experimental data overall, despite the more accurate representation of the contribution from 3L.

4.1.3.5 Signal #5 Sine 1L with Sine Harmonics

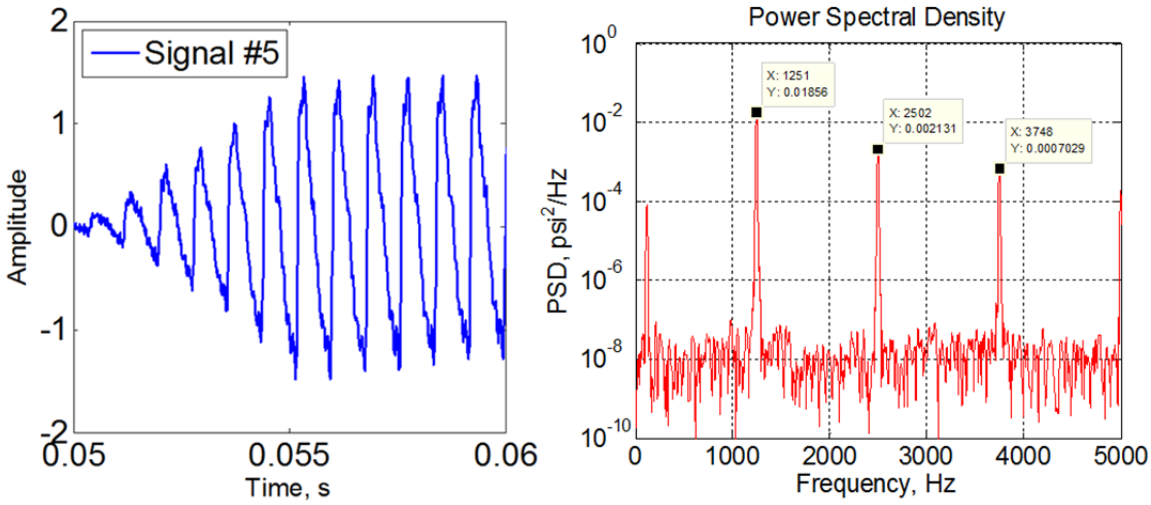

Figure 4.13 For a sine wave with sine harmonics, a) the manufactured signal and b) PSD showing the first three dominant modes detected, $\Delta f = 6$ Hz.

The acoustic wave theory, presented in Sec. 2.2, assumes the steep-fronted pressure oscillations observed during limit cycle are due to the sinusoidal harmonic modes that are excited. Signal #5 represents this idea, with a sinusoidal wave at the 1L frequency of 1250 Hz combined with sine waves up to 7L.

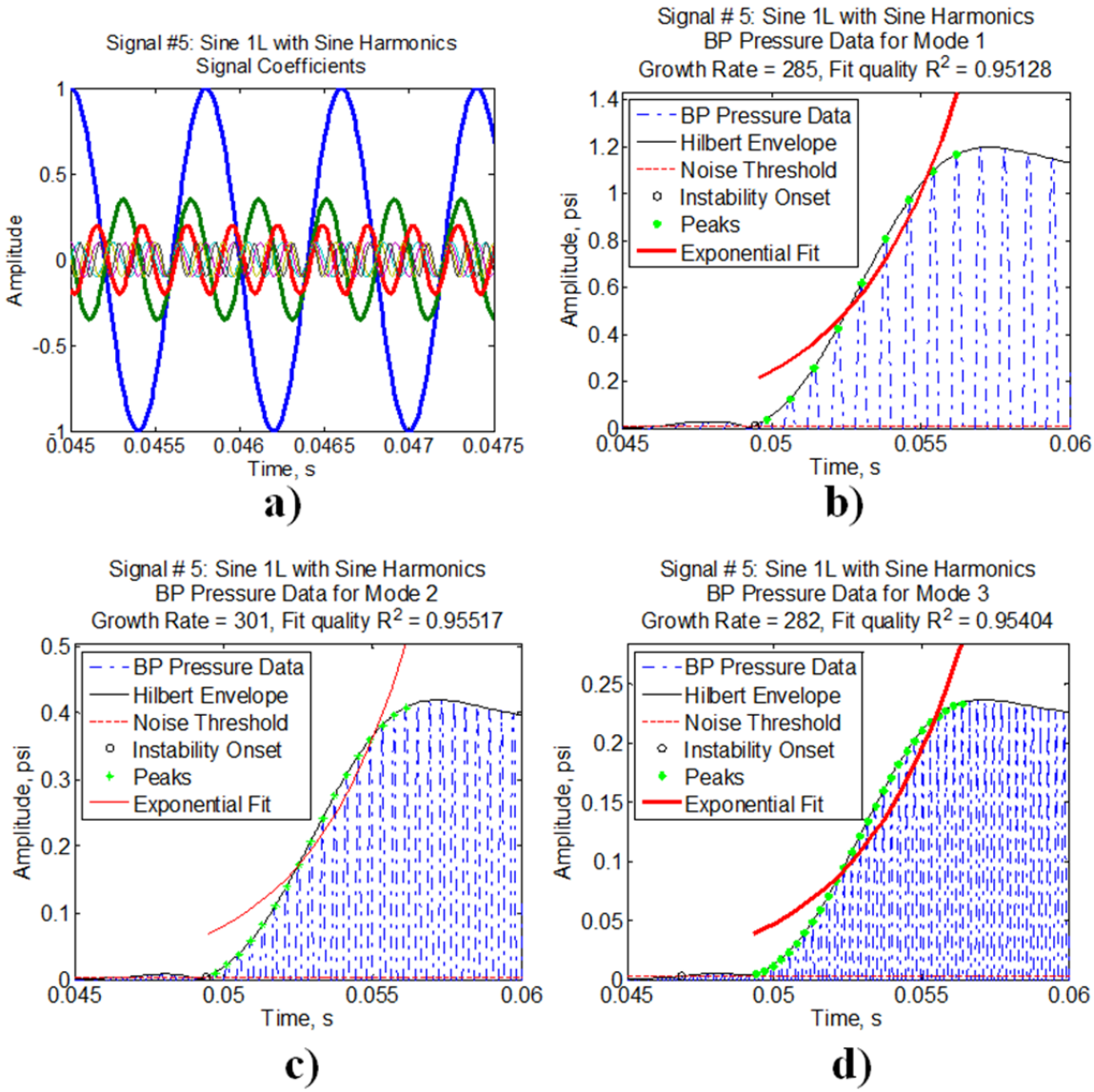

Figure 4.14 For a sine wave with sine harmonics, a) waveform components and traditional analysis results of calculated b) 1L. c) 2L, and d) 3L.

Again, the amplitudes and phases of the 2L and 3L waves relative to the 1L wave are based on experimental observations from the CVRC while the higher harmonics are assumed to be in phase with 1L with 10% relative amplitude, as seen in Figure 4.14a.

The results from the traditional analysis seen in Figure 4.14 show a good agreement between calculated growth rates for 1L, 2L, and 3L as expected, though again the calculated growth rate is much higher than the actual growth rate used to manufacture the composite signal. Additionally, the relative amplitudes of the modes agree well with experimental observations, yet that is to be expected as Signal #5 is best suited to Fourier-based analysis. However, the issue remains that the results from the traditional analysis method are markedly similar for Signal #1, a single steep-fronted wave, and Signal #5, a sine wave with sinusoidal harmonic waves.

4.1.3.6 Summary

Sections 4.1.3.1 to 4.1.3.5 present results from the traditional analysis method outlined in Sec. 3.1 for five manufactured signals. One conclusion from this work is that significantly different growth rates for each mode may be contributed to that mode's transient behavior. If the harmonic content in experimental results was only an artifact of a steep-fronted 1L, the calculated growth rates would appear to be very similar. In addition, a pattern was observed in Sec. 3.1.5 of an increasing growth rate with increasing mode number. Even in the results that display dissimilar growth rates, such as for Signal #4, no such pattern exists in the manufactured signals. Furthermore, Sec. 3.1.5 also exhibits a pattern of sequential excitation of modes (i.e. 1L precedes 2L which precedes 3L). As depicted in Figure

4.15, no such pattern is seen in any of the manufactured signals analyzed. This too supports the idea that the transient behavior observed is not solely a product of Fourier analytical errors.

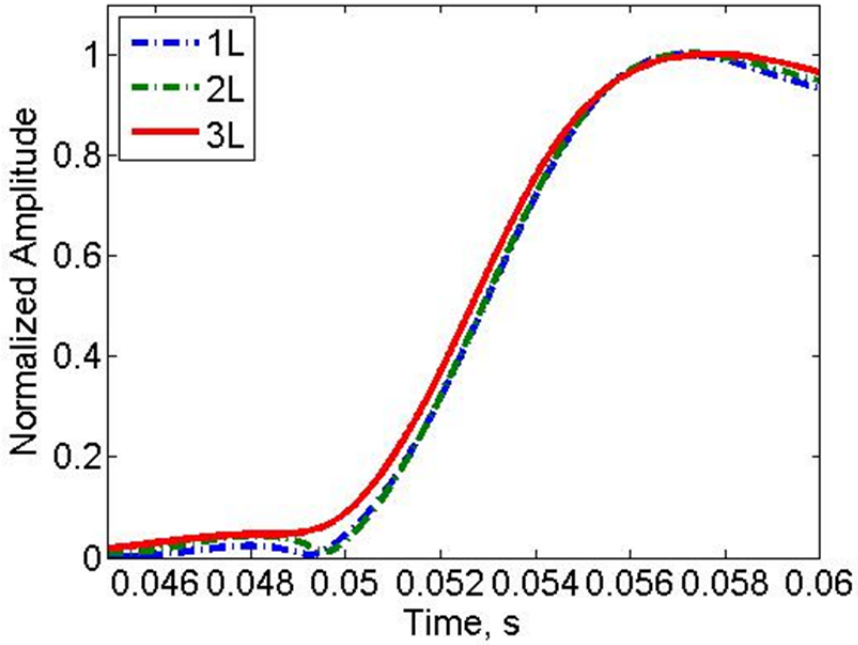

Figure 4.15 Example of artificial harmonic behavior relative to the real signal.

However, as mentioned in Sec. 4.1.3.5, in terms of amplitude and intensity of harmonic modes, the results of Signal #1, a single steep-fronted wave, are qualitatively indistinguishable from the results of Signal #5, a sine wave with sinusoidal harmonic waves. This means that while some of the qualitative characteristics observed from traditional analysis are authentic, this method is unable to properly separate extant harmonic modal behavior from DSP artifacts. So while the traditional Fourier-based method is useful in the study of unstable combustion characteristics, it alone may not fully capture the dynamic behavior in the experiment.

4.2 PC Signal Analysis, Revisited

The IF analysis from the software package PC Signal Analysis provides initial results that agree with traditional analysis for the fundamental frequency but disagree for the harmonic frequencies, as illustrated in Sec. 3.2.4.1. From the initial results, it appears that a significant time lag (on the order of 100 ms) exists between the true onset of 1L and its subsequent harmonics. If the results from IF Analysis prove to be valid, this may be a viable method to distinguish DSP artifacts from true modal signal.

4.2.1 Application to Experimental Data

The discrepancy between the results from traditional analysis and the IF Analysis is unexpected. As previously discussed, the software PC Signal Analysis does not offer user guides or manuals for IF Analysis, so many settings were found in a trial and error method or based on previous analytical work. However, because of the inconsistency in calculated transient modal behavior, these settings were reevaluated. The IF Analysis presented here represents a Finite Impulse Response (FIR) filter, and the difference between results in the transient region may be due to filter order. To further investigate this, the unstable fixed test case is processed with IF Analysis again, this time with a filter order lower than the pass band width. The effect of the filter order is illustrated in Figure 4.16, where the original results from Sec. 3.2.4 are shown in Figure 4.16a and results with a lower filter order are shown in Figure 4.16b. The lower filter order is better able to capture the transient modal behavior. This may be due to the number of data points needed by higher filter orders.

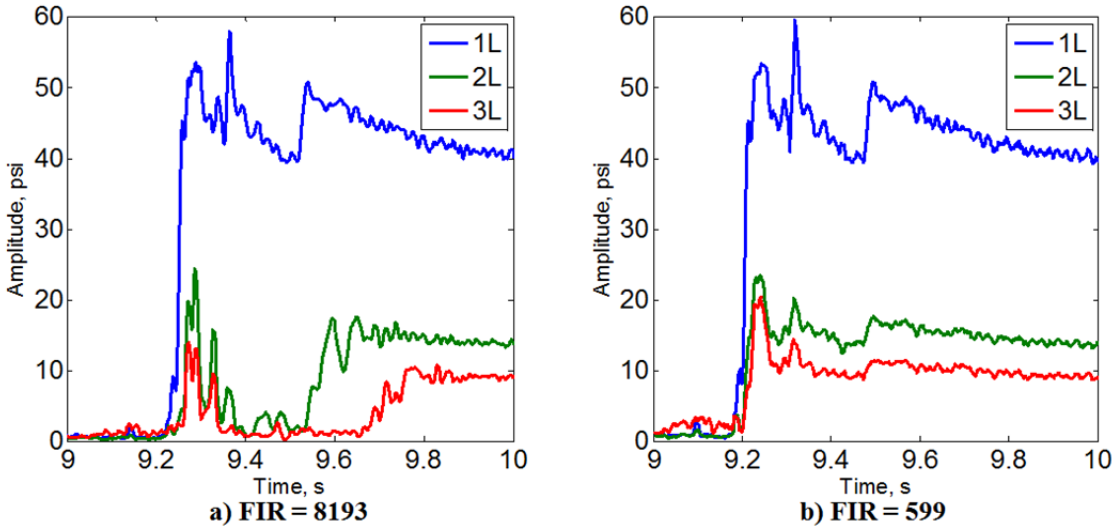

Figure 4.16 For unstable fixed test MSFC3, IF Analysis of 1L, 2L, and 3L at settings a) FIR order = 8193 and b) FIR order = 599 .

Since the results in Figure 4.16b are consistent with results from traditional Fourier-based analysis in Sec. 3.1.5, three other unstable fixed tests were processed through PC Signal's IF Analysis to determine whether or not this behavior is consistent across test cases or if the original results in Sec. 3.2.4 are more accurate. The test cases here come from two separate test series and have slightly different configurations, with MSFC tests at Lop = 5.1 in and VIB tests at Lop = 5.85 in. All results are taken from the 14.5 in PT location.

Figure 4.17 demonstrates that the other unstable fixed tests from the two test series did not show any remarkable difference between times of onset for the first three modes. For all unstable fixed tests considered, results from PC Signal Analysis's IF Analysis are comparable to traditional analytical results when the FIR filter order is smaller than the pass band.

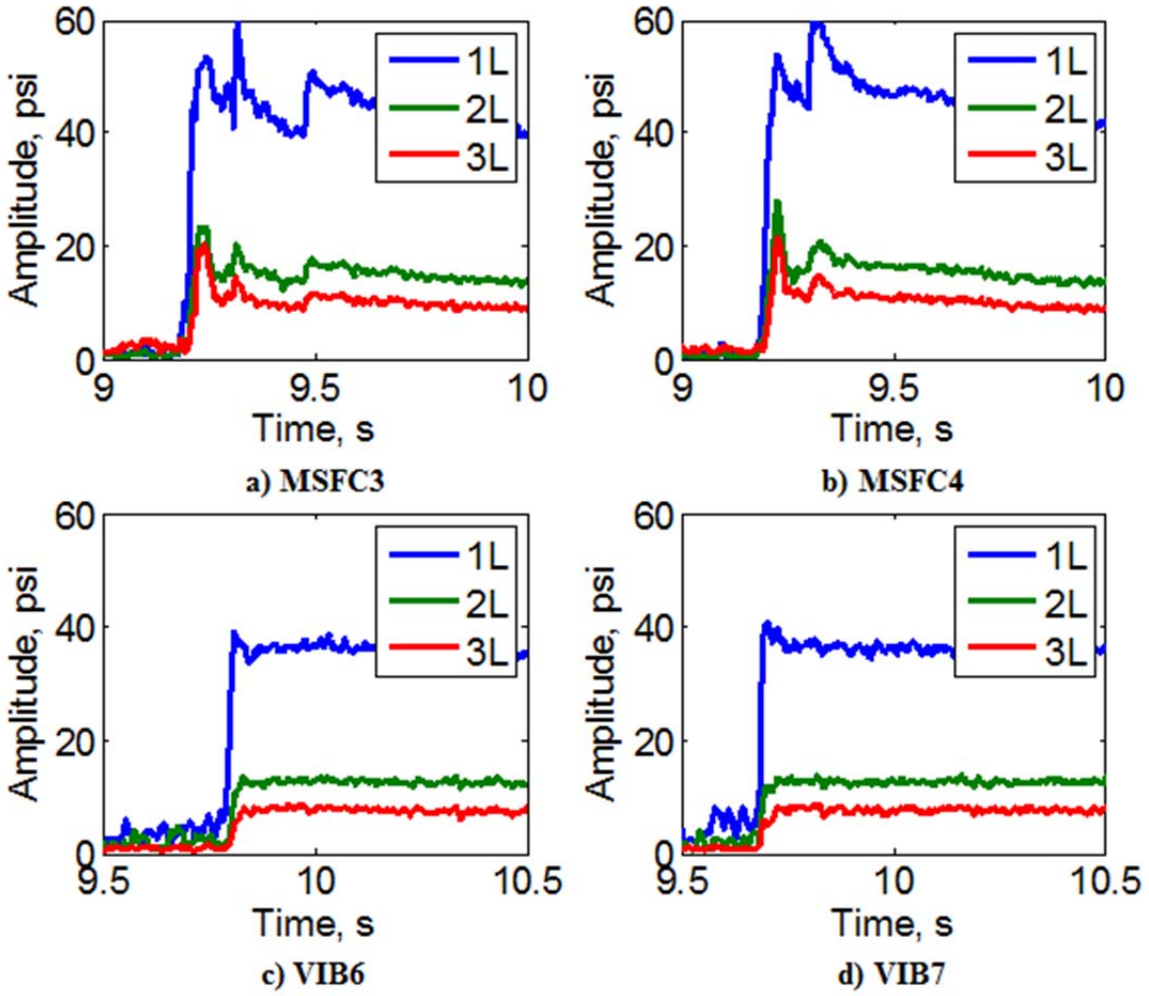

Figure 4.17 IF Analysis of 1L, 2L, and 3L for four unstable fixed tests.

One of the considerations important for the translating tests is the pass band width. In the fixed test cases, the modal frequencies do not change significantly, so a pass band width of 200 Hz is more than sufficient. However, in the translating test cases, the frequencies of the higher modes change significantly as the internal geometry changes, as previously shown in Figure 3.2. For example, the 3L frequency changes from 3900 Hz up to 4400 Hz, seen in Figure 4.21. Because of this, the pass band width requirement increases, so results presented

have a 600 Hz pass band width to properly capture the modal behavior as a function of time and geometry.

Further investigations into several translating tests across test series showed consistent behavior for translating tests as well, with an indiscernible time lag between the excitation of the first three modes and a noticeable time lag between the first three modes as each mode decays from higher mode to lower mode. Seen in Figure 4.18, as the internal geometry changes to an unstable condition, the modes are excited in rapid succession. Then, as the internal geometry transitions to a stable condition, the modes decay in reverse order until a marginally stable limit cycle behavior is reached. Once marginally stable combustion is achieved, the system acts more as a two-mode system with 1L and 2L, supporting Yu's original findings reviewed in Sec. 1.2.3 [20].

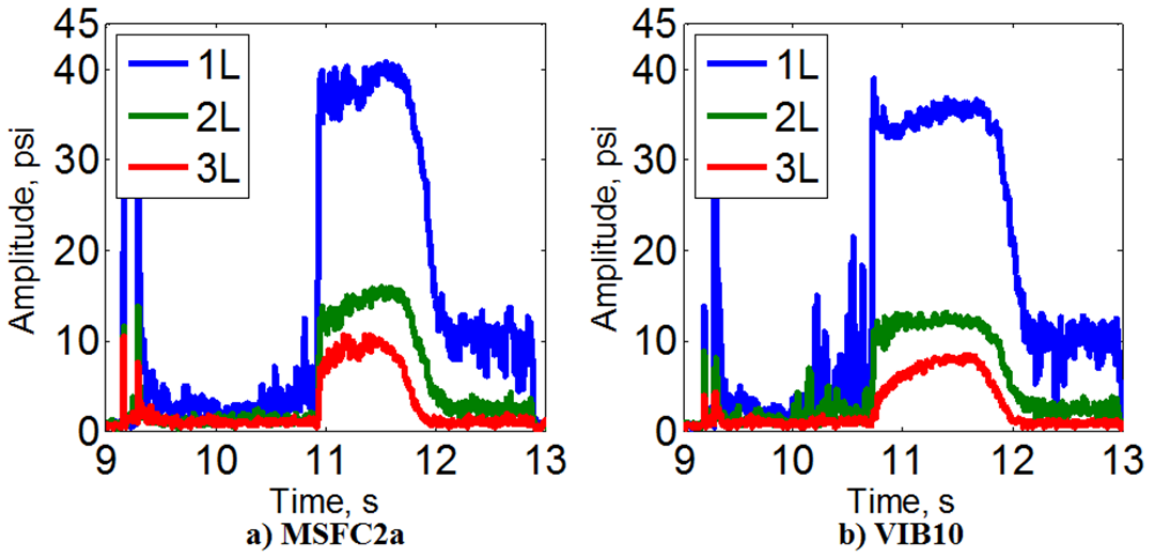

Figure 4.18 IF Analysis of 1L, 2L, and 3L for two translating tests.

Finally, in Sec. 3.2.4.2 and 3.2.4.3, frequency and phase tracking from IF Analysis were explored in an attempt to find alternative indicators of the onset of

unstable combustion besides modal amplitude. As applied to test case MSFC3, there appears to be a qualitative relationship between the increasing amplitude and coherence of the signal at each modal frequency, with a decreasing variance in frequency tied to increasing oscillation amplitude. To continue investigating possible connections between frequency coherence and the excitation of modes, IF Analysis looking at the frequency, amplitude, and phase was performed on the translating test case MSFC2a for the first three modes. The summary of these results for the first three modes are shown in Figure 4.19, Figure 4.20, and Figure 4.21 with the objective of establishing potential relationships between the frequency, amplitude, and/or phase within in each mode. As previously mentioned, the results for the translating test from IF Analysis have a 600 Hz pass band and FIR filter order of 599.

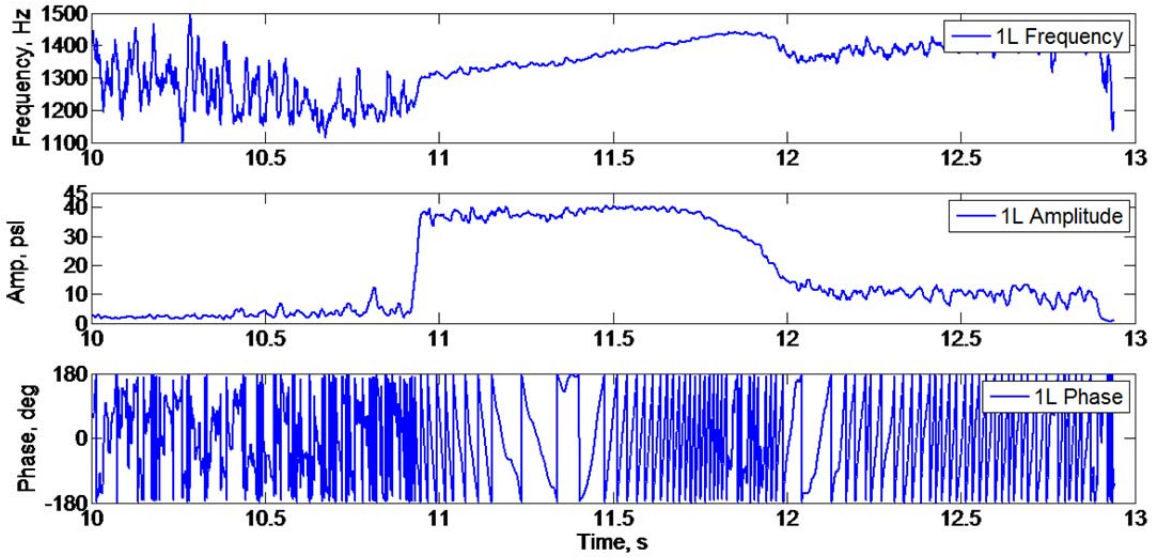

Figure 4.19 Summary of PC Signal Analysis results of 1L for a translating test.

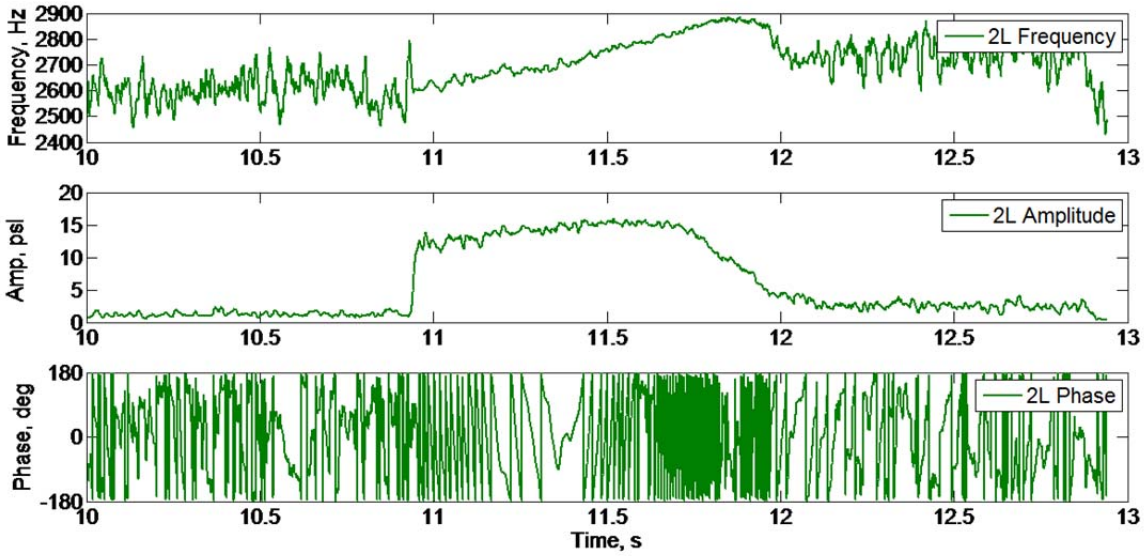

Figure 4.20 Summary of PC Signal Analysis results of 2L for a translating test.

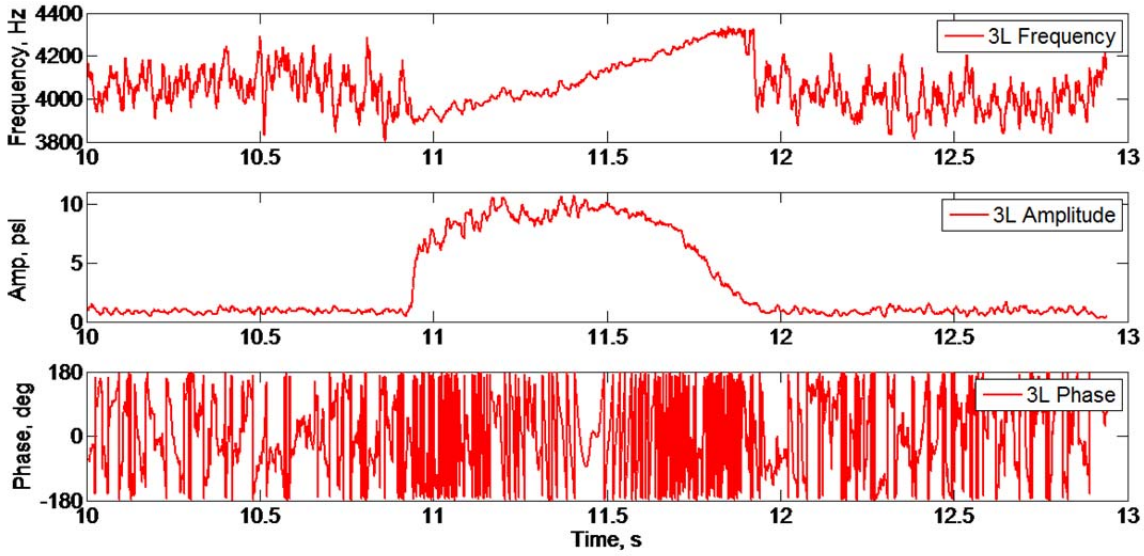

Figure 4.21 Summary of PC Signal Analysis results of 3L for a translating test.

Again, while the results from IF Analysis appear to provide the same qualitative information based on frequency coherence and oscillation amplitude,

these results does not provide a viable quantitative method to establish the time of onset for each mode. Additionally, the phase tracking does not provide useful information for the current study. It is worth reiterating that the results obtained from the IF Analysis for the frequency and phase far exceed those from Matlab's Hilbert function, demonstrating yet again the advantage PC Signal Analysis has when handling experimental data.

4.3 Comparison of Filter Types

The traditional analysis presented in Sec. 3.1 builds off work done by Sisco [4], Feldman [22], and Hardi et al. [59], utilizing a custom Butterworth filter to digitally separate the data into spectral components. However, as Sisco said, the Butterworth filter is most appropriate when the limit cycle amplitude is of most interest, as it has a maximally flat pass band but a slow "roll-off", and it may not respond quickly enough when studying the transition region, as is done in the current study. To investigate the effect of filter type, three digital IIR filters and the results from IF Analysis are compared using both experimental data and the manufactured signals laid out in Sec. 4.1.3.

4.3.1 Overview of Digital Filters

There are two main classifications for filters: infinite impulse response (IIR) and finite impulse response (FIR), with FIR filters used in IF Analysis and IIR filters used in traditional Fourier-based analysis [51]. There are several types of IIR filters that are optimized for application, based on emphasis placed on the pass band or stop band, as previously mentioned in Sec. 3.1.2. There are several classic filter types, including Butterworth, Chebyshev Types I and II, and Elliptic.

Butterworth and Chebyshev Types I and II are compared and applied to the experimental data and manufactured signals to evaluate applicability in this study. More information on digital filter design can be found in Ref. [49–51].

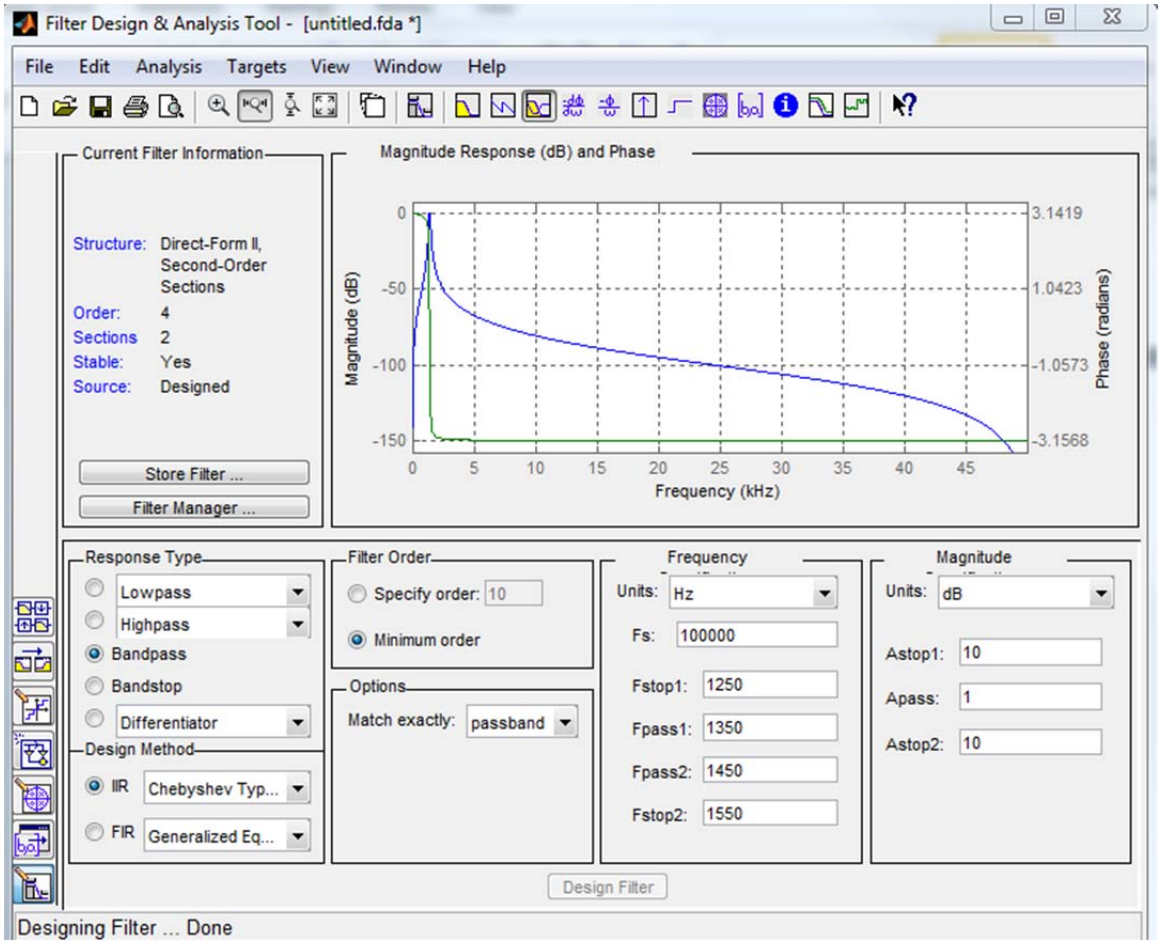

Figure 4.22 User interface of Matlab's Filter Design and Analysis toolbox.

Matlab offers a Filter Design and Analysis (FDA) toolbox, the interface of which is shown in Figure 4.22. The GUI designs the lowest order filter to meet the input requirements. It allows for analysis of the filter response in terms characteristics such as group delay (time delay as a function of frequency), phase response, and magnitude of the filter as a function of frequency [50]. For a band pass IIR filter, users have the option to match exactly the pass band or the stop

band, though this specification appears to only affect the filter design for a Chebyshev Type II filter by adding a slight DC offset to the filtered data. Pass bands in this study have a 600 Hz width centered on the modal frequency and stop bands have a 100 Hz width on either side of the pass band. Allowable ripple in the pass band is restricted to 1 dB while allowable ripple in the stop band is restricted to 10 dB. For each filter design, the only input changed on the FDA tool was the IIR Design Method (filter type).

4.3.1.1 Butterworth Filter

The Butterworth filter type is frequently used, especially in the study of combustion instabilities, for its maximally flat response. This allows for the study of the quantitative behavior of each mode of interest. Sisco specifically chose a Butterworth-type filter to process previous experimental data as his main interest was limit-cycle behavior as opposed to Rosen's more qualitative study of the transition region (see Sec. 1.2) [4,21]. It may not be suitable when the time-varying behavior of the signal is of more interest, as the Butterworth filter has a slow "roll-off" and does not respond quickly to amplitude changes. General filter characteristics for the Butterworth filter type can be seen in Figure 4.23a.

4.3.1.2 Chebyshev Filter

The Chebyshev filter is similar to the Butterworth filter with some notable exceptions. The Chebyshev filter has a faster response than the Butterworth filter and can often use a lower filter order to achieve the same design objectives, which decreases the computational cost [51]. There are two types of Chebyshev filter: Type I minimizes the absolute difference between the ideal and actual frequency

response over the entire pass band by equally distributing the allowable pass band ripple Rp, creating a maximally flat stop band response [50]. Type II is the exact opposite, as it equally distributes the allowable stop band ripple Rs to create a maximally flat pass band response [50]. The key characteristic differences between a Butterworth, Chebyshev Type I, and Chebyshev Type II are qualitatively illustrated in Figure 4.23. In this study, the transition from pass band to stop band, a major characteristic difference between Butterworth and Chebyshev filters, may be important.

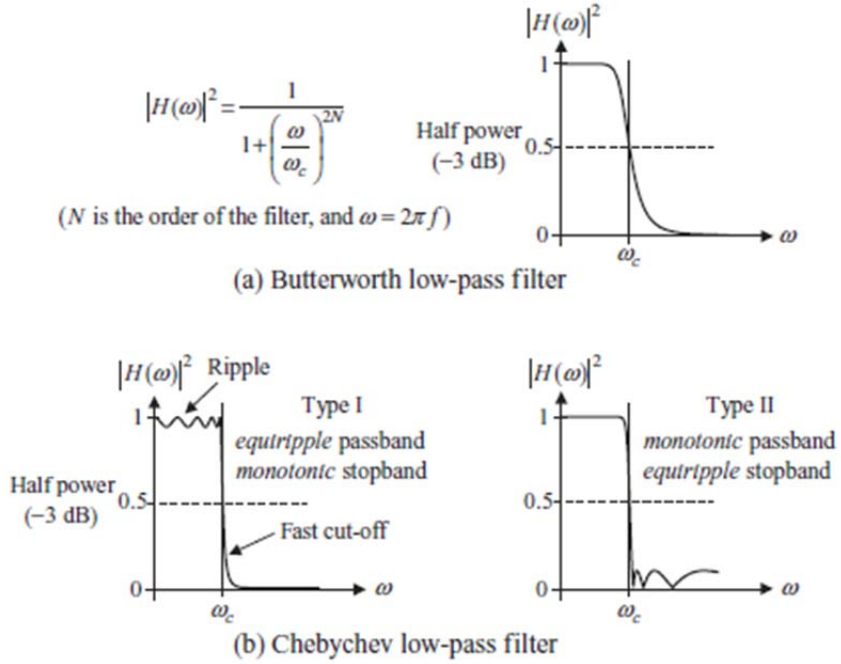

Figure 4.23 Filter characteristics for a) Butterworth type and b) Chebyshev Types I and II. [49]

4.3.2 Application to Manufactured Signals

The five manufactured signals from Sec. 4.1.3 are analyzed to perform side by side comparisons of the three IIR filter types of interest along with the FIR-

based IF Analysis in PC Signal Analysis. Each signal is subject to the same filter (or program setting); that is, the design characteristics for each filter type do not change between signals. The IIR filters have a 600 Hz pass band width, 100 Hz stop band width, 1 dB allowable ripple in the pass band, and 10 dB allowable ripple in the stop band. The FIR-based IF Analysis has a 600 Hz pass band width, 599 FIR filter order, and decimation value of 32.

The objective when comparing these filter types using the manufactured signals is to determine which filter(s) are able to best capture the transient behavior of the signal as well as the limit cycle amplitude, though the transient behavior is more important. Figure 4.24 and Figure 4.25 include an overlay of the final manufactured signal. Since some of the signals have real harmonics of non-negligible amplitudes, the displayed amplitude for the filtered 1L results will not match the total amplitude of the signal.

Figure 4.24 presents the results for Signal #1, a single steep-fronted wave. It appears that PC Signal Analysis' results are the least able to capture the transient behavior of the signal, while the Butterworth filter and Chebyshev Type II filter offer comparable results both for the transient behavior and the total amplitude. The Chebyshev Type I filter also does a better job at reproducing the transient behavior than PC Signal Analysis, but the limit cycle amplitude does not agree with the other filter types' results and as expected provides a lower amplitude value. On closer inspection, it was found that the transient behavior and limit cycle amplitude calculated by three of the filter options corresponds to the amplitude of an equivalent sine wave.

The results for Signals #2-4 are visually indistinguishable from Signal #1. In all cases, the Butterworth type and Chebyshev Type II were most able to

capture the transient behavior of the manufactured signal, though none fully exemplified the transient behavior of a steep-fronted 1L. This is most likely due to the same reason the resultant amplitude does not reflect the original amplitude, as the Fourier-based methods calculate the maximum amplitude for a sine wave at the 1L frequency rather than the actual steep maximum. In addition, Chebyshev Type I results from Signals #2-4 showed a lower amplitude than the other filter types, and IF Analysis results were unable to accurate represent the exponential growth of each signal.

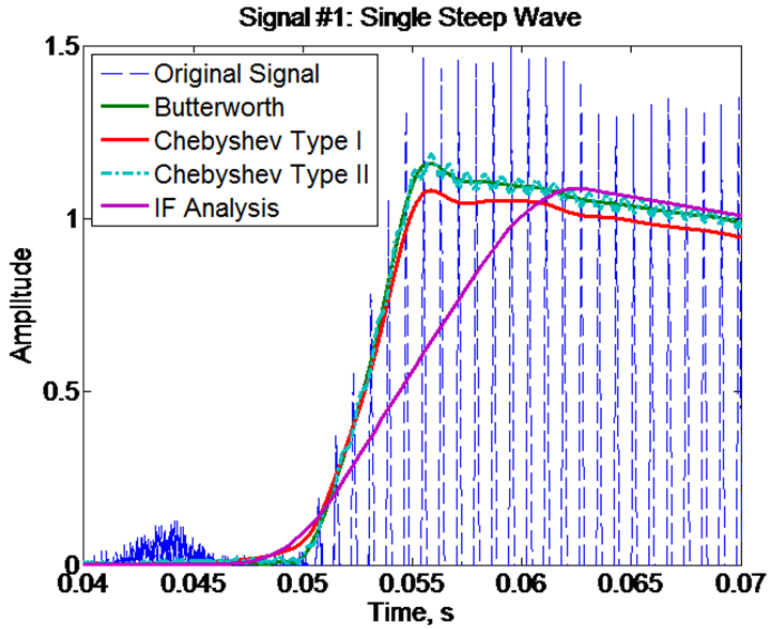

Figure 4.24 Filter comparisons of 1L for a single steep-fronted wave.

Results for Signal #5 seen in Figure 4.25 did not differ from the other manufactured signals, even though the fundamental frequency's waveform was sinusoidal instead of steep-fronted. The three IIR filter types were better able to extract and match the 1L transient behavior, though again the FIR-based IF Analysis's gradual rise to maximum amplitude obscured the true transient behavior.

And yet, IF Analysis along with the Butterworth type and Chebyshev Type II filter properly reproduced the 1L amplitude. The Chebyshev Type I filter again produced an inaccurately lower amplitude.

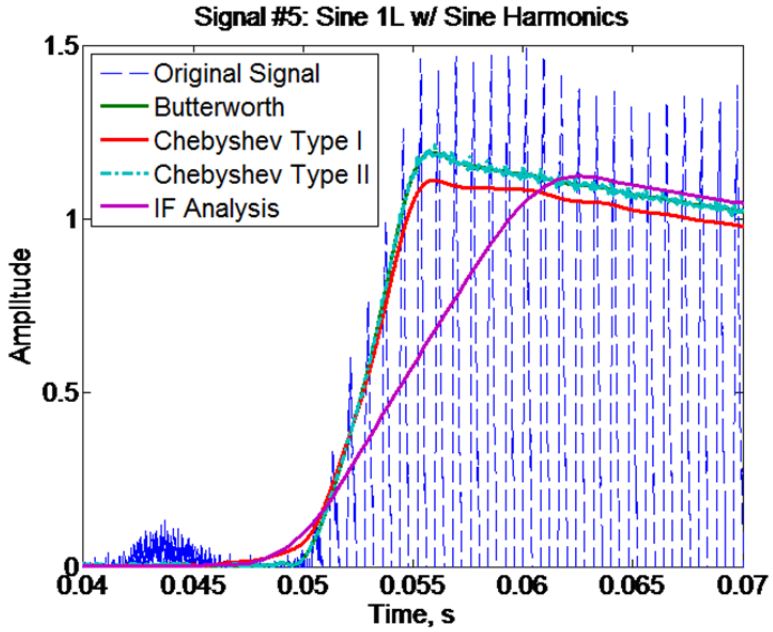

Figure 4.25 Filter comparison of 1L for a sine wave with sine harmonics.

In summary, based on application to the manufactured signals, the Butterworth filter type and the Chebyshev Type II filter are best able to represent both the transient behavior and amplitude of the mode in question, though both struggle when analyzing steep-fronted waves. The Chebyshev Type I filter is also able to represent the transient behavior of the mode but cannot properly extract the modal amplitude. And IF Analysis is able to represent the component amplitude but fails to quickly respond to the rapid amplitude change during the transition.

4.3.3 Application to Experimental Data

While the analysis of manufactured signals aids in the characterization of DSP techniques, oftentimes these techniques are more or less capable when applied to the more erratic experimental data. This is the case with Chebyshev Type II filters, as will be shown. Like before, the features to focus on are the transient behavior and the resultant limit cycle amplitude from each filter. The results from Sec. 4.3.2 suggest that the Butterworth type, Chebyshev Type II, and IF Analysis are able to accurately represent the amplitude of the mode while the Butterworth type and Chebyshev Types I and II are able to capture the transient behavior of the mode. Two experimental cases are examined: a fixed unstable test (MSFC3) and a translating test (MSFC2a).

In the fixed test case (MSFC3), the three IIR filters and FIR-based IF Analysis are applied for the first three modes, with results from Butterworth, Chebyshev Type I, and IF Analysis presented. Figure 4.26, Figure 4.27, and Figure 4.28 show the good agreement between the traditional Fourier analysis and the IF Analysis. Results from IF Analysis do not appear as sensitive to the variability of experimental data and do not show the hard start main ignition event as the traditional analysis results do. In terms of limit cycle amplitude, results from IF Analysis and the Butterworth filter show strong agreement, while the Chebyshev Type I filter shows a slightly lower amplitude, especially for higher harmonic modes.

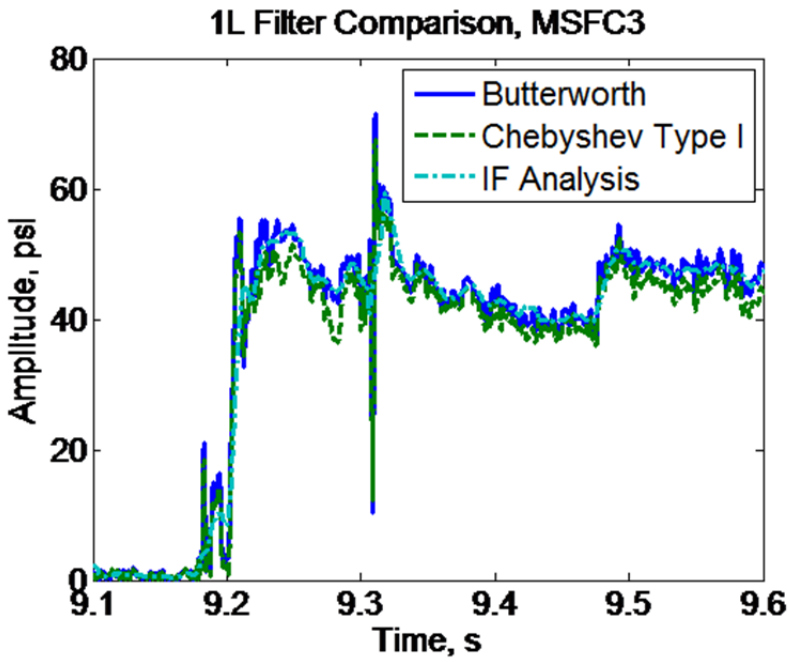

Figure 4.26 Filter comparison of 1L for an unstable fixed test case.

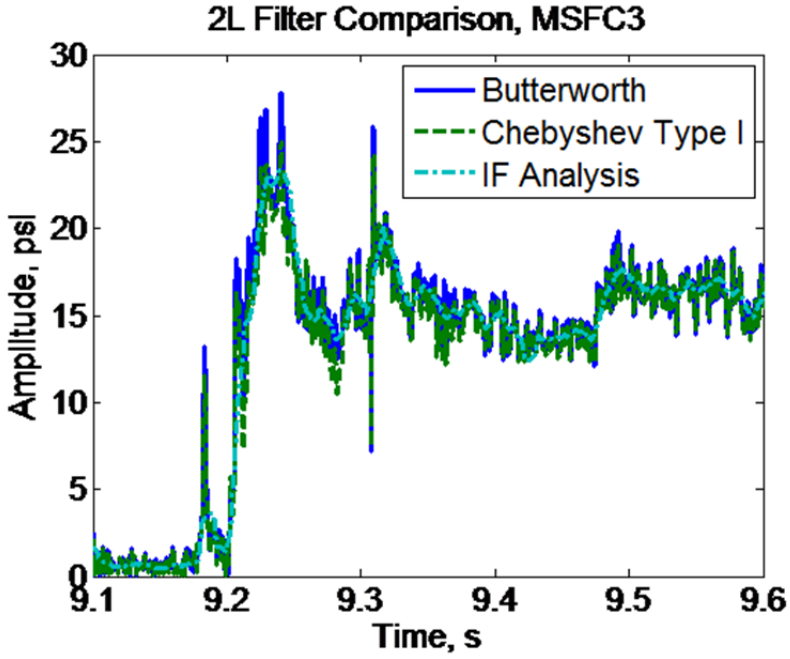

Figure 4.27 Filter comparison of 2L for an unstable fixed test case.

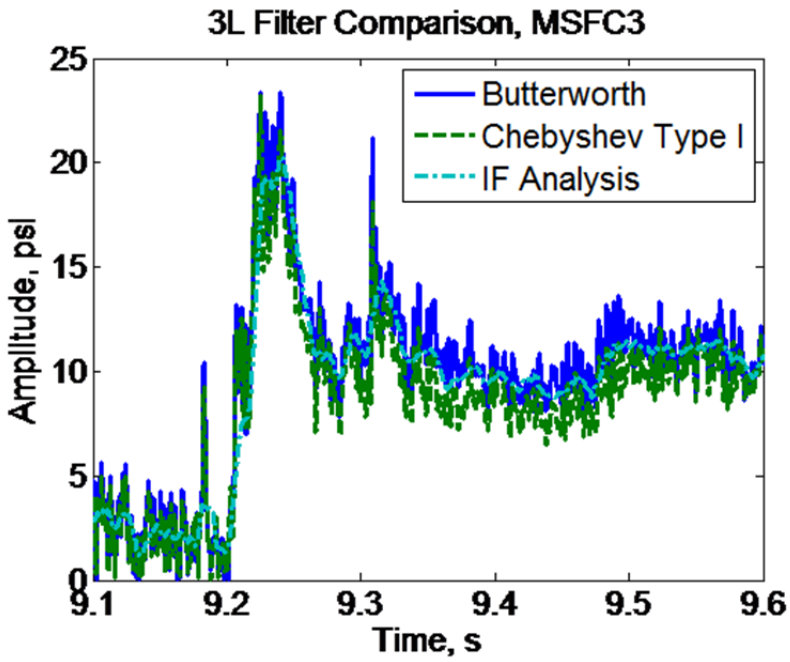

Figure 4.28 Filter comparison of 3L for an unstable fixed test case.

Section 4.2.1 reviewed the consistent modal behavior seen in translating test cases when processed through IF Analysis. This behavior agrees well with Yu's previous CVRC work covered in Sec. 1.2.3, and traditional analysis methods (mainly digital filtering) yield similar results, the extent of which is illustrated in Figure 4.29 – Figure 4.31 [20]. As discussed in Sec. 4.2.1, the frequency of each mode changes considerably during a translating test. The pass band width of all filters applied, both IIR and FIR, is 600 Hz for this reason.

In the study of 1L in a translating test, IF Analysis, Butterworth filters, and Chebyshev Type I filters display comparable limit cycle amplitude and transient behavior from stable to unstable combustion, seen in Figure 4.29. The growth and decay behavior presented by each filter type is indistinguishable from the others. The limit cycle amplitudes calculated from the Butterworth filter and

IF Analysis are essentially identical, though again the Chebyshev Type I filter underestimates this value.

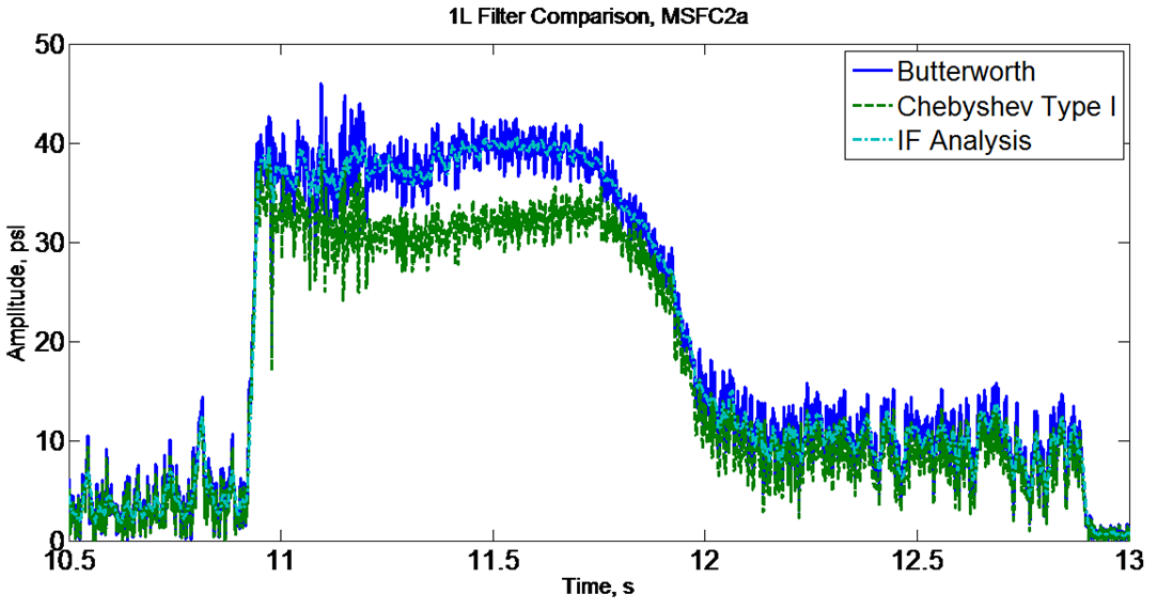

Figure 4.29 Filter comparison of 1L for a translating test case.

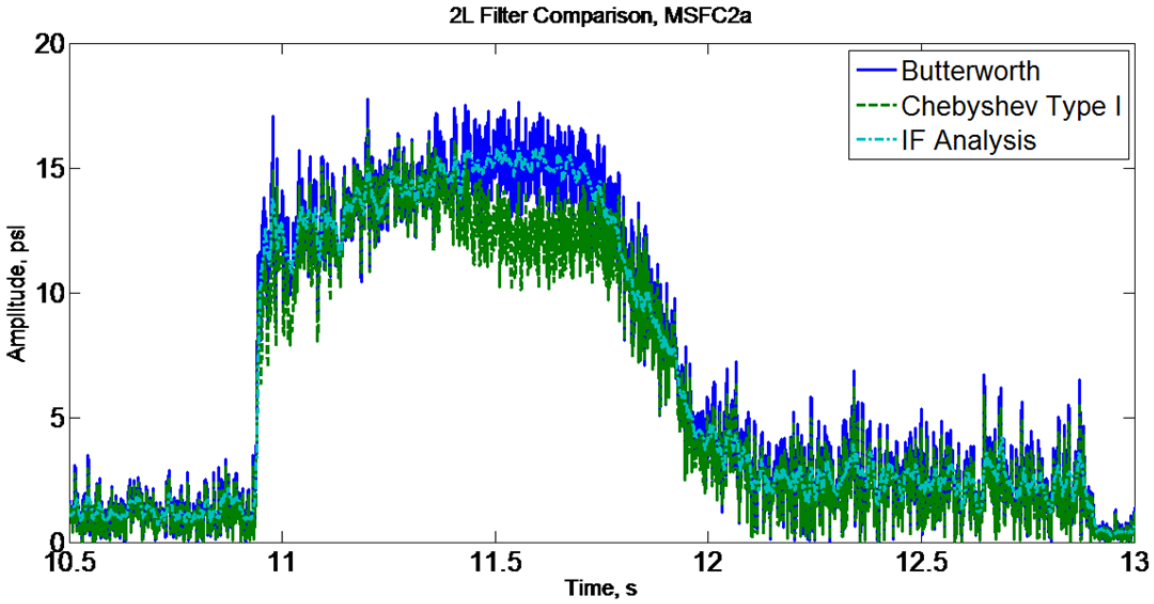

Figure 4.30 Filter comparison of 2L for a translating test case.

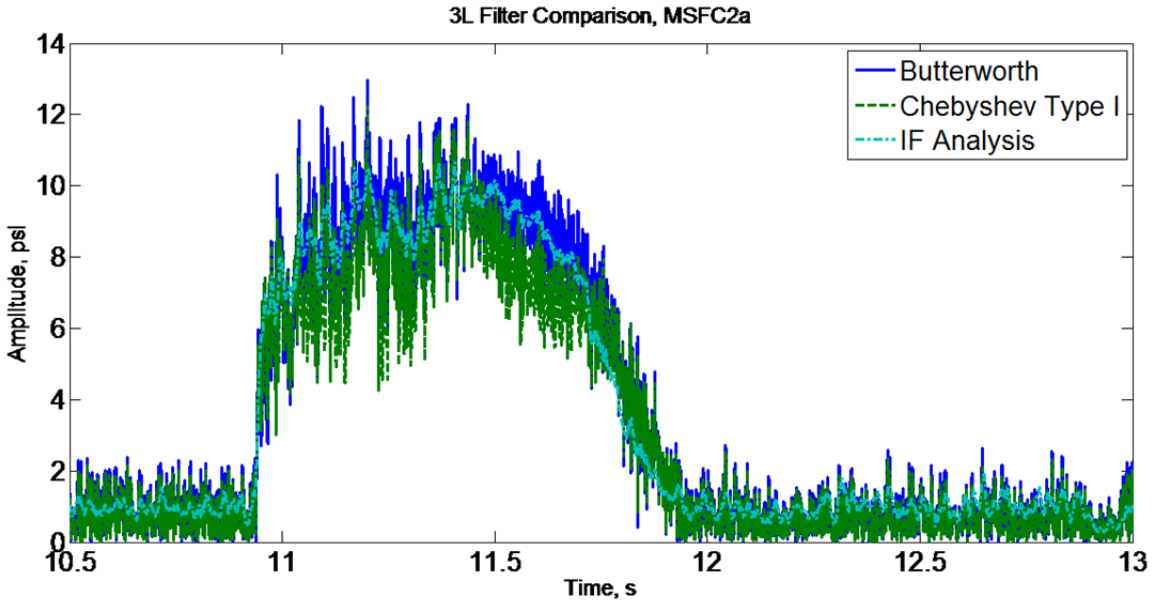

Figure 4.31 Filter comparison of 3L for a translating test case.

The results for 2L and 3L in Figure 4.30 and Figure 4.31 show even closer agreement between the IIR and FIR filters under consideration. IF Analysis again provides less noisy results, but the transient behavior and limit cycle amplitude are otherwise indistinguishable from those seen in the Butterworth and Chebyshev Type I results. Figure 4.30 and Figure 4.31 again suggest that IF Analysis provides results as good as those from the traditional analysis method but does not offer substantial advantages over the traditional analysis method enough to justify the use of IF Analysis over what is normally done.

From the work in Sec. 4.3.2 with the manufactured signals, the Chebyshev Type II filter appears to be a viable candidate as it displays similar responses to the Butterworth type filter. However, as alluded to earlier in this section, the Chebyshev Type II filter does not handle experimental data well. All results from this filter type when applied to experimental data include a significant DC offset

(upwards of 50% maximum amplitude) and the variation in peak amplitude from cycle to cycle is unsuited to the Hilbert transformation as it presents an "envelope" of the signal with a standard deviation on the order of 20% amplitude.

4.3.4 Summary of Results

Digital filter types are more or less appropriate based on the application. In the current study, the main interest was accurately representing the transient behavior as each mode is excited with a secondary interest in limit cycle amplitude. For this, the Butterworth filter type, the Chebyshev Type I and II filter, and FIR-based IF Analysis are surveyed. Section 4.3.2 determined that all of the filter types under consideration are sensitive to steep waves, as the filters are unable to accurately represent the sharp peaks of the maximum amplitude in steep-fronted waveforms. The three IIR filters under consideration were all shown to be sufficient in detecting the transient behavior of the modes, while the IF Analysis results inaccurately expressed a more gradual rise in amplitude. As for the eventual limit cycle amplitude, IF Analysis along with the Butterworth type and Chebyshev Type II filters consistently produced reasonable limit cycle amplitudes that matched each other. The Chebyshev Type I filter systematically underestimated the true value. Section 4.3.3 looked at the applicability to the CVRC's experimental data for both an unstable fixed test case and a translating test case.

Results were for the most part consistent with Sec. 4.3.2, with some notable exceptions. Results from the Chebyshev Type II filter were unusable for experimental data due to its sensitivity to noisy data. The IIR filters and the FIR-based IF analysis provided indistinguishable results for the translating test case,

while for the fixed test case the transient behavior is the same for all filters but the Chebyshev Type I filter provides lower limit cycle amplitude results.

At this time, the Butterworth type filter does not exhibit gross inaccuracies in representing the modal behavior when compared to other digital filter types, and results from this filter type are treated as reasonable preliminary results. Additionally, IF Analysis does not appear to provide a significant advantage over traditional analysis methods. Because of the "black-box" nature of the DSP method, lack of adequate documentation, and guess-and-check specification of settings, IF Analysis from the software PC Signal Analysis does not appear to be a better alternative to traditional Fourier-based analysis.

4.4 Existence of Harmonics

At this point, evidence both for and against the existence of harmonics has been presented. Section 4.1 has shown that distorted wave shapes may produce strong harmonic artifacts in Fourier-based analysis, and Sec. 4.1.3.6 has shown that the sequential and organized behavior of the fundamental mode and its harmonics cannot be attributed to Fourier artifacts alone. However, there are other characteristics of the experimentally observed harmonics that further support the idea that harmonic modes truly exist.

4.4.1 Standing Wave Behavior

In both acoustic wave theory and shock-like wave theory (see Ch.CHAPTER 2), longitudinal combustion instabilities are often treated as standing acoustic waves. Tsuji and Takeno justify representing shock-like waves with equivalent standing waves because of the shock reflections experimentally

observed at locations corresponding to standing wave nodes, seen in Figure 2.4 [17]. Hefner represents two distorted traveling acoustic waves as an equivalent standing wave on account the negating effect on observed amplitude for identical waves traveling in opposite directions, shown in Figure 2.2 [1]. Both of these works support the existence of harmonics, though one makes the assumption of shock-like 1L AND shock-like harmonics. A main difference is the expectation for constant amplitude versus axial location from Tsuji and Takeno, while Hefner assumes the amplitude will depend on the axial position relative to the pressure nodes and antinodes [1,17].

Figure 4.32, Figure 4.33, and Figure 4.34 demonstrate the classical acoustic wave behavior of a standing wave in a closed-closed tube for the first three longitudinal modes. The gold stars indicate the axial location of pressure nodes for each longitudinal mode, the location of minimum amplitude pressure oscillations for the corresponding mode. For 1L, a single pressure node exists at 7.5 in along the axial length of the combustor (see Figure 4.32), two pressure nodes for 2L at 3.75 in and 11.25 in (see Figure 4.33), and three pressure nodes for 3L at 2.5in, 7.5 in, and 12.5 in (see Figure 4.34). All three modes also display a pressure antinode (maximum value) at either end of the combustor. Mode shape analysis from the LEE program has produced similar information for CVRC test cases [20,22,32]. For a standing acoustic wave, it is expected that pressure oscillations of a given mode will have low to no amplitude near one of its pressure nodes. Conversely, near a pressure antinode, pressure oscillations of a given mode should show a maximum amplitude.

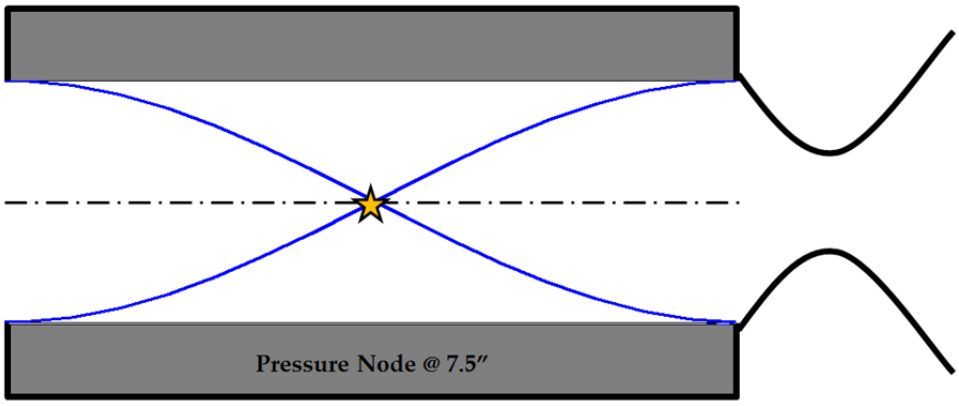

Figure 4.32 Standing wave behavior of 1L in a closed-closed tube.

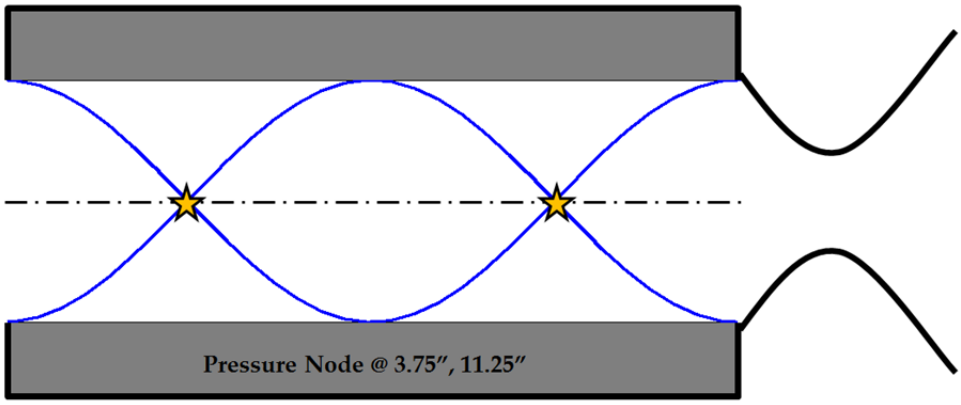

Figure 4.33 Standing wave behavior of 2L in a closed-closed tube.

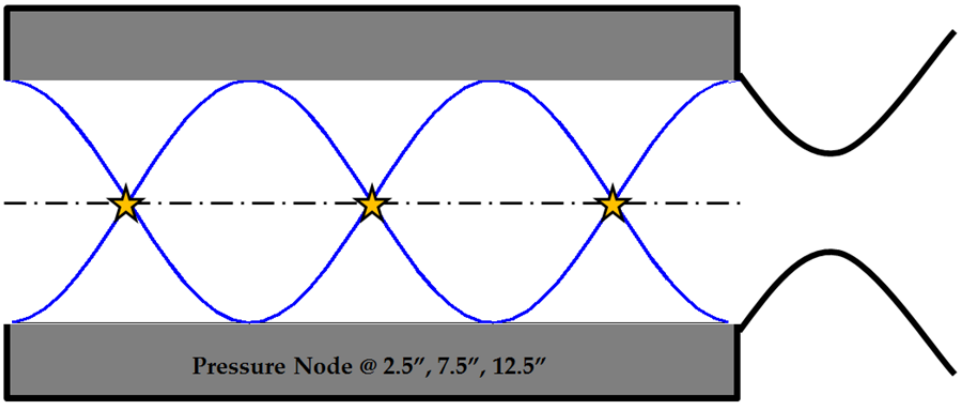

Figure 4.34 Standing wave behavior of 3L in a closed-closed tube.

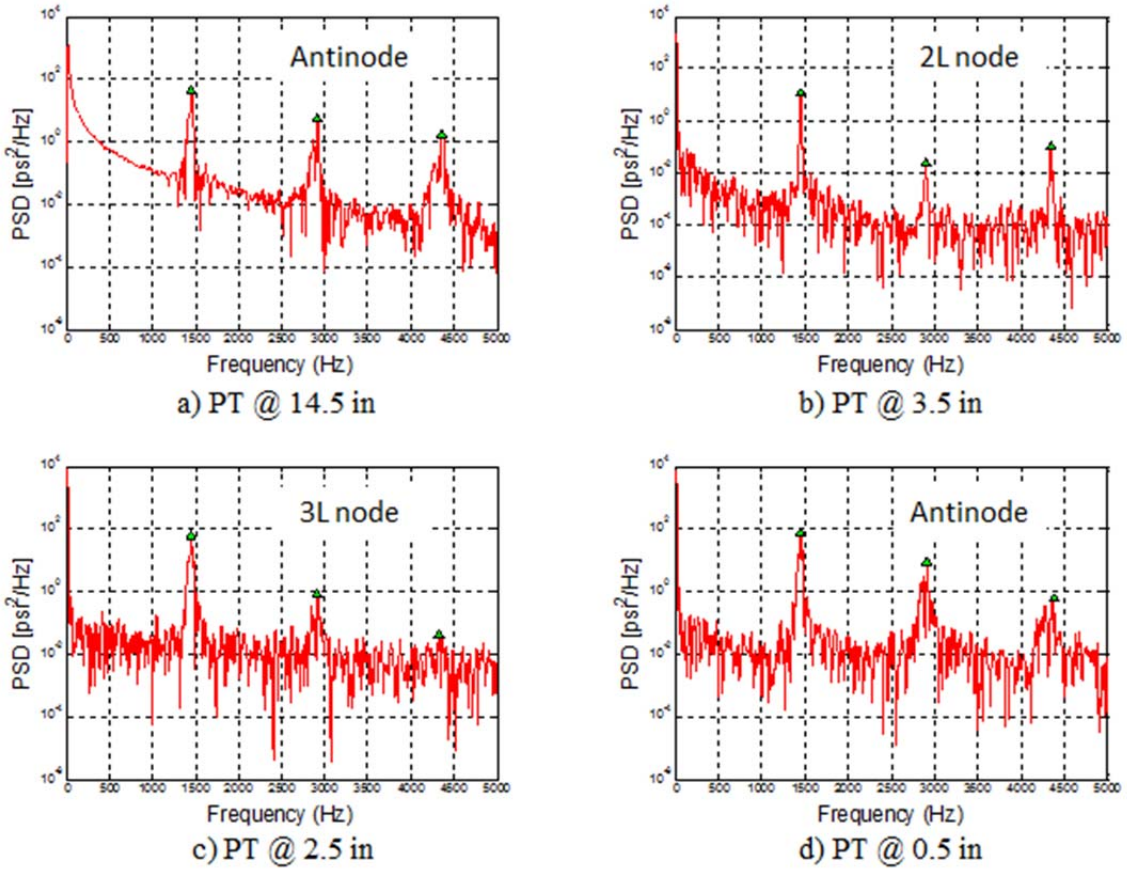

Figure 4.35 PSD results of an unstable fixed test case at four PT locations.

This behavior is most noticeable in the PSD plots for an unstable test. Figure 4.35a and Figure 4.35d show that at axial locations corresponding to pressure antinodes for the first three modes, the intensities calculated correspond to the respective behavior in Sec. 4.1. However, at an axial location near the pressure node for 2L (see Figure 4.35b), the calculated intensity of that frequency decreases while the other two modes are unaffected. Similarly, at an axial location corresponding to the pressure node for 3L (which is near the 2L node), the third mode is nearly indistinguishable from the noise, while the intensity of the second mode is less than at the antinode locations (see Figure 4.35c). This variance of

amplitude for specific modes based on axial location is also demonstrated in Figure 4.16. At the 3.5 in PT location, the amplitude of 2L is barely detectable. The other two modes are not as affected by the proximity to the 2L pressure node, and all three modes display significant amplitudes at the other two PT locations, which correspond to pressure antinodes for all three modes.

Moreover, phase relationships between data acquired on either side of a pressure node can support or refute standing wave behavior. For example, in the case of the third longitudinal mode, a pressure node exists at the 2.5 in axial location. Previously shown in Figure 1.3, high frequency pressure data is recorded at the 1.5 in and 3.5 in axial locations on the CVRC. As these PTs are equidistant from the 3L pressure node, one would expect the BP filtered 3L components from each location to be 180° out of phase. Figure 4.36 confirms that this behavior exists in unstable test cases in the CVRC and supports the existence of harmonic modes during unstable combustion.

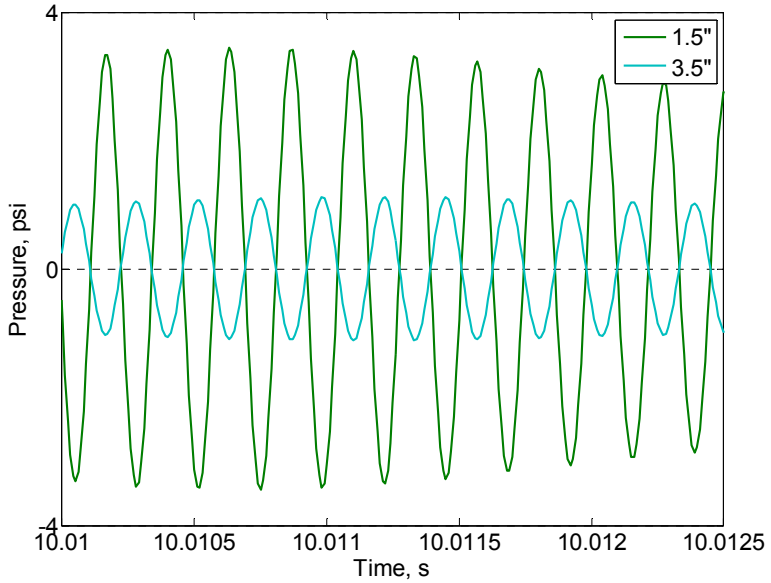

Figure 4.36 Phase relationship of 3L BP results on the side of the 3L node.

4.4.2 POD/DMD Optical Analysis

A secondary path to study the CVRC's combustion dynamics is optical analysis, especially since the CVRC is able to replace the first 5 in of the combustor with a quartz tube for optical access. Previous work on the CVRC by Rosen [21], Feldman [22] and Hardi et al. [59] utilized this optical access to obtain OH* and CH* chemiluminescence data to study the relationship between pressure oscillations and heat addition for both stable and unstable test cases. Two of the analysis techniques applied to the optical data are Proper Orthogonal Decomposition (POD) and Dynamic Mode Decomposition (DMD) [59]. Both techniques decompose the time-varying images into modal components. POD modes do not necessarily correspond to the longitudinal modes under discussion and may in fact include several frequencies. DMD, however, is able to break down the optical information by frequency [59].

In both POD and DMD results, strong harmonic frequencies are observed in unstable test cases. These techniques are not dependent on a sinusoidal assumption and it can be assumed that the harmonic content detected is not artificial. Unfortunately, POD and DMD are not viable options for the study of the transition region for the fundamental and harmonic modes, as these procedures are best applied during limit cycle operation. More information on POD and DMD analysis and results from CVRC experimental data can be found in Ref. [59].

CHAPTER 5. DISCUSSION

5.1 Distinguishing Real Harmonic Signal from DSP Artifacts

The primary concern with this study has been the harmonic modal behavior of longitudinal resonant combustion in the CVRC. However, as explained in Sec. 4.1, if at least some of the attributes of the unstable combustion are truly discontinuous, the transient behavior of the harmonic modes may be obscured by DSP artifacts as a consequence of a non-sinusoidal 1L. From the analysis in Secs. 4.1.3 and 4.2, it is clear that both traditional Fourier analysis methods and IF Analysis from the software PC Signal Analysis are sensitive to the sinusoidal assumption and may provide results that include DSP artifacts. In fact, most of the DSP methods reviewed require a continuous (sinusoidal) assumption, making them susceptible to the appearance of harmonic artifacts.

Section 4.1.3 shows that qualitative behavior of the harmonic modes can be observed using the DSP methods reviewed including traditional Fourier analysis, but the objective here was to establish a relationship that is also dependent on quantitative information such as the number of cycles between modal excitation.

From the current investigation, it appears that DSP artifacts obscure the relevant information to formulate such a relationship. One of the DSP methods not confined by this assumption is wavelet analysis. Though highly sensitive to user inputs, wavelet analysis may be less likely to display DSP artifacts if steep-fronted

wavelet shapes like the Daubechies wavelet are employed. Regardless, until the issue of DSP artifacts can be resolved, studying harmonic behavior in the CVRC will be ineffective.

5.2 Comparison of Fixed vs. Translating Tests

5.2.1 Linear vs. Nonlinear Onset

As discussed by Yu, the onset of instability during translating tests begins in the linear region and transitions to the nonlinear region as the amplitude increases and harmonic modes are excited [20]. However, Sec. 3.1.5 introduces the idea that fixed tests may experience a triggering event (subcritical bifurcation) as a result of the short duration high amplitude ignition events. The source of pressure oscillations can largely affect the transient behavior of the mode(s) as it grows to limit cycle amplitude. As the main concern in the current study is the transient behavior of the fundamental and harmonic modes, significant differences at the onset of instability could make comparison between fixed and translating tests illogical as the results may be characterizing two distinctly different processes. In addition, unstable fixed test cases produce a wider variation in behavior than translating tests. While translating tests may shift to unstable combustion at different Lop lengths, the qualitative behavior is consistent between test cases and test series.

More recent work with the CVRC strives to eliminate the hard start ignition events seen in most experimental data to date. If this can be achieved, the instabilities seen in fixed test cases may then be attributed to self-excited

instabilities as they are in the translating tests. Accomplishing this would make direct comparisons between test types more reasonable.

5.2.2 Stability Characteristics at Onset

Sec. 3.1.5 also touches on the physical differences at the time of instability onset for the fixed and translating tests, namely the difference in oxidizer post lengths at the time of transition from stable to unstable combustion. The internal geometry of the combustor can impact variables such as the characteristic time lag τ, and as introduced in Sec. 2.3 and illustrated in Figure 2.6 and Figure 2.7, the n and τ values of the combustor represent different stability regions. For example, near the stability limits, a change in τ could move the combustor into the linear or nonlinear stability region. At this time, it is believed that as the oxidizer post length increases, the value of τ decreases while the value of n is most likely unchanged [31]. So, different Lop values could create different stability environments in the combustor. In the results presented in Sec. 3.1.5, the oxidizer post length at the time of excitation was 5.1 in for the fixed test and 6.25 in for the translating test. Again, this opens up the possibility that the combustion starts in different stability regions for fixed and translating tests, and direct comparison between the two at this time may be unproductive.

To date, the CVRC fixed test cases have been performed at Lop values corresponding to a stable configuration at 7.8 in, an unstable configuration at 5.1 in, and a marginally stable configuration at 3.9 in. These test cases have served the needs of CFD model validations, but for the current study, fixed test cases at Lop values corresponding to the transition regions in translating tests would be much more relevant. If test cases at these translating transitional configurations occur,

direct comparison between fixed and translating test cases wouldn't be unreasonable. Additionally, the limited number of unstable fixed tests could make side by side quantitative comparisons difficult when the differences in Lop may be changing the stability behavior at onset.

5.3 Isolation of Harmonic Pressure Signal

A key way to confirm or deny the existence of harmonic modes would be to isolate the harmonic pressure signal. One way to do this would be to place a pressure transducer at the axial location corresponding to a pressure node for the fundamental frequency. Section 4.4.1 identifies this location as the midpoint of the combustor length, in this study at the 7.5 in location. The midpoint corresponds to a pressure node for 1L and 3L and a pressure antinode for 2L, as previous illustrated in Figure 4.32 – Figure 4.34. Then, the dynamic pressure signal recorded at this location could be mainly attributed to a harmonic mode, in this case 2L, supporting the existence of harmonic modes in longitudinal combustion instabilities.

Until the harmonic pressure component(s) can be isolated, analysis efforts along the lines of the current study may continue to be ineffectual, since at this time all PT locations are dominated by 1L.

CHAPTER 6. CONCLUSION

The current study started with the intention to establish a heuristic relationship between the excitation of the fundamental mode and the consequent excitation of higher harmonic modes for longitudinal combustion instabilities in liquid rocket engines. During this study, sizable issues with the traditional analysis results became apparent (namely the existence of harmonic artifacts in Fourier-based analyses for discontinuous waveforms), requiring a major digression from the original intent. Several DSP methods were tested, with Fourier-based analysis and IF Analysis from the software PC Signal Analysis explored in more detail. While a couple DSP methods have been conclusively eliminated, the remainder have the potential to provide relevant modal information.

Further assessment of IF Analysis and components of the traditional Fourier-based analysis provided mixed results. It was shown that the components used in the traditional analysis presented are reasonably suited to the study of modal behavior in combustion instabilities when compared to alternative options. However, deficiencies were also exposed, particularly the inability to correctly interpret amplitude information from sharp peaks in a waveform. Continued use of IF Analysis showed the sensitivity of the results to filter settings like pass band width and FIR filter order. What was originally thought to be a potential ability of IF Analysis to distinguish between DSP artifacts and real modal behavior proved

to be the result of non-optimal settings. The traditional Fourier-based analysis results closely match results from IF Analysis and bring in to question whether or not IF Analysis is worth using. Both methods have been shown to be very sensitive to the sinusoidal assumption.

6.1 Harmonics Exist

At the conclusion of the current study, it has been shown that harmonic modes do exist in the CVRC. Behavioral patterns observed in Sec. 3.1.5 were shown to be independent of Fourier artifacts in Sec. 4.1.3, in particular the sequential excitation of modes and the increasing growth rate with increasing mode number. An independent modal decomposition analysis of optical data from the CVRC further validated the existence of harmonic modes during unstable combustion.

6.2 Artifacts of Harmonics Exist

Unfortunately, at the conclusion of the current study, it has also been shown that artifacts from DSP methods do appear in the current results for harmonic modes. At this time, it is unclear how to distinguish between artifacts and real details of harmonic modal behavior. Until a procedure can be established to identify and remove the data artifacts, it cannot be stated with certainty that the observed harmonic behavior is a result of the combustion instability characteristics instead of the DSP method.

6.3 Evaluation of Signal Processing Methods

A number of DSP methods for high frequency applications were tested and assessed in the current study. The main abilities desired from a DSP method for this application were a fine time resolution on the order of 1 ms, protection against user bias, consistency between runs, reasonable computational requirements of both the user and the computer, and ability to distinguish real harmonic signal components from noise and/or data artifacts.

The oscillation decrement, a form of signal autocorrelation analysis, is one of the DSP methods eliminated during this study. Previously used by the Russian space agency and more recently by Sisco as an indicator of instantaneous combustor damping levels, application of the oscillation decrement to the experimental CVRC data showed an inability to handle multiple frequencies, especially sinusoidal waveforms [4]. Data artifacts from lower modes would appear in the results of higher modes, and it was unclear if the indication of instability onset changed for different frequencies. Additionally, the time scale required for comparison between modes was not available through the oscillation decrement. While fitting for general characterization of a combustor, the oscillation decrement is not a suitable DSP method when comparing modes.

Another DSP method that was quickly eliminated from consideration was matched filtering. Originally pursued because of the *a priori* knowledge of the frequencies of interest, matched filtering is similar to a brick wall filter that searches for when the input signal matches the specified signal. However, due to the distortion of the waveform during the transition to unstable combustion, matched filtering is inappropriate for this application.

A recent buzzword in the aerospace community, wavelet analysis has the potential to provide useful information about harmonic modal behavior, especially in the case of discontinuous waveforms. However, this method is highly sensitive to user-defined wavelet characteristics such as wavelet shape and shape factor. Wavelet analysis requires more computational power than the other methods reviewed and has the steepest learning curve. Until more analysis using steep-fronted wavelets have been performed, the appropriateness of wavelet analysis for the current application cannot be explicitly stated. Should future analysis provide similar results to those presented in the current study, wavelet analysis may not be worth the additional effort. However, the ability to differentiate between or completely eliminate data artifacts from harmonic modal behavior would justify the use of this DSP method.

Traditional Fourier-based analysis was not completely disqualified in the current study. While it was proven that results from Fourier-based analysis include data artifacts, it was also shown that qualitative behavior of the harmonic modes is distinguishable through this DSP method. In essence, traditional Fourier-based analysis as has been applied to CVRC experimental data to date provides useful information in the study of harmonic modes, but the results should not be used alone. Supplemental DSP methods that could better provide quantitative information would be more appropriate in the current study.

The IF Analysis from the software package PC Signal Analysis has also not been completely discounted. At its core a Fourier-based analysis, the IF Analysis provides results nearly identical to those from the traditional DSP method. However, IF Analysis is better able to handle experimental data and can produce frequency and phase information that Matlab's routine is unable to provide.

Additionally, the capabilities of this signal processing software have yet to be fully explored. One roadblock to the continued use of this software is the lack of documentation and steep learning curve. Further analysis may need to be done before completely ruling out PC Signal Analysis as a viable method to study harmonic behavior, especially if it can be shown that frequency and/or phase information is relevant.

6.4 Future Tasks

The CVRC is an active experiment at Purdue University, offering the chance for future experimental and analytical efforts. The main tasks that would most benefit the continuation of the current study are the addition of a PT at the 7.5 in location corresponding to a 1L pressure node, the elimination of hard start ignition events, and the execution of fixed test cases at Lop corresponding to transition length in translating tests. These tasks, however, are wholly experimental and time-dependent on others.

A task that can be done immediately is the continued exploration of wavelet analysis, testing and comparing different wavelet shapes and shape factors. A good comparison might look at the calculated onset times for each mode as a function of shape factor to see how much impact user defined settings may have on results. This would be a non-trivial task, and any efforts in this direction should consider continued use of David Kittel's Matlab routine [55,56]. An essential portion of this task will involve modification of the routine to accommodate alternative wavelet shapes and the development of criteria to evaluate how suitable the shape(s) may be to this study.

An additional analytical task would be continued fake signal analysis, with the variation from the work presented in Sec. 4.1 being the staggered onset of harmonic modes. For example, instead of creating a composite waveform and then exponentially growing this waveform, individual components can each exponentially grow to the relative amplitude previously used and may begin at a different time than the 1L component. This may help to distinguish the behavior of extant harmonic signal if the artificial harmonics appear with the onset of 1L while the real modal behavior appears at known later times. Plus, direct comparisons can be made between the filtered results and the original component signals. And fake signal analysis of signals with an exponential decay could aid in the interpretation of translating test data.

Finally, once real harmonic signal can be distinguished from Fourier artifacts, analytical efforts can work toward heuristic relationships between the onset of the fundamental mode and higher harmonics.

LIST OF REFERENCES

LIST OF REFERENCES

[1] Harrje, D. T., Reardon, F. H. (eds.), Liquid Propellant Rocket Combustion Instability, NASA SP-194, Washington, D.C., 1972.

[2] Culick, F. E. C., "Combustion Instabilities in Liquid-Fuelled Propulsion Systems - an Overview," AGARDograph, 1988.

[3] Culick, F. E. C., Yang, V., "Overview of Combustion Instabilities in Liquid Propellant Rocket Engines." In: Yang, V., Anderson, W. E., (eds.). *Liquid Rocket Engine Combustion Instability*, Vol. 169, Progress in Aeronautics and Astronautics, AIAA; 1995, pp. 3–38.

[4] Sisco, J., "Measurement and Analysis of an Unstable Model Rocket Combustor," Ph.D. Dissertation, Aeronautics and Astronautics Dept., Purdue University, West Lafayette, IN, 2007.

[5] Culick, F. E. C., "Some Recent Results for Nonlinear Acoustics in Combustion Chambers," *AIAA Journal*, Vol. 32, No. 1, 1994, pp. 146–169.

[6] Natanzon, M.S., "Low Frequency Oscillations in Liquid Rocket Combustion Chambers." In: Culick, F. E. C., (ed.). *Combustion Instability*, Vol. 222, Progress in Aeronautics and Astronautics, AIAA; 1999, pp. 1–42.

[7] Natanzon, M. S., "High-Frequency (Acoustic) Oscillations in a Combustion Chamber." In: Culick F. E. C. , (ed.). *Combustion Instability*, Vol. 222, Progress in Aeronautics and Astronautics, AIAA; 1999, pp. 95–124.

[8] Sujith, R. I., [2008, December 8]. Aerospace - Acoustic Instabilities in Aerospace Propulsion. Online video lectures. National Programe on Technology Enhanced Learning, YouTube. Accessed Jan - May 2014.

[9] Crocco, L., Cheng, S. I., "High Frequency Combustion Instability in Rocket Engines with Distributed Combustion." *Symposium (International) on Combustion*, The Combustion Institute, Vol. 4, 1953, pp. 865–880.

[10] Mitchell, C. E., "Analytical Models for Combustion Instability." In: Yang, V., Anderson, W. E., (eds.). *Liquid Rocket Engine Combustion Instability*, Vol. 169, Progress in Aeronautics and Astronautics, AIAA; 1995, pp. 403–430.

[11] Bracco, F., "Standing Acoustic Waves in a Confined, Non-Uniform Gas." *Journal of Sound and Vibration*. Vol. 41, 1975: pp. 301–309.

[12] Yang, V., Anderson, W. E. , (eds.). *Liquid Rocket Engine Combustion Instability*. Vol. 169, Progress in Aeronautics and Astronautics, AIAA; 1995.

[13] Yang, V., Wicker, J. M., Yoon, M. W., "Acoustic Waves in Combustion Chambers." In: Yang, V., Anderson, W. E., (eds.). *Liquid Rocket Engine Combustion Instability*, Vol. 169, Progress in Aeronautics and Astronautics, AIAA; 1995, pp. 357–376.

[14] Natanzon, M. S., *Combustion Instability*. Culick, F.E.C. (ed.). Vol. 222, Progress in Aeronautics and Astronautics, AIAA. Reston, Virginia: 1999.

[15] Hutt, J. J., Rocket, M., "High-Frequency Injection-Coupled Combustion Instability." In: Yang, V., Anderson, W. E., (eds.). *Liquid Rocket Engine Combustion Instability*, Vol. 169, Progress in Aeronautics and Astronautics, AIAA; 1995, pp. 345–356.

[16] Zucrow, M. J., Osborn, J. R., "An Experimental Study of High-Frequency Combustion Pressure Oscillations." *Journal of Jet Propulsion*. Vol. 28, 1958: pp. 654 – 659.

[17] Tsuji, H., Takeno, T., "An Experimental Investigation on High-Frequency Combustion Oscillations." *Symposium (International) on Combustion*. 1965: pp. 1327–1335.

[18] Miller, K. J., "Experimental Study of Longitudinal Instabilities in a Single Element Rocket Combustor," Ph.D. Dissertation, Aeronautics and Astronautics Dept., Purdue University, West Lafayette, IN, 2005.

[19] Smith, R. J., "Computational Modeling of High Frequency Combustion Instability in a Single-Element Liquid Rocket Engine," M.S. Dissertation, Aeronautics and Astronautics Dept., Purdue University, West Lafayette, IN, 2006.

[20] Yu, Y., "Experimental and Analytical Investigations of Longitudinal Combustion Instability in a Continuously Variable Resonance Combustor (CVRC)," Ph.D. Dissertation, Aeronautics and Astronautics Dept., Purdue University, West Lafayette, IN, 2009.

[21] Rosen, S. C., "Combustion Instabilities in the Transition Region of an Unstable Model Rocket Combustor," M.S. Dissertation, Aeronautics and Astronautics Dept., Purdue University, West Lafayette, IN, 2011.

[22] Feldman, T. W., "Unstable Combustion Processes for a Single Element Shear/Coax Injector in a Longitudinal Combustor," M.S. Dissertation, Aeronautics and Astronautics Dept., Purdue University, West Lafayette, IN, 2013.

[23] Fisher, S. C., Dodd, F. E., Jensen, R. J., "Scaling Techniques for Liquid Rocket Combustion Stability Testing." In: Yang, V., Anderson, W. E., (eds.). *Liquid Rocket Engine Combustion Instability*, Vol. 169, Progress in Aeronautics and Astronautics, AIAA; 1995, pp. 545–564.

[24] Hulka, J., "Instability Phenomena in Liquid Oxygen/Hydrocarbon Rocket Engines." In: Yang, V., Anderson, W. E., (eds.). *Liquid Rocket Engine Combustion Instability*, Vol. 169, Progress in Aeronautics and Astronautics, AIAA; 1995, pp. 73–88.

[25] Crocco, L., Cheng, S. I., "Theory of Combustion Instability in Liquid Propellant Rocket Motors," AGARDograph, 1956.

[26] Mitchell, C. E., Crocco, L., Sirignano, W. A., "Nonlinear Longitudinal Instability in Rocket Motors with Concentrated Combustion," *Combustion Science and Technology* , Vol. 1, 1969: pp. 35–64.

[27] Pal, S., Kalitan, D., Woodward, R., Santoro, R., "Performance and Stability Characteristics of a Uni-Element Swirl Injector for Oxygen-Rich Stage Combustion Cycles," NASA Report, 2004: pp. 1–11.

[28] Zinn, B. T., Lores, M. E., "Application of the Galerkin Method in the Solution of Non-linear Axial Combustion Instability Problems in Liquid Rockets," *Combustion Science and Technology,* Vol. 4, 1971: pp. 269–278.

[29] Lores, M. E., Zinn, B. T., "Nonlinear Longitudinal Combustion Instability in Rocket Motors," *Combustion Science and Technology*, Vol. 7. 1973: pp. 245–256.

[30] Feldman, T. W., Harvazinski, M. E., Merkle, C. L., Anderson, W. E., "Comparison Between Simulation and Measurement of Self-Excited Combustion Instability". *48th AIAA/ASME/SAE/ASEE Joint Propulsion Conference & Exhibit*, 30 July-01 August 2012, Atlanta, Georgia.

[31] Harvazinski, M. E., Huang, C., Sankaran, V., Feldman, T. W., Anderson, W. E., Merkle, C. L., "Combustion Instability Mechanisms in a Pressure-coupled Gas-gas Coaxial Rocket Injector." *49th AIAA/ASME/SAE/ASEE Joint Propulsion Conference*, 14-17 July 2013, San Jose, CA.

[32] Yu, Y., O'Hara, L., Sisco, J., Anderson, W. E., "Experimental Study of High-Frequency Combustion Instability in a Continuously Variable Resonance Combustor (CVRC)." 47*th AIAA Aerospace Sciences Meeting,* 05-08 January 2009, Orlando, FL.

[33] Lang, W., "Harmonic Frequency Generation by Oscillating Flames." *Combustion and Flame,* Vol. 83, 1991: pp. 253–262.

[34] Bowman, C. T., "Experimental Investion of High Frequency Longitudinal Combustion Instability in Gaseous Propellant Rocket Motors," Ph.D. Dissertation, Aerospace and Mechanical Sciences Dept, Princeton University, Princeton, New Jersey, 1967.

[35] Natanzon, M. S., "Nonlinear Effects." In: Culick, F. E. C., (ed.). *Combustion Instability*, Vol. 222, Progress in Aeronautics and Astronautics, AIAA; 1999, pp. 125–146.

[36] Flandro, G., Majdalani, J., Sims, J., "Nonlinear Longitudinal Mode Instability in Liquid Propellant Rocket Engine Preburners." *40th AIAA/ASME/SAE/ASEE Joint Propulsion Conference*, 11-14 July 2004, Fort Lauderdale, FL.

[37] Harrje, D., Sirignano, W., "Nonlinear Aspects of Combustion Instability in Liquid Propellant Rocket Motors," NASA Progress Report No. 553-d, 1964.

[38] Flandro, G., "Approximate Analysis of Nonlinear Instability with Shock Waves." *18th AIAA/SAE/ASME Joint Propulsion Conference*, 21-23 June 1982, Cleveland, OH.

[39] Sirignano, W. A., Crocco, L., Harrje, D., "A Theoretical Study of Non-Linear Combustion Instability: Longitudinal Mode." NASA Technical Report No. 677, 1964.

[40] Sirignano, W. A., "A Theory of Axial-Mode Shock-Wave Oscillations in a Solid-Rocket Combustor." *Symposium (International) on Combustion*, Vol. 12, 1969: pp. 129–137.

[41] Culick, F. E. C., "Non-Linear Growth and Limiting Amplitude of Acoustic Oscillations in Combustion Chambers." *Combustion Science and Technology*, Vol. 3, 1971: pp. 1–16.

[42] Burnley, V. S., Culick, F. E. C., "Some Dynamics of Acoustic Oscillations with Nonlinear Combustion and Noise," *International Journal of Energetic Materials and Chemical Propulsion*, Vol. 4, 1997: pp. 1-6.

[43] Sterling, J. D., Zukoski, E. E., "Nonlinear Dynamics of Laboratory Combustor Pressure Oscillations." *Combustion Science and Technology*, Vol 77, 1991: pp. 225–238.

[44] Sterling, J. D., "Nonlinear Analysis and Modelling of Combustion Instabilities in a Laboratory Combustor." *Combustion Science and Technology*, Vol. 89, 1993: pp. 167–79.

[45] Margolis, S., "The Nonlinear Dynamics of Intrinsic Acoustic Oscillations in a Model Pulse Combustor." *Combustion and Flame*, Vol. 322, 1994: pp. 311–322.

[46] Sirignano, W. A., Crocco, L. "A Shock Wave Model of Unstable Rocket Combustors." *AIAA Journal*; Vol. 2, 1964: pp. 1285–1296.

[47] Clayton, R. M., Rogero, R. S., "Experimental Measurements on a Rotating During Liquid Rocket Wave Observed Resonant." NASA Technical Report No. 32-788, 1965.

[48] Clayton, R. M., Rogero, R. S., Sotter, J., "An Experimental Description of Destructive Liquid Rocket Resonant Combustion." *AIAA Journal*; Vol. 6, 1968: pp. 1252–1259.

[49] Shin, K., Hammond, J., *Fundamentals of Signal Processing for Sound and Vibration Engineers*. West Sussex, England: John Wiley & Sons Ltd.; 2008.

[50] "Signal Processing Toolbox™ User's Guide R 2014 a." Natick, MA: The MathWorks, Inc.; 2014.

[51] Losada, R. A., "Digital Filters with MATLAB ®". Natick, MA: The MathWorks, Inc.; 2008.

[52] Misiti, M., Misiti, Y., Oppenheim, G., Poggi, J. M., "Wavelet Toolbox™ User's Guide R 2014 a." Natick, MA: The MathWorks, Inc.; 2014.

[53] Zeytinoglu, M., Wong, K., "Detection of Harmonic Sets." *IEEE Transactions on Signal Processing*; Vol. 43, No. 11, 1995: pp. 2618–2630.

[54] "Wavelet Toolbox: Wavelet Shapes." University of Prague: Department of Radio Engineering, n.d. Web. 16 Oct 2013.

[55] Kittel, D. E., Mares, O. J., Son, S. F., "Measuring Time-Resolved Detonation Velocity Using Wavelet Analysis and Microwave Interferometry." Review of Scientific Instruments. Submitted for publication July 2014.

[56] Kittel, D. E., Mares, O. J., Son, S. F., "A Comparison of Wavelet, Quadrature, and Peak-to-Peak Methods for Determining Shock Velocity from Microwave Interferometer Data." *15th International Detonation Symposium*, 13-18 July 2014, San Francisco, CA.

[57] "PC-SIGNAL: Basic Module: User Manual." Huntsville, AL: AI Signal Research, Inc.; 2003.

[58] PC Signal Analysis, Software Package, Ver. 2.0, AI Signal Research, Inc., Huntsville, AL, 2013.

[59] Hardi, J. S., Hallum, W. Z., Huang, C., Anderson, W. E., "Development of Validation Approaches for Numerical Simulation of Combustion Instability using Flame Imaging." *50th AIAA/ASME/SAE/ASEE Joint Propulsion Conference*, 28-30 July 2014, Cleveland, OH.